WATER RESOURCES RESEARCH, VOL. 26, NO. 9, PAGES 1981–2014, SEPTEMBER 1990

Geochemical Modeling of the Madison Aquifer in Parts of Montana, Wyoming, and South Dakota

L. NIEL PLUMMER,[1] JOHN F. BUSBY,[2] ROGER W. LEE,[3] AND BRUCE B. HANSHAW[1]

Stable isotope data for dissolved carbonate, sulfate, and sulfide are combined with water composition data to construct geochemical reaction models along eight flow paths in the Madison aquifer in parts of Wyoming, Montana, and South Dakota. The sulfur isotope data are treated as an isotope dilution problem, whereas the carbon isotope data are treated as Rayleigh distillations. All reaction models reproduce the observed chemical and carbon and sulfur isotopic composition of the final waters and are partially validated by predicting the observed carbon and sulfur isotopic compositions of dolomite and anhydrite from the Madison Limestone. The geochemical reaction models indicate that the dominant groundwater reaction in the Madison aquifer is dedolomitization (calcite precipitation and dolomite dissolution driven by anhydrite dissolution). Sulfate reduction, $[Ca^{2+} + Mg^{2+}]/Na^{+}$ cation exchange, and halite dissolution are locally important, particularly in central Montana. The groundwater system is treated as closed to CO_2 gas from external sources such as the soil zone or cross-formational leakage but open to CO_2 from oxidation of organic matter coupled with sulfate reduction and other redox processes occurring within the aquifer. The computed mineral mass transfers and modeled sulfur isotopic composition of Madison anhydrites are mapped throughout the study area. Carbon 14 groundwater ages, adjusted for the modeled carbon mass transfer, range from modern to about 23,000 years B.P. and indicate flow velocities of 7–87 ft/yr (2.1–26.5 m/yr). Most horizontal hydraulic conductivities calculated from Darcy's Law using the average ^{14}C flow velocities are within a factor of 5 of those based on digital simulation. The calculated mineral mass transfer and adjusted ^{14}C groundwater ages permit determination of apparent rates of reaction in the aquifer. The apparent rate of organic matter oxidation is typically 0.12 μmol/L/yr. Sulfate and, to a lesser extent, ferric iron are the predominant electron acceptors. The (kinetic) biochemical fractionation of ^{34}S between sulfate and hydrogen sulfide is approximately −44‰ at 25°C, with a temperature variation of −0.4‰ per °C. The rates of precipitation of calcite and dissolution of dolomite and anhydrite typically are 0.59, 0.24, and 0.95 μmol/L/yr, respectively.

INTRODUCTION

This report describes some of the results of a modeling study [*Busby et al.*, 1990] to determine the geochemical reactions controlling water chemistry in the Madison aquifer underlying approximately 120,000 square miles of the northern Great Plains in parts of Montana, South Dakota, and Wyoming.

Several earlier studies [*Hanshaw et al.*, 1978; *Plummer and Back*, 1980; *Back et al.*, 1983; *Busby et al.*, 1983] have recognized dedolomitization as the predominant reaction in the Madison aquifer. Dedolomitization refers to the net dissolution of dolomite and precipitation of calcite caused by dissolution of anhydrite. *Plummer and Back* [1980] and *Back et al.* [1983] evaluated reactions in the calcite-dolomite-anhydrite system in a limited portion of the Madison aquifer near the Black Hills in western South Dakota. *Busby et al.* [1983] presented chemical and isotopic data collected in the present study area.

Because of the diversity of the hydrochemical conditions, the aquifer was divided into eight regional subsets of the flow system, and several other reactions beyond the dedolomitization reaction were considered in order to interpret the observed water chemistry. The original data base of *Busby et al.* [1983] was supplemented with sulfur isotope data for dissolved sulfide species, permitting quantification of sulfate reduction. These data combined with the chemical and carbon isotope data of *Busby et al.* [1983] have allowed refinement of geochemical mass balance models [*Plummer et al.*, 1983] on a regional scale. The geochemical mass balance models have been used to adjust the ^{14}C data, permitting hydrochemical estimation of water age, apparent reaction rates, regional flow velocities, and hydraulic conductivities, the latter of which are compared with digital simulation results of *Downey* [1984, 1986].

GEOHYDROLOGIC SETTING

The geohydrology of the Madison aquifer is summarized from reports by *Grossman* [1968], *Smith* [1972], *Sando* [1976*a*, *b*], *Peterson* [1978, 1981], *Thayer* [1981], *Brown et al.* [1984], *MacCary et al.* [1983], *Downey* [1984, 1986], and *Cooley et al.* [1986].

The major physiographic features in the area include the Big Horn Mountains, the Laramie Mountains, the Big Snowy Mountains, the Hartville uplift, and the Black Hills (Figure 1). These highland features are the principal recharge areas to the Madison aquifer [*Downey*, 1984]. Extensive undulating plains dissected by streams lie between the uplift areas and the regional discharge area for the aquifer system in eastern North and South Dakota.

The Madison aquifer in this report is composed of the Madison Limestone or Group where divided or stratigraphic equivalents. The Madison Group, from oldest to youngest, consists of the Lodgepole Limestone, the Mission Canyon Limestone, and the Charles Formation of Mississippian age.

The Lodgepole Limestone is a cyclic carbonate sequence consisting largely of fossiliferous to micritic dolomite and limestone units that are argillaceous and thinly bedded in

[1]U.S. Geological Survey, Reston, Virginia.
[2]U.S. Geological Survey, Austin, Texas.
[3]U.S. Geological Survey, Nashville, Tennessee.

Paper number 90WR00212.

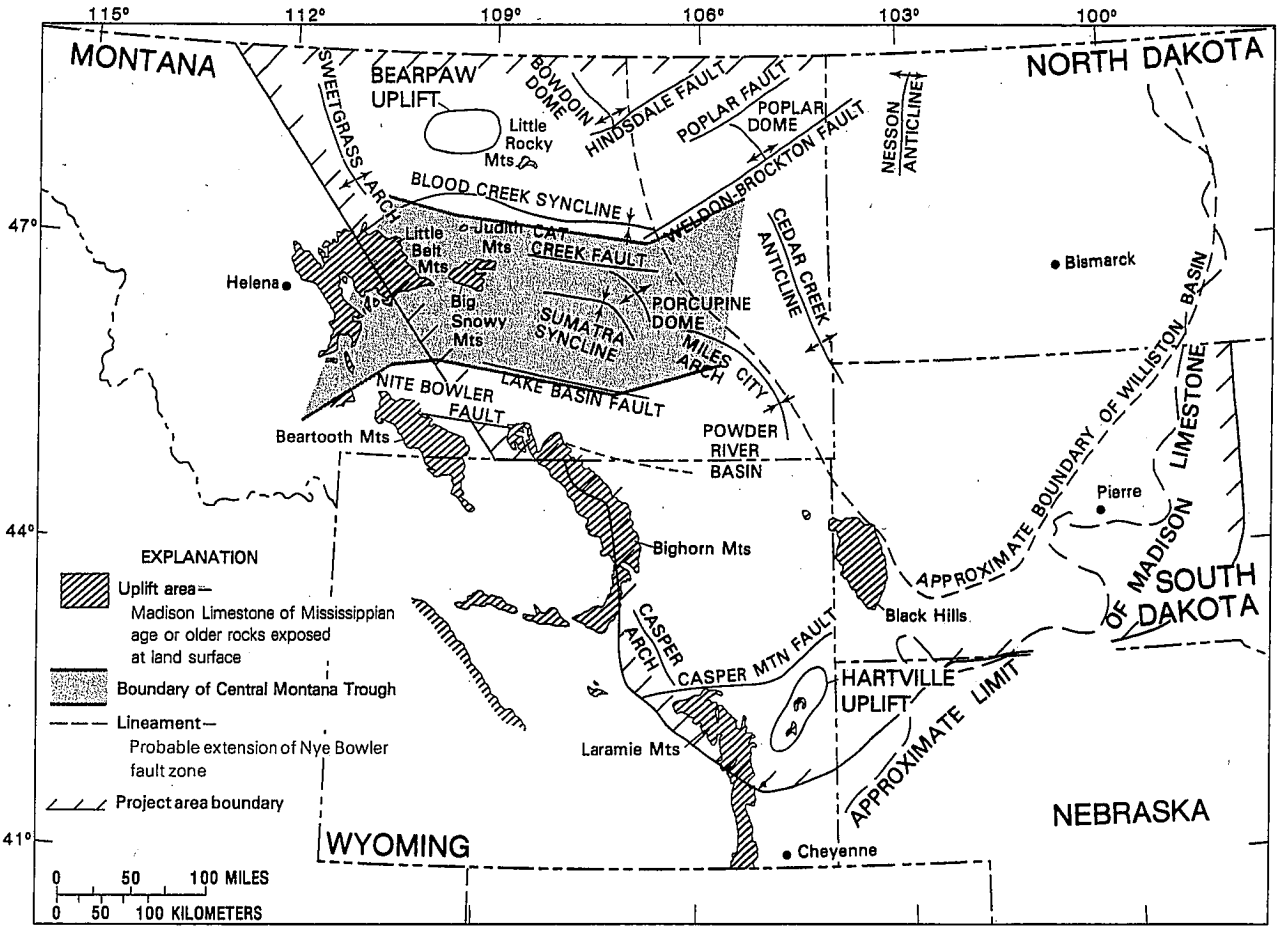

Fig. 1. Map showing location of major structural and physiographic features in the study area. Modified from *Peterson* [1981].

most of the study area [*Smith*, 1972]. The thickness of the unit ranges from 0 to more than 900 ft (274 m) in the study area and averages about 300 (91.4 m).

The Mission Canyon Limestone grades from a coarsely crystalline limestone at its base to finer crystalline limestone with evaporite minerals near the top. The sequence contains one evaporite cycle and shares a second with the lower part of the overlying Charles Formation. Bedded evaporites are absent in most of Wyoming and South Dakota but occur in southeastern Montana. The evaporite deposits thicken in the Central Montana trough (Figure 1), reaching their maximum areal extent in the Williston basin to the north. The thickness of the Mission Canyon Limestone ranges between 0 and about 650 ft (198 m) and averages about 300 ft (91.4 m).

The Charles Formation is the uppermost unit of the Madison Group. It is a marine evaporite sequence consisting of anhydrite and halite with interbedded dolomite, limestone, and argillaceous units. The thickness of the Charles Formation ranges from 0 to more than 295 ft (89.9 m) with an average thickness of about 98 ft (29.9 m) in the study area. Pre-Jurassic erosion has removed most of the Charles Formation in the western and southern parts of the study area.

The major minerals in the Madison Limestone are calcite, dolomite, and anhydrite [*Thayer*, 1981; R. G. Deike, U.S. Geological Survey, written communication, 1984]. Minor quantities of geothite, hematite, and quartz also are common. Nodular anhydrite occurs throughout the Mission Canyon Limestone. R. G. Deike (written communication, 1984) also reported the presence of talc, fluorite, and chalcedony in the Mission Canyon Limestone penetrated by well HTH 1 (well 14 in Wyoming, Table 1) and amphibole in the Charles Formation penetrated by the same well. *Thayer* [1981] reported one example of dedolomite (calcite pseudomorph after dolomite) in HTH 1. The most common clay minerals in the system are kaolinite and illite, some of which are mixed-layer illite-smectite. Smectites also occur but in quantities subordinate to those of other clay minerals.

Because the sulfate and carbonate rocks of the Madison Limestone are relatively soluble in water, the development of karst (solution) features is common. *Sando* [1974] describes ancient karst features, including enlarged joints, sink holes, caves, and solution breccias, that developed in the Madison Limestone in north central Wyoming. He further indicates that most of the openings were filled with sand and residual products reworked by a transgressive sea during Late Mississippian time. Large and extensive cave systems in outcrop areas of the Madison Limestone in the Bighorn Mountains and in the Black Hills are further evidence of the importance of the dissolution process in the development of secondary permeability in limestone units.

Overlying the Charles Formation in parts of Montana and South Dakota are rocks of Late Mississippian age belonging to the Big Snowy Group. The Big Snowy Group is composed mainly of shales and sandstones with minor limestone beds

and was considered a confining unit of the underlying Madison aquifer [*Downey*, 1984].

The relationship of the Madison aquifer to other bedrock aquifers in the northern Great Plains is illustrated in Figure 2. *Downey* [1984, 1986] developed a digital simulation model of the hydrologic system with two major aquifers and two confining units, as shown in Figure 2. Figure 3 shows the predevelopment potentiometric surface in the Madison aquifer given by *Downey* [1984] and locates wells studied in this report. Well numbers are keyed to the tables.

Downey [1984] found that the Madison aquifer functioned as a confined aquifer with recharge in the western highlands and a general direction of flow toward the northeast (Figure 3). Major discharge areas for the aquifer are along the subcrop of the Madison Limestone in east central South Dakota and eastern North Dakota and in the saline lakes in northern North Dakota and saline springs and seeps in the Canadian province of Alberta [*Grossman*, 1968; *Downey*, 1984].

Recharge entering the groundwater flow system in the Black Hills follows two general paths. One component flows north along the front of the Black Hills and then to the east in response to structural and hydrologic controls. The other component flows south along the front of the Black Hills and then to the east, also in response to structural and hydrologic control. Very little water recharged from the Black Hills enters the Madison aquifer in the Powder River basin of Wyoming [*Downey*, 1984, 1986].

The same general situation occurs for recharge waters entering the Madison aquifer from the Big Horn Mountains. Waters entering the northern end of the Big Horn Mountains flow to the east, whereas waters entering along the flanks of the mountains are diverted to the north by structural features along the eastern front of the mountain range.

Little recharge to the groundwater flow system occurs from the Laramie Mountains, and the recharge that does enter the system in this region moves toward the center of the Powder River Basin [*Downey*, 1984].

Figure 4 shows the regional distribution of dissolved solids within the Madison aquifer and locations of wells studied in this report. The area in east central Montana bounded by the Cat Creek fault and Porcupine dome forms an area of elevated dissolved-solids concentration, indicating a possible retardation of flow by geologic structure near the Big Snowy mountains. The large dissolved-solids concentration also could result from greater abundance of soluble minerals in the aquifer. In eastern Wyoming a set of anticlines and minor faults along the western front of the Black Hills diverts recharge north and south around the Black Hills and away from the Powder River basin of Wyoming. In southeastern Wyoming the Casper Mountain fault and Casper arch appear to retard flow north from the Laramie Range.

The possibility of substantial cross-formational leakage into the Madison aquifer from underlying Cambrian and Ordovician strata was considered during formulation of the geochemical models and rejected. This conclusion was based on the hydrologic modeling results of *Downey* [1984, 1986], which show that vertical hydraulic conductivity between the Cambrian-Ordovician and Madison aquifers is less than 10^{-6} ft/d (0.3×10^{-6} m/d) throughout the study area. This compares to horizontal hydraulic conductivities within the Madison aquifer ranging from approximately 1–10 ft/d (0.3–3 m/d). This comparison indicates that on a regional scale, cross-formational leakage between the Madison and Cambrian-Ordovician aquifers can be neglected.

Busby et al. [1983] observed relatively depleted sulfur isotope values for dissolved SO_4 in waters from the Madison aquifer in northeast Wyoming. Because of the similarity of these isotope values to values expected for anhydrites from the overlying evaporites in the Pennsylvanian Minnelusa Formation, these authors concluded that lowered heads in the Madison, due to oil field secondary recovery procedures, have caused downward leakage into the Madison in northeast Wyoming. However, this conclusion is not supported by the data of *Downey* [1984, 1986], which show that the vertical hydraulic conductivity is approximately 6–7 orders of magnitude less than the horizontal hydraulic conductivity within the Madison aquifer in northeast Wyoming. Using a nonlinear regression groundwater modeling approach, *Cooley et al.* [1986] found no evidence of vertical leakage in the Madison aquifer within the uncertainties of the hydrologic data on which the modeling was based. A later section of this study demonstrates that the relatively depleted sulfur isotope values for dissolved SO_4 in northeast Wyoming are consistent with an observed regional pattern throughout the study area, possibly representing variations in the Mississippian depositional environment.

By use of the digital simulation results of *Downey* [1984, 1986] and the dissolved solids map (Figure 4), eight regional subsets (flow paths) of the flow system were identified (Figure 5). For each flow path an average recharge water composition was defined on the basis of the chemistry of waters near the beginning of the flow path. Waters that had passed through the soil zone but had not interacted significantly with the rock matrix were used to define the chemistry of the recharge water.

Generally, recharge waters were selected from springs and wells located within the recharge area with temperatures less than the mean annual air temperature of 15°C, sulfate concentrations of less than 100 mg/L, unadjusted ^{14}C content of at least 50% modern, and tritium content greater than 10 tritium units (TU). Wells and springs were selected for sampling on the basis of records of the U. S. Geological Survey. Wells selected represented a point source of water in some formation of the Madison Group and were free of contamination or chemical pretreatment. Table 1 lists all wells and springs sampled, their total depth, interval sampled, lithologic unit, and recharge and flow path designation. All wells and springs are located on Figures 3 and 4 and identified by index numbers given in the tables.

HYDROCHEMISTRY

Samples were collected for measurement of major and minor elements using the methods described by *Brown et al.* [1970] and are reported by *Busby et al.* [1983]. Only the subset of those data judged useful in the geochemical model are presented in this report. Field determinations were made for *p*H, alkalinity, temperature, and specific conductance, following the methods of *Wood* [1976].

Samples were collected for the analysis of ^{14}C, tritium, $\delta^{13}C$, δD, and $\delta^{18}O$ using methods described by *Busby et al.* [1983]. The $\delta^{34}S$ content of sulfate was determined for $BaSO_4$ samples precipitated in the field. The $\delta^{34}S$ content of hydrogen sulfide was determined for cadmium sulfide samples precipitated in the field from acidified (to *p*H 4) water samples. See *Busby et al.* [1990] for additional details.

TABLE 1. Wells and Springs Sampled

State	Well Number	Well Name	Total Depth, ft	Interval Sampled, ft	Water Yielding Unit*
MT	2	Gore Hill	755	679–699	1
MT	3	Great Falls High School	426	400–426	1
MT	4	Bozeman Fish Hatchery	200	115–200	1
MT	5	Bough Ranch	1299	1266–1299	1
MT	6	McLeod Warm Spring	spring	...	1
MT	7	Big Timber Fish Hatchery	spring	...	1
MT	8	Hanover Flowing Well	751	...	2
MT	9	Vanek Warm Spring	spring	...	2
MT	10	Lewistown Warm Spring	spring	...	1
MT	11	Blue Water Spring	spring	...	1
MT	12	Landusky Spring	spring	...	2
MT	13	Lodgepole Warm Spring	spring	...	2
MT	14	HTH 3	7175	4373–4422	2
MT	15	Keg Coulee	...	6457–6516	2, 3
MT	16	Texaco C115X	6768	6079–6768	2
MT	17	Sumatra	6854	6152–6854	2, 3, 4
MT	18	Sleeping Buffalo	3199	3130–3199	2
MT	19	Sarpy Mine	...	...	...
MT	20	Mysee Flowing Well	5102	5039–5102	2
MT	21	Colstrip	9337	7795–8340	2, 3
MT	22	Moore	F.W.	...	2
MT	23	Ranch Creek	7260	7169–7260	1
MT	24	Belle Creek	7190	6991–7190	1
MT	26	Gas City	7598	7434–7598	2
MT	27	Buckhorn Exeter	6519	6174–6335	1
SD	1	Kosken	...	2661–2936	1
SD	2	McNenny	220	144–220	1
SD	3	Provo	3845	...	1
SD	4	Rhoads Fork	F.W.	...	1
SD	5	Spearfish	879	650–879	5
SD	6	Fuhs	551	548–551	1
SD	7	Delzer 1	4557	...	...
SD	8	Delzer 2	5453	...	...
SD	9	Cascade Spring	spring	...	...
SD	10	Evans Plunge	spring	...	1
SD	11	Kaiser	...	689–781	5
SD	12	Jones Spring	spring	...	...
SD	13	Black Hills Cemetery	...	...	5
SD	14	Streeter Ranch	938	928–938	5
SD	16	Cleghorn Spring	spring	...	1
SD	17	Lein	3921	...	5
SD	18	Ellsworth AFB	4436	...	5
SD	19	Philip	4009	3783–4009	2
SD	20	Dupree	4501	...	3
SD	21	Hamilton	3760	...	1
SD	22	Hilltop Ranch	...	3379–4101	1
SD	23	Eagle Butte	4324	...	1
SD	24	Midland	3320	3166–3320	1
SD	25	Murdo	3314	...	1
SD	26	Prince	2838	2700–2746	1
SD	27	Bean	3510	3199–3510	5
WY	1	Mock Ranch	1594	...	1
WY	2	Denius 1	...	...	3
WY	3	Denius 2	...	942–3143	3
WY	4	Denius 3	...	...	3
WY	5	Hole in the Wall	432	...	1
WY	6	Story Fish Hatchery	764	...	1
WY	7	Mobil	1112	...	1
WY	8	Conoco 44	...	2680–2880	1
WY	9	Shidler	6155	5141–6155	1
WY	10	MKM	7178	6391–7178	1
WY	11	Conoco 175	...	8845–9154	1
WY	12	Barber Ranch Spring	1467	...	...
WY	13	Devils Tower	479	450–469	1
WY	14	HTH 1	4341	2431–2595	2
WY	15	Upton	3159	2900–3159	4
WY	16	Coronado 2	4521	4085–4521	1
WY	17	Osage	3071	2684–3071	1
WY	18	JBJ	6880	6476–6880	1
WY	19	Seeley	2816	2716–2816	1
WY	20	Voss	2738	2467–2738	1

TABLE 1. (Continued)

State	Well Number	Well Name	Total Depth, ft	Interval Sampled, ft	Water Yielding Unit*
WY	21	Newcastle	2637	2618–2637	1
WY	22	Self	3596	3169–3596	1
WY	23	Martens Madison	...	640–718	1
WY	24	Mallo Camp	spring	...	1
WY	25	Ranch A	...	...	1

Three dots indicate that data are not available. One foot = 0.3048 m. The states are designated by MT, Montana; SD, South Dakota; WY, Wyoming. F.W. indicates flowing well, total depth unknown.

*Water yielding units are (1) Madison Limestone, (2) Mission Canyon Limestone; (3) Lodgepole Limestone; (4) Charles Formation, (5) Pahasapa Limestone (Madison Limestone equivalent in western South Dakota).

Saturation State

In order to investigate thermodynamic controls on the water composition, equilibrium speciation calculations were made using WATEQF [*Plummer et al.*, 1976]. These calculations provide saturation indices (SI) of minerals that may be reacting in the system. The SI of a particular mineral is defined as

$$SI = \log \frac{IAP}{K_T} \quad (1)$$

where IAP is the ion activity product of the mineral-water reaction and K_T is the thermodynamic equilibrium constant adjusted to the temperature of the given sample. Pertinent thermodynamic data used in these calculations have been revised from the original WATEQF [*Plummer et al.*, 1976] and are summarized in Table 2. The full water analyses for major and minor elements are given elsewhere [*Busby et al.*, 1983] and were used to calculate the saturation indices given in Table 3.

Calculated values of the saturation indices of gypsum, calcite, and dolomite are shown as a function of dissolved-sulfate concentration in Figure 6. As dissolved sulfate increases, the waters approach gypsum saturation. Although gypsum is not known to occur in the Madison Limestone, the saturation calculation is made with respect to gypsum because the temperature dependence of the gypsum equilibrium constant is known more reliably than that of anhydrite. For the temperature and salinity ranges of waters from the Madison aquifer, waters in equilibrium with anhydrite would appear slightly undersaturated with gypsum, as expected by the small difference in Gibbs free energy between the two phases. Therefore most waters from the Madison aquifer with SO_4 contents of more than approximately 14 mmol/kg H_2O probably are saturated with respect to anhydrite (Figure 6).

Slight oversaturation of many of the waters with respect to calcite is expected under conditions of dedolomitization necessary to cause precipitation of calcite. The degree of oversaturation required for calcite precipitation in the Madison aquifer is not known, however. Thermodynamic calculations accounting for pressure effects on the calcite equilibrium constant using molar volume data of *Millero* [1982] indicate that waters in equilibrium with calcite at a depth of approximately 5000 ft (1524 m) would appear oversaturated with calcite with a saturation index not greater than 0.16 if rapidly brought to the surface. This is a maximum estimate of the apparent oversaturation due to pressure differences because it does not account for pressure effects on the aqueous carbonate species [*Aggarwal et al.*, 1990]. In addition, the calcite cements accompanying the dedolomitization reaction may contain significant amounts of sulfate, which can enhance solubility relative to pure calcite [*Busenberg and Plummer*, 1985]. It is likely that all these processes contribute to the observed oversaturation with respect to pure stoichiometric calcite. Many of the waters are quite warm, typically 50°–80°C. Because of the elevated temperature there is significant potential for CO_2 outgassing during field measurement of *p*H. However, significant *p*H error is discounted because the *p*H measurements were made in a closed flow cell to minimize the effects of CO_2 outgassing. Most water samples were clear, indicating little evidence of gas bubble formation.

Except for some waters with very low sulfate concentrations, the Madison aquifer is near saturation with dolomite (Figure 6), if we accept an uncertainty of ±0.50 in the saturation index. The WATEQF calculations also indicate that celestite saturation is approached as sulfate exceeds 14 mmol/L. Because the high-sulfate waters are near saturation with calcite, anhydrite, and celestite, an application of the Gibbs phase rule to the $CaCO_3$-$CaSO_4$-$SrSO_4$ system at constant temperature and pressure indicates that these waters cannot also be in equilibrium with strontianite. At calcite, anhydrite, and celestite equilibrium, the strontianite

LOWER CRETACEOUS ROCKS	UPPER BOUNDARY
CHARLES FORMATION AND BIG SNOWY GROUP OF MISSISSIPPIAN AGE, AND PENNSYLVANIAN, PERMIAN, TRIASSIC, AND JURASSIC ROCKS	CONFINING UNIT
LODGEPOLE AND MISSION CANYON LIMESTONES OF THE MADISON GROUP, AND MADISON LIMESTONE	MADISON AQUIFER
SILURIAN AND DEVONIAN ROCKS AND BAKKEN FORMATION OF DEVONIAN AND MISSISSIPPIAN AGE	CONFINING UNIT
UPPER PART OF DEADWOOD, AND WINNIPEG, RED RIVER, AND STONY MOUNTAIN FORMATIONS OF CAMBRIAN TO ORDOVICIAN AGE	CAMBRIAN-ORDOVICIAN AQUIFER
PRECAMBRIAN ROCKS	LOWER BOUNDARY

Fig. 2. Relationship between geologic units and units in digital simulation of flow system used by *Downey* [1984].

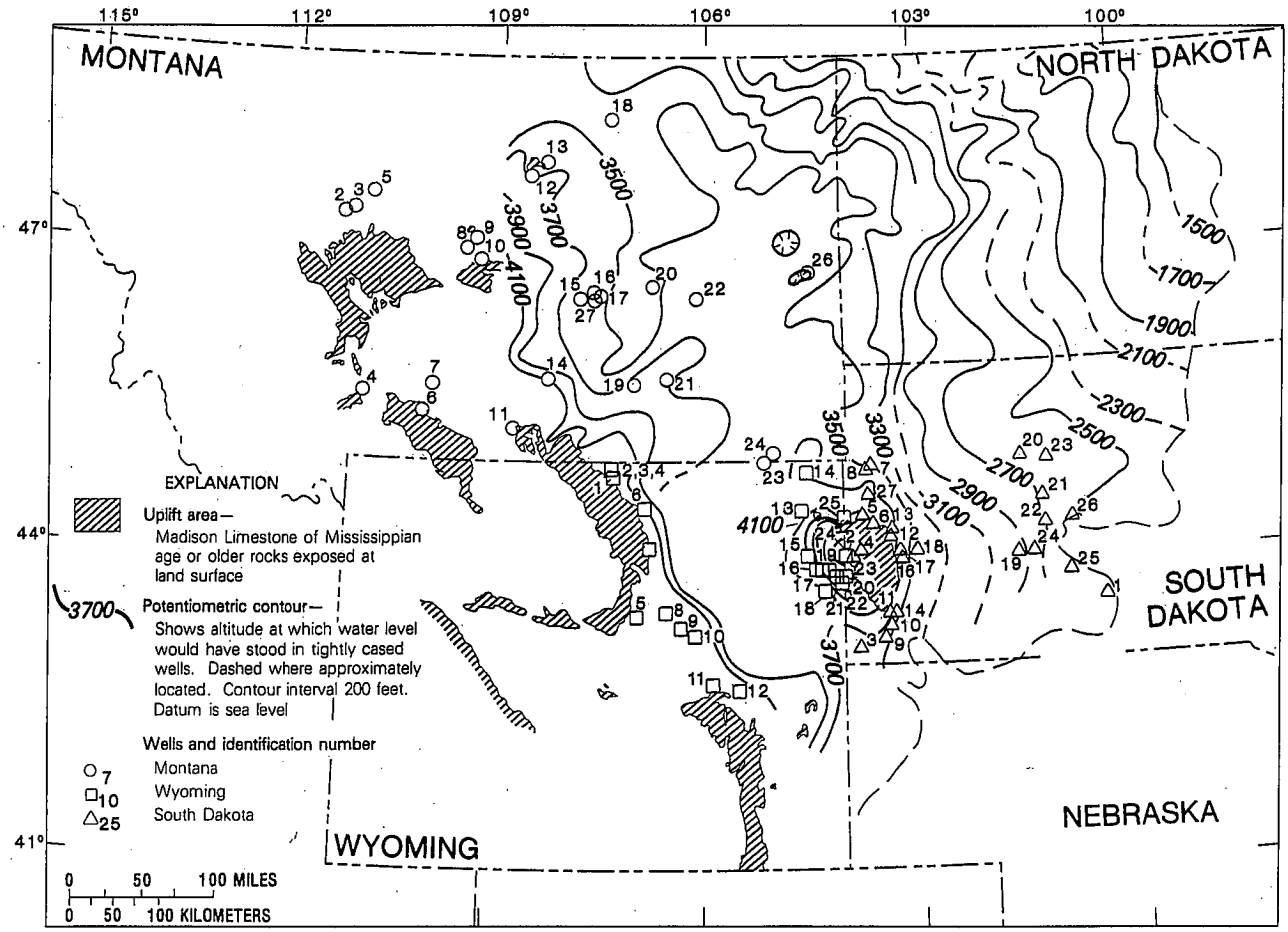

Fig. 3. Predevelopment potentiometric surface of the Madison aquifer, showing location and identification of wells and springs sampled. Identification numbers are keyed to the tables. Modified from *Downey* [1984].

saturation index is defined for a particular temperature and pressure by

$$SI_S = \log \frac{K_C K_{Cel}}{K_{An} K_S} \quad (2)$$

where K denotes the equilibrium constant and the subscripts C, Cel, An, and S refer to calcite, celestite, anhydrite, and strontianite, respectively. Using thermodynamic data from Table 2, SI_S is expected to be near -1.4 (25°C) in waters from the Madison aquifer, which compares well with the observed SI_S of -1.2 ± 0.2 calculated by WATEQF and data of Table 2.

The WATEQF results show considerable variation for barite and siderite saturations, partly reflecting larger uncertainties in the analytical data for dissolved barium and iron. The calculations indicate, however, that most waters of the Madison aquifer probably are saturated or oversaturated with barite and undersaturated with siderite. Most of the waters are oversaturated with respect to quartz but either saturated or slightly undersaturated with respect to chalcedony throughout the temperature range [*Back et al.*, 1983; *Busby et al.*, 1983].

In addition to providing SI information, the equilibrium speciation calculations yield information on other parameters of use during the modeling process. These include P_{CO_2}, the redox state (RS) of the water [*Parkhurst et al.*, 1980], the total concentration of inorganic carbon (molal units), and a conversion of the total concentrations of the other analyzed elements to molal units. The molal concentrations (or millimoles per kilogram of water) of the elements and redox state are summarized in Table 4 for the average recharge water of each flow path and for each subsequent well on the flow path.

Analysis of Trend

The thermodynamic calculations discussed above determine which minerals may react reversibly and which may react irreversibly in the Madison aquifer. On the basis of these calculations, it is likely that anhydrite dissolves irreversibly in most of the system, whereas the water remains at or near saturation with calcite and dolomite. It is appropriate then to choose dissolved sulfate as a reaction progress variable in examining trends in the water quality data.

Changes in predominant cations and anions are depicted (on a mole percent basis) on the trilinear diagram for each flow path in Figure 7. No single flow path shows the entire evolutionary trend, but combined, the eight flow paths complete different segments of the overall set of reactions in the aquifer. The evolutionary path for cations proceeds from a predominance of calcium and magnesium to sodium predominance. The anions proceed from a predominance of bicarbonate to sulfate to chloride. This is the commonly observed "major-ion evolution sequence" [*Freeze and Cherry*, 1979, p. 241], which was first recognized by *Che-*

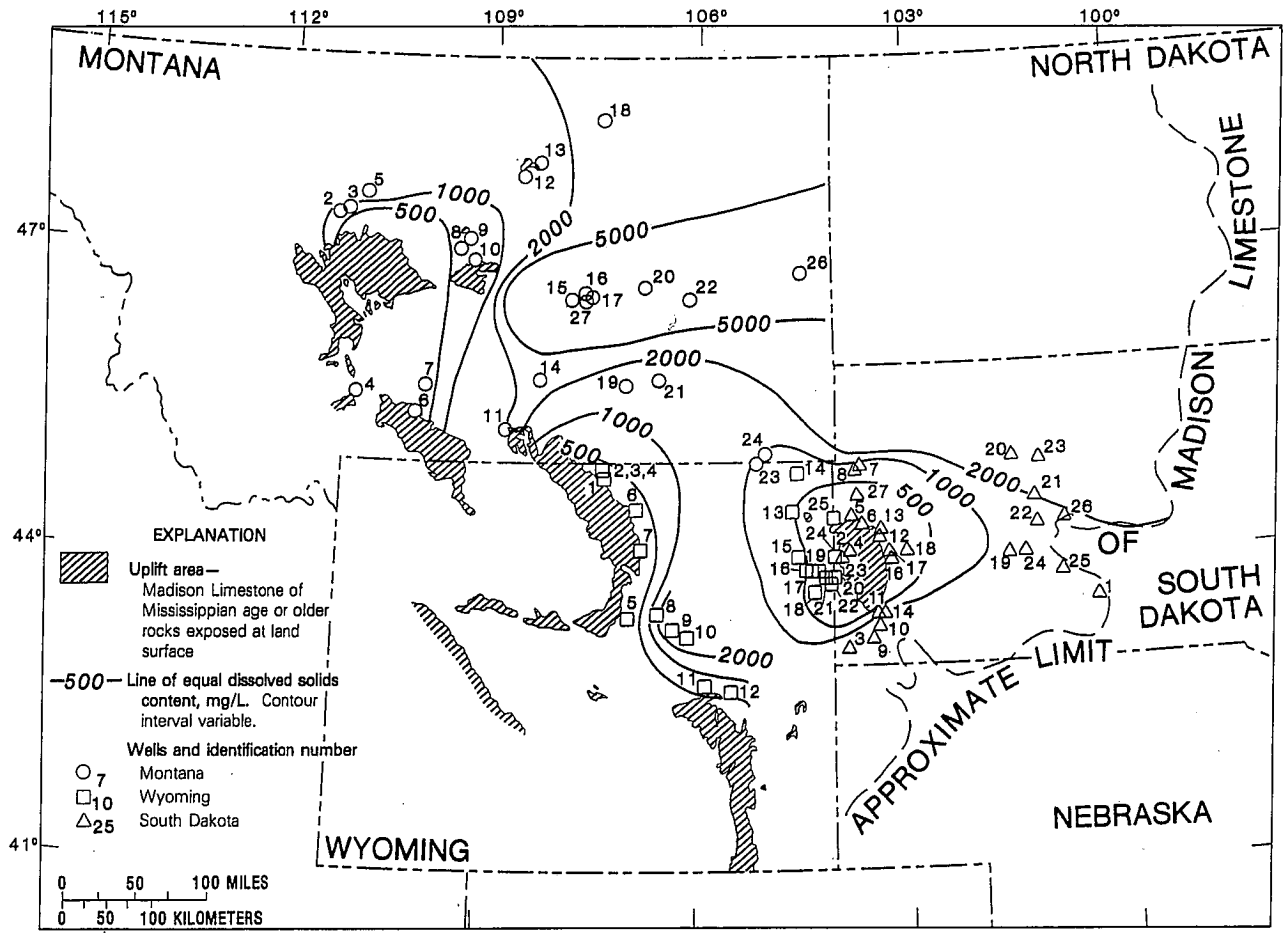

Fig. 4. Map showing dissolved solids content for the Madison aquifer and location of wells sampled. Identification numbers are keyed to the tables.

botarev [1955]. In the Madison aquifer this trend indicates that the major element chemistry is determined initially by dissolution of calcite and dolomite, followed by dissolution of anhydrite and, along several flow paths, dissolution of halite.

There are distinct differences in the extent of reaction progress along each flow path (Figure 7). Flow paths 1, 4, 7, and 8 begin as calcium-magnesium-bicarbonate-type waters but are significantly affected by anhydrite dissolution. Flow paths 2, 3, and 5 are affected significantly by halite dissolution. Flow path 6 is controlled predominantly by carbonate mineral reactions. Flow path 4 represents a relatively mature water in which dissolution of anhydrite dominates over dissolution of the carbonate minerals. Although waters along flow paths 2, 3, and 5 are dominated by halite dissolution, these flow paths also show evidence of earlier evolution in the calcite-dolomite-anhydrite reaction system. For example, flow paths 3 and 5 begin with waters similar in composition to those at the end of flow paths 1 and 8; and the initial well on flow path 2 is predominantly calcium-magnesium-bicarbonate. It is expected that more samples from wells along the beginnings of flow paths 2, 3, and 5 would show the full reaction path from predominantly $Ca > Mg : HCO_3$ to $Ca > Mg : SO_4 > HCO_3$ waters.

Although the trilinear diagram (Figure 7) indicates changes in the relative proportions of cations and anions, more reaction information may be gained by examining actual changes in concentrations as a function of reaction progress (sulfate concentration). Systematic increases in both calcium and magnesium as sulfate increases are shown in Figure 8. Accompanying the increase in dissolved sulfate as a decrease in pH and an increase in P_{CO_2} (Figure 9).

These trends are consequences of the dedolomitization reaction, as discussed by *Hanshaw et al.* [1978] and *Back et al.* [1983]. Beginning with recharge water near saturation with calcite and dolomite, dissolution of anhydrite adds calcium to the groundwater, causing precipitation of calcite. Calcite precipitation causes the pH to decrease (Figure 9) (due to H^+ released from HCO_3^- during incorporation of CO_3^{2-} in calcite). The decrease in pH increases the proportion of $H_2CO_3^*$ ($\equiv H_2CO_3^\circ + CO_2^\circ$) in solution and thus increases the P_{CO_2} (Figure 9). The decrease in CO_3^{2-} concentration with decreasing pH causes the water to be undersaturated with respect to dolomite, which leads to dolomite dissolution and an increase in dissolved magnesium (Figure 8). The mass of anhydrite and dolomite dissolved in this dedolomitization process exceeds the mass of calcite precipitated, resulting in a net increase in dissolved calcium (Figure 8). Although these trends in Ca, Mg, pH, and P_{CO_2} with SO_4 are evident in the waters from the Madison aquifer (Figures 8 and 9), there is considerable variation between sampling points and flow paths. This variation is due to several factors, including differences in recharge water composition on differing flow paths, temperature variations, and

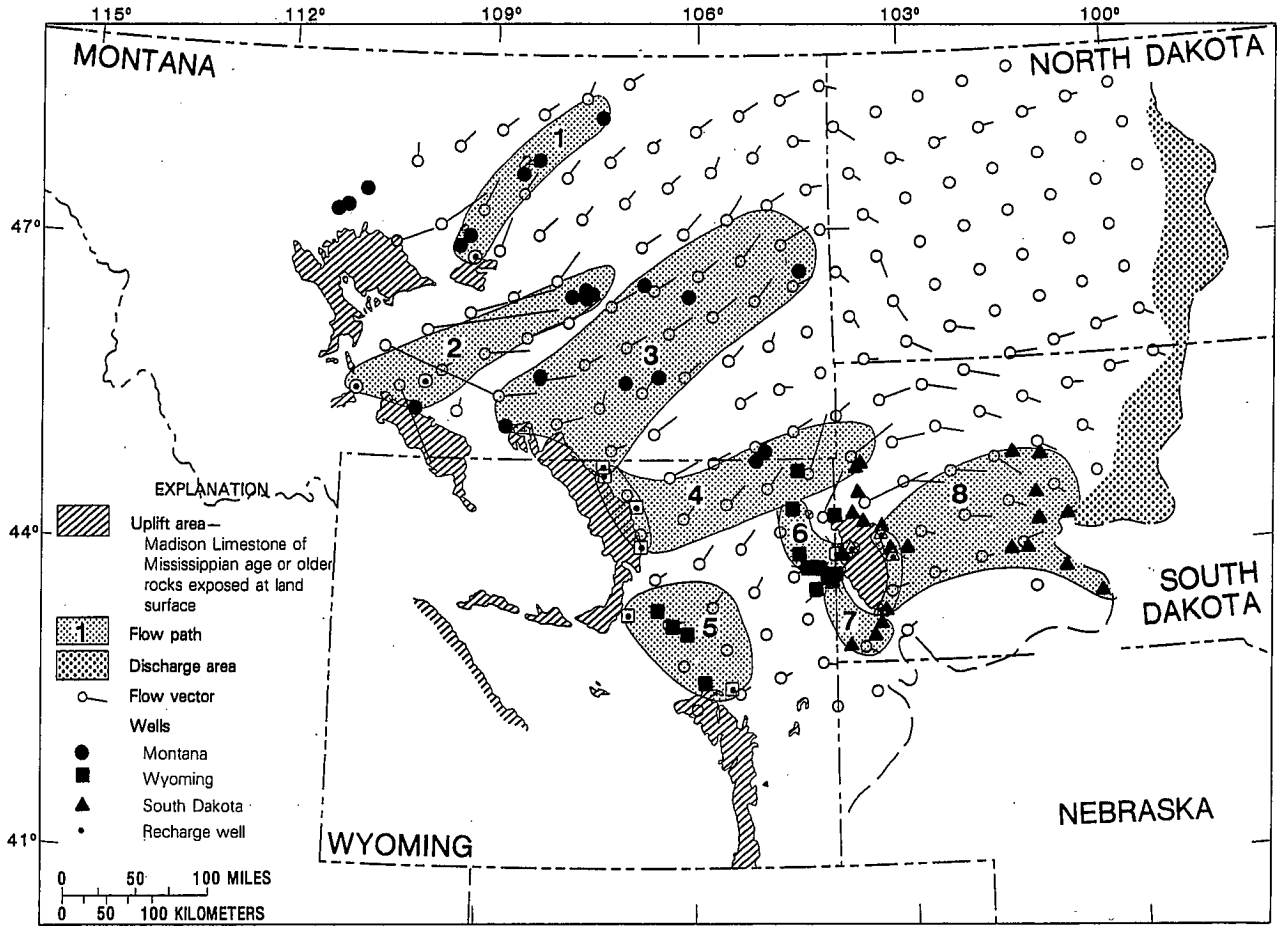

Fig. 5. Vector map of the Madison aquifer flow system from J. S. Downey (written communication, 1984) showing location of wells and flow paths studied. Solid shapes denote location of all wells sampled in the Madison aquifer: squares (Wyoming), circles (Montana), and triangles (South Dakota). Numbers 1–8 identify flow paths. Location of representative discharge wells (Table 1) are given. Open circles (no vector) correspond to flow velocities of less than 2 ft/yr (0.6 m/yr), and the greatest flow velocities range from 50 to 75 ft/yr (15.2 to 22.9 m/yr) [*Downey*, 1986].

the occurrence of other reactions in addition to the dedolomitization reaction.

Two trends are evident in total alkalinity as a function of dissolved sulfate (Figure 10). Most waters show a decrease in alkalinity with increasing sulfate, except for waters associated primarily with flow paths 2 and 3 which have some of the largest alkalinity concentrations (>300 mg/L, as HCO_3^-) with large concentrations of dissolved sulfate. The decrease in alkalinity is to be expected for evolutionary paths following the dedolomitization reaction, but increases in alkalinity concentrations (flow paths 2 and 3) indicate the occurrence of other reactions. Some oil field waters have been shown to contain large contribution of carboxylic acid anions to the total alkalinity at temperatures in excess of 80°C [*Carothers and Kharaka*, 1978; *Surdam et al.*, 1989]. Most of the Madison waters sampled have temperatures below 80°C and are thought not to contain significant contributions of carboxylic acid anions in the alkalinity. Although dissolved organic carbon (DOC) was not measured, significant contributions of carboxylic acid anions to the alkalinity would have resulted in excessively large indications of oversaturation with respect to carbonate minerals, which was not observed (Figure 6, Tables 3–4). Cation exchange could contribute additional HCO_3^- along flow paths 2 and 3, in addition to the dedolomitization reaction. In this case the uptake of Ca^{2+} and Mg^{2+} and release of Na^+ from exchange sites on clay minerals causes dissolution of carbonate minerals. The additional CO_3^{2-} released from carbonate mineral dissolution reacts with dissolved $H_2CO_3^*$, resulting in excess HCO_3^-, which is balanced by Na^+ released from cation exchange.

There are additional contributions of sodium (and potassium) from chloride sources. Figure 11 shows the variation in sodium, potassium, and chloride with sulfate. Generally, waters with large concentrations of sodium also have large concentrations of potassium and chloride, indicating evaporite sources for these ions. Sodium and chloride concentrations are small and nearly independent of sulfate along flow paths 1, 4, 6, 7, and 8. At sulfate concentrations larger than about 8 mmol/kg H_2O, flow paths 2, 3, and 5 have much larger concentrations of sodium, potassium, and chloride than elsewhere in the Madison aquifer (Figure 11). Because the molal concentrations of sodium plus potassium are similar to the concentration of chloride for flow path 5, it is likely that evaporite minerals are the primary source for these ions there. Figure 11 also shows that the concentrations of sodium plus potassium significantly exceed that of chloride for flow paths 2 and 3 at sulfate concentrations greater than about 8 mmol. These are the same waters that contain unusually large concentrations of bicarbonate (Figure

TABLE 2. Summary of Revised Thermodynamic Data

Reaction	Mineral	ΔH_r^o	log K	Analytical Expression	Reference
Species					
$Ca^{2+} + HCO_3^- = CaHCO_3^+$		4.11	1.095	$\log K_{CaHCO_3^+} = 1209.120 + 0.31294T - 34765.06/T - 478.782 \log T$	1
$Ca^{2+} + CO_3^{2-} = CaCO_3^o$		3.556	3.224	$\log K_{CaCO_3^o} = -1228.732 - 0.299444T + 35512.75/T + 485.818 \log T$	1
$CO_2(g) = CO_2(aq)$		−4.776	−1.468	$\log K_H = 108.3865 + 0.01985076T - 6919.53/T - 40.45154 \log T + 669365./T^2$	1
$CO_2(aq) + H_2O = H^+ + HCO_3^-$		2.177	−6.352	$\log K_1 = -356.3094 - 0.06091964T + 21834.37/T + 126.8339 \log T - 1684915./T^2$	1
$HCO_3^- = H^+ + CO_3^{2-}$		3.561	−10.329	$\log K_2 = -107.8871 - 0.03252849T + 5151.79/T + 38.92561 \log T - 563713.9/T^2$	1
$Sr^{2+} + HCO_3^- = SrHCO_3^+$		6.05	1.18	$\log K_{SrHCO_3^+} = -3.248 + 0.014867T$	2
$Sr^{2+} + CO_3^{2-} = SrCO_3^o$		5.22	2.81	$\log K_{SrCO_3^o} = -1.019 + 0.012826T$	2
$Sr^{2+} + SO_4^{2-} = SrSO_4^o$		1.6	2.55	...	3
Minerals					
$CaCO_3 = Ca^{2+} + CO_3^{2-}$	calcite	−2.297	−8.480	$\log K_C = -171.9065 - 0.077993T + 2839.319/T + 71.595 \log T$	1
$CaCO_3 = Ca^{2+} + CO_3^{2-}$	aragonite	−2.589	−8.336	$\log K_A = -171.9773 - 0.077993T + 2903.293/T + 71.595 \log T$	1
$CaMg(CO_3)_2 = Ca^{2+} + Mg^{2+} + 2CO_3^{2-}$	dolomite	−9.436	−17.09	...	4
$SrCO_3 = Sr^{2+} + CO_3^{2-}$	strontionite	−0.40	−9.271	$\log K_{Stront} = 155.0305 - 7239.594/T - 56.58638 \log T$	2
$SrCO_4 = Sr^{2+} + SO_4^{2-}$	celestite	0.228	−6.578	$\log K_{Celest} = 73.415 - 3603.341/T - 29.8115 \log T$	5
$CaSO_4 \cdot 2H_2O = Ca^{2+} + SO_4^{2-} + 2H_2O$	gypsum	−0.028	−4.602	$\log K_{Gyp} = 82.090 - 3853.936/T - 29.8115 \log T$	6
$CaSO_4 = Ca^{2+} + SO_4^{2-}$	anhydrite	−4.3	−4.384	...	7
$FeCO_3 = Fe^{2+} + CO_3^{2-}$	siderite	−6.14	−10.57	...	8
$BaSO_4 = Ba^{2+} + SO_4^{2-}$	barite	6.141	−9.978	...	9

References are 1, *Plummer and Busenberg* [1982]; 2, *Busenberg et al.* [1984]; 3, *Smith and Martell* [1976]; 4, *Robie et al.* [1978]; 5, calculated from the data of *Gallo* [1935] for $SrSO_4$ precipitated, as given by *Seidell* [1958] and consistent with $SrSO_4^o$ data of *Smith and Martell* [1976]; 6, calculated from the data of *Marshall and Slusher* [1966] using the aqueous model of WATEQF; 7, log K of *Harvie and Weare* [1980] adjusted for consistency with log K_{gyp} and ΔH_r^o from *Parker et al.* [1971]; 8, log K of *Smith* [1918] recalculated using aqueous model of WATEQF at 30°C and adjusted to 25°C using ΔH_r^o from *Parker et al.* [1971]; 9, *Parker et al.* [1971]. Three dots indicate that the analytical expression is not available, and for these ΔH_r^o is the standard enthalpy of reaction, in kilocalories per mole at 25°C. The Van't Hoff relation was used to define temperature dependence of equilibrium constants.

10). Thus there is a tendency to form sodium bicarbonate waters along flow paths 2 and 3. The sodium bicarbonate waters are expected to evolve from several possible mechanisms [*Foster*, 1950; *Thorstenson et al.*, 1979; *Chapelle and Knobel*, 1985; *Chapelle et al.*, 1987; *Lee and Strickland*, 1988]. In the Madison aquifer it is likely that sodium bicarbonate waters form from the dissolution of carbonate minerals accompanying the exchange of calcium and magnesium for sodium on clay minerals in the presence of sulfate reduction.

Most of the waters downgradient from recharge areas contain traces of hydrogen sulfide (H_2S); and in some cases such as along flow paths 2 and 3, H_2S concentrations greater than 100 mg/L have been observed. Therefore, in addition to the dissolution and precipitation reactions discussed above, the possibility of redox reactions, especially sulfate reduction, need to be considered. Sulfate reduction alone also could contribute to the excess bicarbonate along flow paths 2 and 3 (Figure 10). The data will be examined more closely with mass balance models in conjunction with the carbon and sulfur isotopic data to determine the extents of ion exchange and sulfate reduction.

On the basis of the analysis of saturation state and chemical trends, the reactions along each flow path can be summarized as follows: Flow paths 1, 4, 7, and 8 are primarily examples of the dedolomitization reaction caused by irreversible dissolution of anhydrite at or near calcite-dolomite saturation. Flow paths 2 and 3 combine the dedolomitization reaction with dissolution of halite and a potassium chloride source such as sylvite, sulfate reduction, and ion exchange (Ca^{2+} and Mg^{2+} for Na^+). Flow path 5 shows evidence for the dedolomitization reaction accompanied by halite dissolution. Flow path 6 is controlled primarily by CO_2-carbonate mineral reactions, with only small quantities of anhydrite dissolution.

MASS BALANCE REACTION MODELS

We now attempt to test the above reaction hypotheses by constructing geochemical mass balance models for the changes in water composition between the recharge water and each downgradient well. In modeling the chemical evolution of water and rock in the Madison system, use is made of the fact that the correct reaction model will describe both the observed chemical and isotopic composition of aqueous and solid phases. Inclusion of isotopic data in reaction modeling provides additional criteria for testing reaction hypothesis. The modeling approach that follows is similar to that of *Plummer et al.* [1983].

TABLE 3. Results of Thermodynamic Speciation Calculations

Well Name	Flow Path	State	Well Number	Log P_{CO_2}	Saturation Indices: Calcite	Aragonite	Dolomite	Gypsum	Anhydrite	Siderite	Strontianite	Celestite	Barite
Lewistown Big Spring	R1	MT	10	−2.40	0.01	−0.15	−0.27	−1.41	−1.80	−1.46	−1.37	−1.68	···
Hanover Flowing Well	F1	MT	8	−2.38	0.25	0.11	0.35	−1.33	−1.60	−1.75	−1.03	−1.45	···
Vanek Warm Spring	F1	MT	9	−2.17	0.14	−0.01	0.06	−0.96	−1.24	−1.58	−1.15	−1.09	···
Landusky Spring	F1	MT	12	−2.01	0.15	0.00	0.20	−0.43	−0.70	−1.85	−1.18	−0.60	···
Lodgepole Warm Spring	F1	MT	13	−1.80	0.11	−0.03	0.22	−0.46	−0.61	−1.98	−1.22	−0.58	···
Sleeping Buffalo	F1	MT	18	−1.81	0.18	0.04	0.20	−0.07	−0.15	−0.81	−1.21	−0.22	···
Bozeman Fish Hatchery	R2	MT	4	−2.60	0.19	0.04	0.01	−2.26	−2.68	−0.74	−1.82	−3.17	···
Big Timber Fish Hatchery	R2	MT	7	−2.37	0.05	−0.11	−0.27	−2.20	−2.59	−1.86	−1.53	−2.66	···
Mcleod Warm Spring	F2	MT	6	−2.14	0.02	−0.13	−0.10	−1.52	−1.74	···	−1.72	−2.07	···
Sumatra	F2	MT	17	−0.83	0.18	0.07	−0.16	−0.58	−0.48	−1.76	−0.88	−0.37	0.09
Keg Coulee	F2	MT	15	−0.88	0.05	−0.07	−0.26	−0.42	−0.38	−0.77	−1.14	−0.34	0.41
Texaco C115X	F2	MT	16	−0.68	0.07	−0.04	−0.38	−0.38	−0.28	−1.64	−1.13	−0.30	···
Mock Ranch	R3	WY	1	−2.20	−0.01	−0.16	−0.33	−2.68	−3.07	−1.65	−1.93	−3.49	−0.06
Denius 1	R3	WY	2	−2.32	−0.11	−0.26	−0.25	−2.39	−2.80	−0.98	−1.94	−3.12	···
Colstrip	F3	MT	21	−0.89	0.12	0.02	−0.60	−0.41	−0.30	−0.68	−1.10	−0.36	···
Sarpy Mine	F3	MT	19	−1.20	0.27	0.16	0.00	−0.28	−0.18	−0.41	−1.00	−1.27	−0.60
Gas City	F3	MT	26	−0.70	0.56	0.46	0.52	−0.31	−0.20	−0.94	−0.66	−0.25	0.32
Bluewater Spring	F3	MT	11	−2.08	0.37	0.22	0.09	−0.04	−0.38	−2.48	−1.19	−0.47	1.70
Moore	F3	MT	22	−0.88	0.48	0.37	0.45	−0.30	−0.20	−1.71	−0.74	−0.24	0.39
Mysse Flowing Well	F3	MT	20	−0.94	0.29	0.17	0.42	−0.15	−0.11	−1.93	−1.10	−0.28	0.92
Story Fish Hatchery	R4	WY	6	−2.06	−0.32	−0.48	−1.11	−3.08	−3.51	···	−2.64	−4.31	···
Mobil	R4	WY	7	−2.14	−0.59	−0.75	−1.35	−2.88	−3.32	−1.39	−2.59	−3.78	···
Mock Ranch	R4	WY	1	−2.20	−0.01	−0.16	−0.33	−2.68	−3.07	−1.65	−1.93	−3.49	−0.06
Denius 1	R4		2	−2.32	−0.11	−0.26	−0.25	−2.39	−2.80	−0.98	−1.94	−3.12	···
HTH 1	F4	WY	14	−1.57	0.18	0.05	0.25	−0.78	−0.82	0.79	−1.12	−0.84	0.88
Ranch Creek	F4	MT	23	−1.47	0.23	0.10	0.33	−0.74	−0.75	−1.63	−1.09	−0.80	···
Belle Creek	F4	MT	24	−1.52	0.35	0.22	0.56	−0.70	−0.68	−1.13	−1.01	−0.80	0.77
Delzer 1	F4	SD	7	−2.57	0.37	0.23	0.43	−0.08	−0.32	0.52	−0.89	−0.17	1.26
Delzer 2	F4	SD	8	−1.41	0.25	0.13	0.27	−0.05	−0.04	0.38	−1.21	−0.25	0.76
Hole in the Wall	R5	WY	5	−1.94	−0.48	−0.64	−0.92	−2.98	−3.41	−1.78	−2.48	−3.88	···
Barber Ranch Spring	R5	WY	12	−2.17	−0.02	−0.17	−0.29	−2.09	−2.41	−1.61	−1.72	−2.65	···
Conoco 175	F5	WY	11	−1.74	0.07	−0.04	−0.04	−0.99	−0.94	0.54	−1.50	−1.30	0.28
Conoco 44	F5	WY	8	−1.85	0.21	0.07	0.26	−0.57	−0.72	−0.20	−1.29	−0.86	0.90
MKM	F5	WY	10	−1.21	0.20	0.10	−0.22	−0.43	−0.32	0.65	−1.27	−0.63	0.05
Shidler	F5	WY	9	−1.90	0.18	0.05	0.05	−0.45	−0.43	0.20	−1.37	−0.74	···
Mallo Camp	R6	WY	24	−2.23	0.12	−0.04	−0.06	−3.33	−3.76	···	NS	NS	NS
Rhoads Fork	R6	SD	4	−1.98	−0.09	−0.25	−0.60	−3.03	−3.50	···	−2.49	−4.36	···
Seeley	F6	WY	19	−1.91	−0.05	−0.20	−0.31	−2.34	−2.70	−1.73	−1.96	−3.12	−0.12
Coronado 2	F6	WY	16	−1.63	0.08	−0.05	0.33	−2.23	−2.31	···	−1.71	−2.79	···
Newcastle	F6	WY	21	−1.76	−0.02	−0.16	−0.02	−1.96	−2.17	···	−1.81	−2.56	···
Osage	F6	WY	17	−1.75	0.01	−0.13	−0.06	−1.89	−2.13	···	−1.89	−2.61	···
Upton	F6	WY	15	−1.69	−0.03	−0.17	−0.02	−1.36	−1.57	···	−1.10	−1.24	···
Devils Tower	F6	WY	13	−1.84	0.00	−0.15	−0.21	−1.17	−1.48	−1.68	NS	NS	0.41
Rhoads Fork	R7	SD	4	−1.98	−0.09	−0.25	−0.60	−3.03	−3.50	···	−2.49	−4.36	···
Voss	F7	WY	20	−1.82	0.12	−0.02	0.27	−2.00	−2.21	···	−1.66	−2.59	···
Self	F7	WY	22	−1.85	0.16	0.02	0.36	−1.67	−1.85	−1.39	−1.51	−2.14	···
JBJ	F7	WY	18	−1.58	−0.71	−0.84	−1.44	−1.32	−1.37	···	−1.46	−0.83	···
Evans Plunge	F7	SD	10	−1.55	−0.03	−0.17	−0.34	−0.68	−0.84	···	−1.53	−0.97	···
Cascade Spring	F7	SD	9	−1.61	0.10	−0.05	−0.30	−0.06	−0.33	···	−1.46	−0.46	···
Jones Spring	R8	SD	12	−1.75	−0.06	−0.21	−0.45	−2.77	−3.13	···	−2.32	−3.90	···
Kaiser	R8	SD	11	−2.11	−0.15	−0.30	−0.51	−2.52	−2.86	−1.07	−1.94	−3.17	−0.18
Cleghorn Spring	R8	SD	16	−2.19	−0.30	−0.45	−0.79	−2.33	−2.71	···	−2.40	−3.32	···
Lein	F8	SD	17	−2.12	−0.19	−0.34	−0.48	−2.53	−2.91	−2.03	−2.18	−3.41	−0.14
McNenney	F8	SD	2	−1.86	−0.17	−0.32	−0.74	−1.50	−1.88	···	−1.65	−1.86	···
Ellsworth AFB	F8	SD	18	−1.57	0.03	−0.10	0.12	−1.27	−1.29	···	−1.64	−1.69	···
Fuhs	F8	SD	6	−1.79	−0.09	−0.25	−0.18	−1.28	−1.68	−2.22	−1.84	−1.92	0.58
Philip	F8	SD	19	−1.18	0.03	−0.09	−0.09	−0.57	−0.51	···	−1.42	−0.76	···
Kosken	F8	SD	1	−1.34	−0.05	−0.17	−0.36	−0.53	−0.48	···	−1.52	−0.73	···
Midland	F8	SD	24	−1.24	0.13	0.01	0.04	−0.44	−0.36	···	−1.34	−0.63	···
Murdo	F8	SD	25	−1.32	0.01	−0.11	−0.17	−0.41	−0.38	−0.19	−1.39	−0.56	···
Prince	F8	SD	26	−1.40	−0.01	−0.13	−0.25	−0.23	−0.21	−0.88	−1.42	−0.38	0.96
Hilltop Ranch	F8	SD	22	−1.36	0.06	−0.05	−0.12	−0.26	−0.20	−0.44	−1.36	−0.42	···
Hamilton	F8	SD	21	−1.32	0.05	−0.07	−0.10	−0.20	−0.17	0.03	−1.36	−0.36	−0.43
Eagle Butte	F8	SD	23	−1.45	0.23	0.11	0.40	−0.24	−0.24	0.24	−1.06	−0.29	···
Dupree	F8	SD	20	−1.47	0.17	0.04	0.18	−0.22	−0.20	−0.83	−1.10	−0.23	···

NS, no sample (missing cation data). Three dots indicate that cation concentration below detection. Detection limits are Fe < 10 μg/L; Ba < 100 μg/L. The states are designated by MT, Montana; SD, South Dakota; WY, Wyoming.

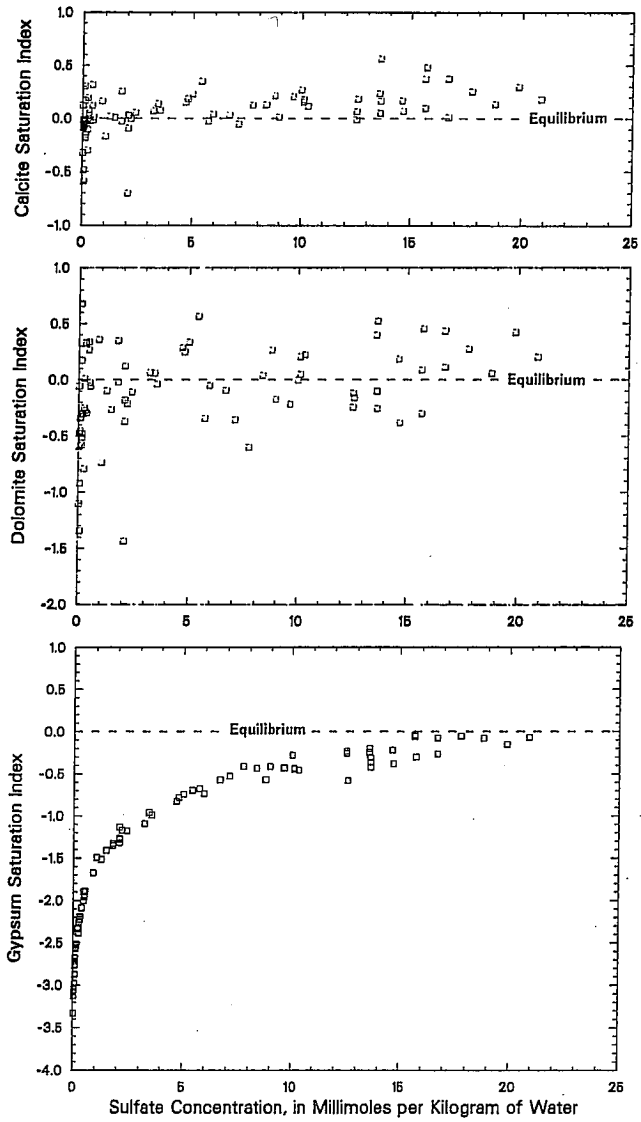

Fig. 6. Comparison of calcite, dolomite, and gypsum saturation indices as a function of total dissolved sulfate content for wells and springs in the Madison aquifer.

Equations

The chemical evolution of the water along a flow path is constrained by relationships of conservation of mass and electrons that are represented by the equations

$$\sum_{p-1}^{P} \alpha_p b_{p,k} = \Delta m_{T,k,|k=1,j} \tag{3}$$

$$\sum_{p=1}^{P} u_p \alpha_p = \Delta \mathrm{RS} \tag{4}$$

Equation (3) relates the change in total moles of the kth element in solution along the flow path $\Delta m_{T,k}$ (final water minus initial water) to the sum of the net moles of that element entering or leaving solution from dissolution, precipitation, biological degradation, gas transfer, and so forth of P phases along the flow path, where the mass transfer coefficient α_p is the number of moles of the pth mineral entering (positive) or leaving (negative) the solution, and $b_{p,k}$ is the stoichiometric coefficient of the kth element in the pth mineral. There are j equations of the form of (3), one for each of the j elements (excluding hydrogen and oxygen) required to define the composition of the P phases (minerals) considered in the model. Thus a reaction model is a particular choice of phases that react to give the actual final water composition.

Because the reactions include changes in oxidation state, (4) provides an additional constraint. Equation (4) follows from the fact that hydrated electrons do not exist in aqueous solution. If electron transfer takes place (that is, there is a redox reaction), the electrons transferred are conserved among the dissolved species and the masses (α_p) of P phases in the model. Equation (4) relates the sum of operational valences of the constituents in the pth plausible phase (u_p) and the stoichiometric coefficient of the pth plausible phase in the mass balance calculation to ΔRS (the difference in redox state; final minus initial water). The operational valence (ν_i for species and u_p for phases) is defined by *Parkhurst et al.* [1980] and *Plummer et al.* [1983] and in some cases differs from the recognized oxidation state.

In (4) the change in the redox state of the solution ΔRS is calculated from the analytical data, as is Δm_T, and includes the (operational) valence ν_i of the ith species in solution. The term ΔRS is defined as

$$\Delta \mathrm{RS} = \mathrm{RS}_{(\mathrm{final})} - \mathrm{RS}_{(\mathrm{initial})} = \sum_{i=1}^{I} \nu_i m_{i(\mathrm{final})} - \sum_{i=1}^{I} \nu_i m_{i(\mathrm{initial})} \tag{5}$$

where m_i is the molality of the ith species in solution. (The initial condition refers to the recharge area and final condition indicates the downgradient well.) The change in the redox state is then set equal to the number of electrons transferred among the P phases (equation (4)).

The mass transfers of sulfur-bearing phases (anhydrite and pyrite) can be estimated accurately by a sulfur mass balance equation and an isotope balance equation for ^{34}S. In the form of (3) the sulfur isotope balance equation is

$$\sum_{p=1}^{P} \alpha_p b_{p,S} \delta^{34}S_p = \Delta m_{T,^{34}S_T} \tag{6}$$

where

$$\Delta m_{T,^{34}S_T} = (m_{T,S}\delta^{34}S_T)_{\mathrm{final}} - (m_{T,S}\delta^{34}S_T)_{\mathrm{initial}} \tag{7}$$

The term $b_{p,S}$ is the stoichiometric coefficient of sulfur in the pth phase; $\delta^{34}S_p$ is the sulfur isotopic composition, in per mil of the pth phase; $m_{T,S}$ and $\delta^{34}S_T$ denote the total molality of sulfur in solution (sulfate plus sulfide species) and the average isotopic composition, in per mil, of total dissolved sulfur, respectively; and α_p is the mass transfer of the pth phase in units of m.

The data required to solve a mass balance reaction model are (1) the set of phases thought to be reacting along the flow path, (2) the concentrations of the elements in the initial and final waters that correspond to the composition of the chosen phases, and (3) the isotopic composition of sulfur. The analytical data and redox state used in mass balance model-

TABLE 4. Concentrations of the Major Elements and Redox State Used in Mass Balance Models

Well Name	Flow Path	State	Well Number	Temperature, °C	pH	Ca	Mg	Na	K	Cl	SO_4	H_2S	C	Fe	RS
Recharge 1	R1			10.6	7.58	1.87	1.15	0.10	0.02	0.05	1.46	···	3.31	0.0007	21.99
Hanover Flowing Well	F1	MT	8	20.4	7.63	2.10	1.19	0.12	0.03	0.04	1.77	···	3.42	0.0002	24.29
Vanek Warm Spring	F1	MT	9	19.6	7.40	3.25	1.65	0.16	0.03	0.07	3.44	···	3.53	0.0005	34.77
Landusky Spring	F1	MT	12	20.4	7.24	6.50	4.08	1.79	0.24	0.54	10.11	···	3.81	0.0005	75.93
Lodgepole Warm Spring	F1	MT	13	31.6	7.08	6.50	3.96	3.44	0.31	1.89	10.32	···	3.72	0.0004	76.83
Sleeping Buffalo	F1	MT	18	40.9	7.00	12.77	4.95	13.53	0.67	5.38	20.89	0.001	2.81	0.0079	136.58
Recharge 2	R2			9.7	7.74	1.26	0.68	0.22	0.04	0.05	0.26	···	3.85	0.0010	16.96
Mcleod Warm Spring	F2	MT	6	24.6	7.40	1.77	0.95	0.07	0.04	0.03	1.25	···	3.35	0.0000	20.90
Sumatra	F2	MT	17	83.7	6.61	5.52	1.41	78.78	3.35	65.27	12.57	1.358	6.31	0.0004	97.92
Keg Coulee	F2	MT	15	61.7	6.50	8.78	2.19	65.63	3.09	56.74	13.61	1.682	6.78	0.0070	105.44
Texaco C115X	F2	MT	16	84.7	6.40	8.03	2.15	74.42	3.86	59.61	14.67	3.898	6.37	0.0009	105.68
Recharge 3	R3			9.9	7.55	1.20	1.01	0.02	0.02	0.02	0.16	···	4.30	0.0010	18.14
Colstrip	F3	MT	21	97.5	6.52	5.50	1.15	6.10	1.72	2.71	7.72	0.118	3.58	0.0061	60.39
Sarpyk Mine	F3	MT	19	83.0	6.70	8.00	2.10	2.09	1.26	0.59	10.01	0.085	2.99	0.0100	71.86
Gas City	F3	MT	26	91.5	6.61	9.28	2.52	61.24	2.83	53.90	13.61	1.594	7.54	0.0018	108.62
Bluewater Spring	F3	MT	11	14.3	7.29	13.26	2.76	3.10	0.07	0.07	15.65	···	3.97	0.0002	109.81
Moore	F3	MT	22	86.9	6.67	9.54	2.82	74.44	3.35	68.14	15.72	0.561	6.02	0.0004	117.26
Mysse Flowing Well	F3	MT	20	63.0	6.61	11.28	4.54	31.89	2.54	17.85	19.86	0.259	6.87	0.0004	146.13
Recharge 4	R4			8.7	7.43	1.12	0.85	0.05	0.02	0.02	0.11	···	4.05	0.0012	16.86
HTH 1	F4	WY	14	46.2	6.99	4.50	1.81	1.57	0.19	1.52	4.79	···	3.99	0.1040	44.93
Ranch Creek	F4	MT	23	52.7	6.94	4.75	1.89	1.65	0.20	1.58	5.00	···	4.05	0.0004	46.21
Belle Creek	F4	MT	24	56.2	7.01	5.00	1.98	1.65	0.20	1.61	5.42	···	3.95	0.0009	48.30
Delzer 1	F4	SD	7	22.8	7.51	12.76	4.54	1.57	0.90	0.71	16.70	0.001	1.88	0.1418	107.99
Delzer 2	F4	SD	8	55.6	6.77	13.76	4.54	1.96	0.31	1.89	17.74	0.005	3.45	0.1023	120.46
Recharge 5	R5			12.0	7.36	1.14	1.05	0.22	0.04	0.08	0.21	···	4.45	0.0004	19.07
Conoco 175	F5	WY	11	65.0	7.07	2.75	1.03	3.35	0.25	1.98	3.54	0.002	2.23	0.0430	30.24
Conoco 44	F5	WY	8	32.2	7.17	6.00	2.51	16.57	0.64	13.85	8.76	0.009	3.98	0.0156	68.54
MKM	F5	WY	10	88.1	6.71	7.26	1.69	33.17	1.77	33.97	9.61	0.002	2.81	0.1240	69.13
Shidler	F5	WY	9	56.0	7.08	7.50	2.02	21.37	0.90	17.53	10.12	0.004	2.00	0.0431	68.83
Recharge 6	R6			6.7	7.48	1.54	0.97	0.05	0.02	0.02	0.03	···	5.46	0.0000	21.99
Seeley	F6	WY	19	13.0	7.30	1.65	1.11	0.06	0.03	0.02	0.18	···	5.51	0.0004	23.09
Coronado 2	F6	WY	16	39.8	7.16	1.40	1.11	0.08	0.04	0.02	0.29	···	5.13	···	22.28
Newcastle	F6	WY	21	25.0	7.20	1.60	1.19	0.11	0.04	0.03	0.49	···	5.34	···	24.29
Osage	F6	WY	17	23.4	7.20	1.75	1.11	0.09	0.04	0.02	0.52	···	5.54	···	25.27
Upton	F6	WY	15	25.7	7.12	2.20	1.69	0.11	0.06	0.02	1.77	···	5.25	···	31.63
Devils Tower	F6	WY	13	17.1	7.20	2.75	1.56	0.16	0.04	0.07	2.19	···	5.03	0.0005	33.23
Recharge 7	R7			5.7	7.35	1.65	0.95	0.04	0.02	0.01	0.03	···	5.73	0.0000	23.11
Voss	F7	WY	20	26.1	7.30	1.57	1.19	0.11	0.04	0.05	0.45	···	5.56	···	24.94
Self	F7	WY	22	29.5	7.30	1.82	1.28	0.11	0.05	0.06	0.90	···	5.00	0.0004	25.39
JBJ	F7	WY	18	45.1	6.70	1.82	0.91	0.48	0.12	0.21	2.08	···	2.20	···	21.28
Evans Plunge	F7	SD	10	30.5	6.90	5.25	1.69	3.75	0.28	3.11	5.73	0.001	4.59	···	52.76
Cascade Spring	F7	SD	9	20.0	6.89	13.51	3.42	1.18	0.13	0.88	15.65	···	4.87	···	113.41
Recharge 8	R8			13.2	7.34	1.33	0.81	0.23	0.05	0.06	0.15	0.001	4.67	0.0007	19.58
Lein	F8	SD	17	11.9	7.41	1.15	1.03	0.10	0.05	0.04	0.15	···	4.31	0.0002	18.11
McNenney	F8	SD	2	11.5	7.18	2.17	0.99	0.09	0.04	0.02	1.04	···	4.96	···	26.07
Ellsworth AFB	F8	SD	18	49.0	7.01	2.27	1.36	0.21	0.09	0.03	2.08	···	3.80	···	27.70
Fuhs	F8	SD	6	10.7	7.21	2.20	2.59	0.25	0.09	0.11	2.08	0.002	6.41	0.0002	38.14
Philip	F8	SD	19	68.0	6.65	5.50	2.39	0.78	0.19	0.62	6.67	0.000	3.57	···	54.28
Kosken	F8	SD	1	63.5	6.68	6.00	1.98	1.18	0.28	1.13	7.09	0.004	2.83	···	53.82
Midland	F8	SD	24	71.0	6.69	6.75	2.72	1.09	0.25	0.79	8.34	0.001	3.26	···	63.06
Murdo	F8	SD	25	59.1	6.68	7.50	2.68	2.00	0.33	1.72	8.97	0.004	3.24	0.0251	66.78
Prince	F8	SD	26	57.0	6.67	10.25	3.42	3.14	0.51	3.11	12.52	0.004	2.80	0.0075	86.30
Hilltop Ranch	F8	SD	22	66.0	6.70	9.00	3.17	3.70	0.33	4.52	12.52	0.002	2.77	0.0154	86.21
Hamilton	F8	SD	21	58.5	6.66	10.50	3.71	1.48	0.38	1.36	13.56	0.041	3.22	0.0538	94.27
Eagle Butte	F8	SD	23	54.7	6.84	9.75	4.53	2.62	0.72	1.78	13.56	0.027	3.54	0.0538	95.60
Dupree	F8	SD	20	56.5	6.82	9.75	3.88	4.80	1.26	3.39	14.61	0.029	3.17	0.0054	100.29

All concentrations are in millimoles per kilogram of water; C denotes total dissolved inorganic carbon. The redox state (RS) is in milliequivalents per kilogram water. For the Madison waters, RS = $6SO_4 - 2H_2S + 4C + 2Fe$, where SO_4, H_2S, C, and Fe are the respective total concentrations in millimoles per kilogram water (see equation (5)). Missing values of H_2S were not determined in the field and are expected to be below detection (<0.001 mmol/kg H_2O). Some laboratory values of H_2S reported by *Busby et al.* [1983] were found to be erroneous and are excluded. Missing Fe values are below the detection of 10 μg/L. The letter in front of the flow path number indicates recharge waters (R) or waters on the flow path. See Table 3 for individual wells or springs used to define the average recharge water compositions. The states are designated by MT, Montana; SD, South Dakoka; and WY, Wyoming.

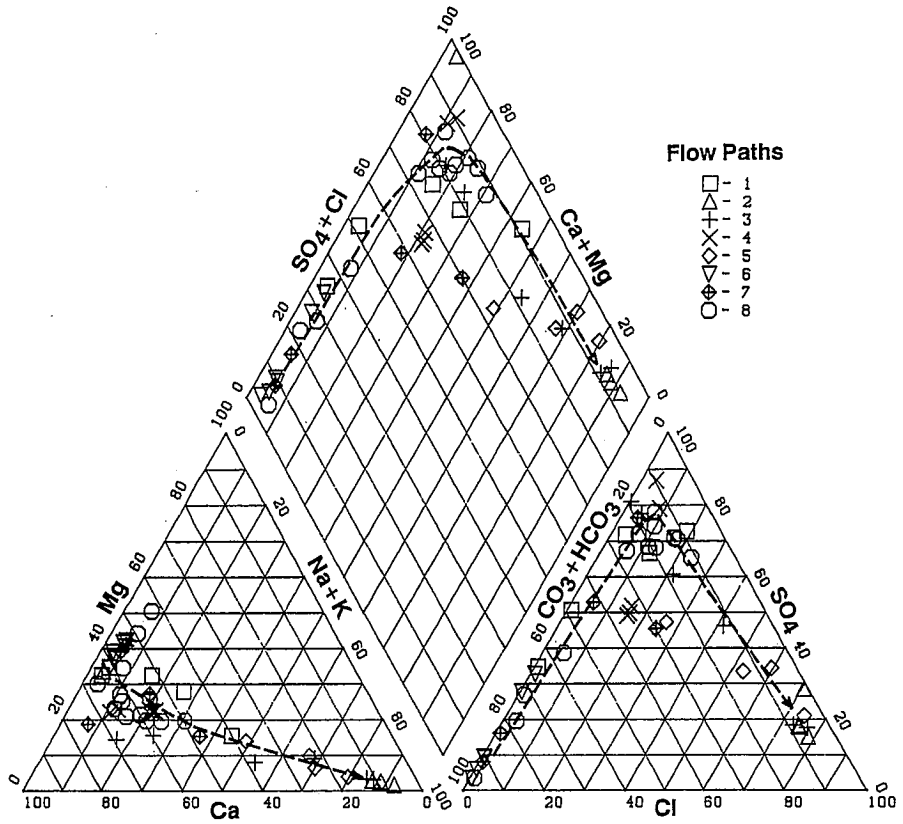

Fig. 7. Trilinear diagram for waters from the Madison aquifer showing evolutionary trends in the major ionic composition along each flow path (mole percent). The arrows show the combined evolutionary paths for all reactions in the Madison aquifer.

ing of the Madison aquifer are summarized in Table 4, and the sulfur isotope data are given in Table 5.

Although the sulfur isotopic composition of dissolved sulfate is known for nearly all the wells or springs sampled in the Madison aquifer, the sulfur isotopic composition of dissolved sulfide was obtained for only 12 wells (Table 5). As a result, it was necessary to use an estimation procedure to calculate the anhydrite and pyrite mass transfers elsewhere in the Madison aquifer, based on the parameter $^{34}\Delta$ [*Pearson and Rightmire*, 1980]

$$^{34}\Delta = \delta^{34}S_{SO_4} - \delta^{34}S_{H_2S} \quad (8)$$

There are relatively few observations of $^{34}\Delta$ from carbonate aquifers reported in the literature for comparison with $^{34}\Delta$ values from the Madison aquifer. *Rye et al.* [1981] show that for the Floridan aquifer system (Florida), $^{34}\Delta$ approaches that expected for isotopic equilibrium (based on experimental data of *Ohmoto and Rye* [1979] at 200°–350°C, extrapolated to 25°C). Values of $^{34}\Delta$ in the Edwards aquifer (Cretaceous Edwards Limestone in Texas) (F. J. Pearson, Jr., and P. L. Rettman, unpublished data, 1976) and Madison aquifer probably result from kinetic fractionation during biologically mediated sulfate reduction. The kinetic fractionation in the Edwards and Madison aquifers appears to be a linear function of temperature (Figure 12) and is approximated by

$$^{34}\Delta = 54 - 0.40t \quad (9)$$

where t is temperature in degrees Celsius.

In calculating the anhydrite and pyrite mass transfers, all measured values of $\delta^{34}S_{SO_4}$ and $\delta^{34}S_{H_2S}$ for the groundwater have been used where available (Table 5). For other wells, $\Delta m_{T,^{34}S_T}$ was estimated using (9) with the measured temperature and $\delta^{34}S_{SO_4}$. These estimates were used in the mass balance models to calculate the anhydrite and pyrite mass transfers elsewhere in the Madison aquifer, as described below.

As a test of the magnitude of potential uncertainties due to the use of (9) (in lieu of actual data on the sulfur isotopic composition of dissolved sulfide), the sulfur isotope mass balance calculation of the anhydrite and pyrite mass transfers was made using (3) and (6) for wells with $\delta^{34}S$ measurements for both SO_4 and H_2S (Table 5) and compared with results using the approximation of (9).

The largest deviation of $\delta^{34}S_{H_2S}$ values obtained from (9) relative to the measured values is ±10‰ (Dupree and Moore wells, Table 5). This uncertainty in $\delta^{34}S_{H_2S}$ translates to a maximum uncertainty in the pyrite mass transfer of 37% and in the anhydrite mass transfer of less than 0.7%. Specifically, for the Dupree well, the measured $\delta^{34}S_{H_2S}$ is −4.77‰, which compares to the estimated (equation (9)) value of $\delta^{34}S_{H_2S}$ of −15.1‰. Using the measured $\delta^{34}S_{H_2S}$, α_{pyrite} is −0.127 mmol, which compares to −0.080 mmol using the estimated value. The anhydrite mass transfer is 14.744 and 14.648 using the measured and estimated value of $\delta^{34}S_{H_2S}$, respectively.

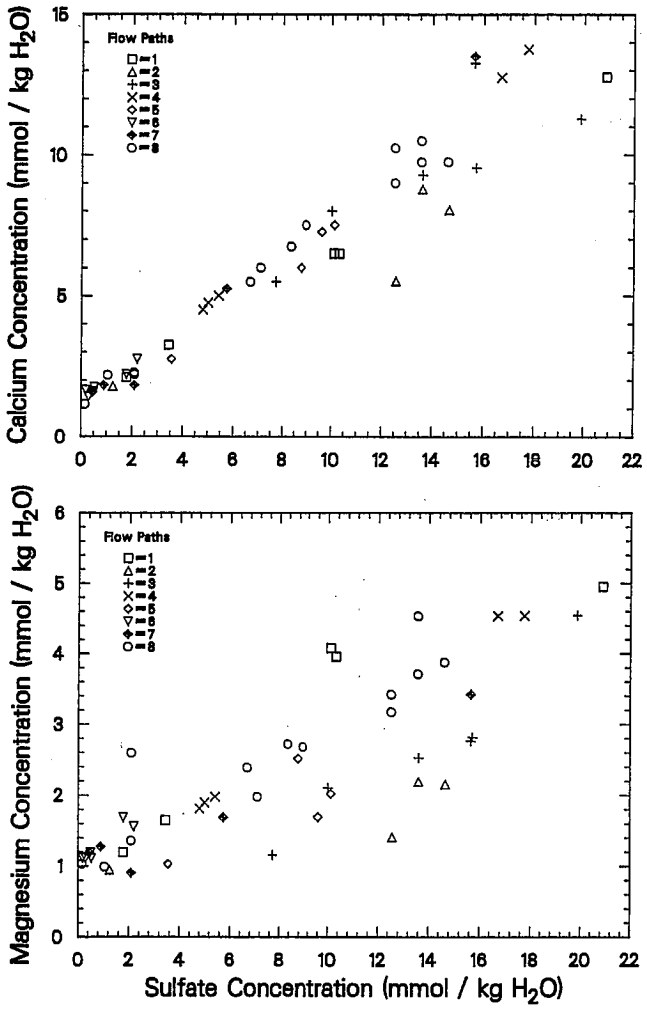

Fig. 8. Comparison of concentrations of dissolved calcium and magnesium as a function of dissolved sulfate content for waters from the Madison aquifer.

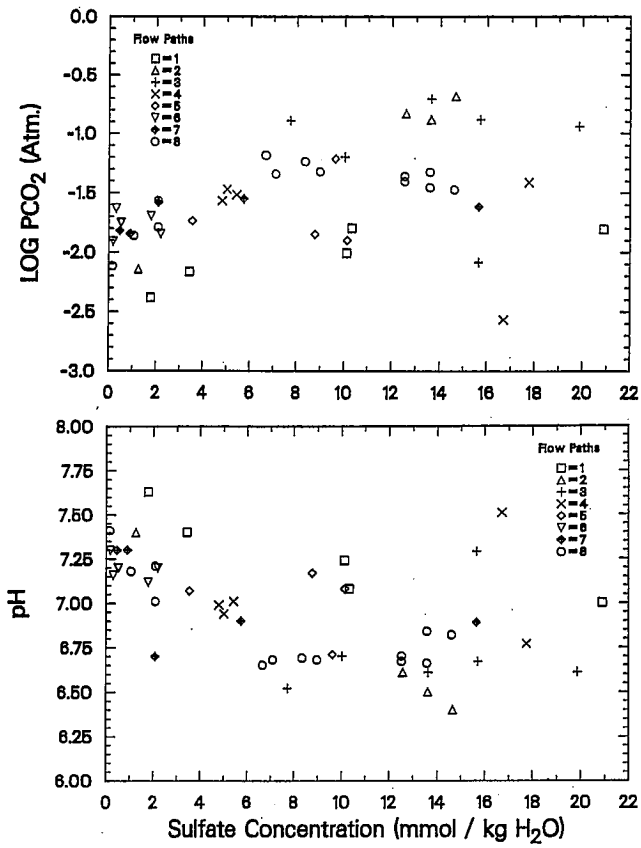

Fig. 9. Comparison of pH and (calculated) P_{CO_2} as a function of dissolved sulfate content for waters from the Madison aquifer.

Plausible Phases

The most obvious phases to include in the mass balance modeling, based on the analysis of the chemical trends, calculated values of SI, and the mineralogy, are summarized in Table 6. Even though we have chosen a likely set of reactants and products for the Madison aquifer, and even though the reaction models presented below are consistent with all chemical and isotopic observations for the system, the results should always be considered nonunique because of the possibility of other reactants and products which are not included in Table 6 [*Plummer*, 1984].

Organic matter (CH_2O) is included as the most likely electron donor for bacterially mediated sulfate reduction. The formula CH_2O denotes carbon of valence zero. Sulfate reduction is known to occur because of the presence of dissolved-sulfide species in many wells (Table 4) and the occurrence of sulfate-reducing bacteria as facultative thermophiles in one of the test wells drilled by the Madison Limestone Project [*Olson et al.*, 1981; *Blankennagel et al.*, 1979]. If sufficient sources of dissolved iron are available for precipitation of pyrite, sulfate reduction can occur in the absence of large concentrations of dissolved sulfide species. Therefore ferric hydroxide and pyrite have been included in

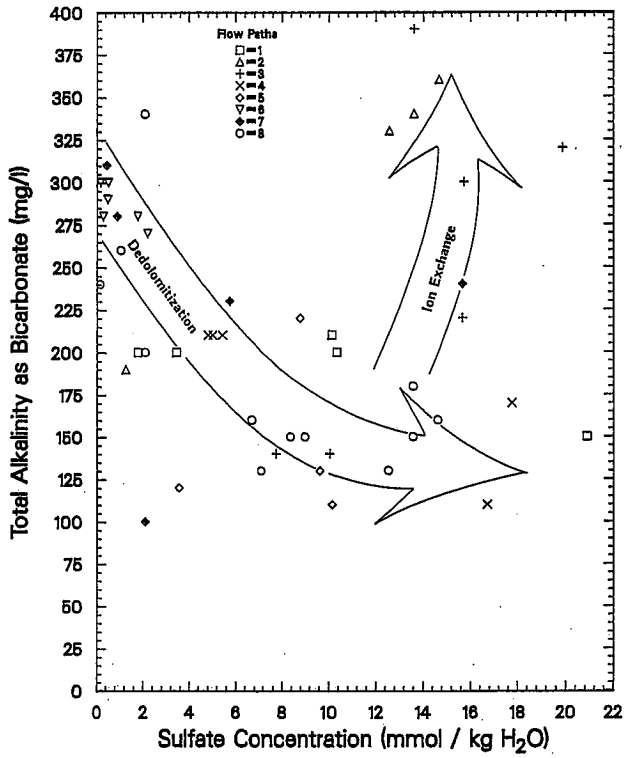

Fig. 10. Trends in total alkalinity of waters from the Madison aquifer as a function of dissolved sulfate content.

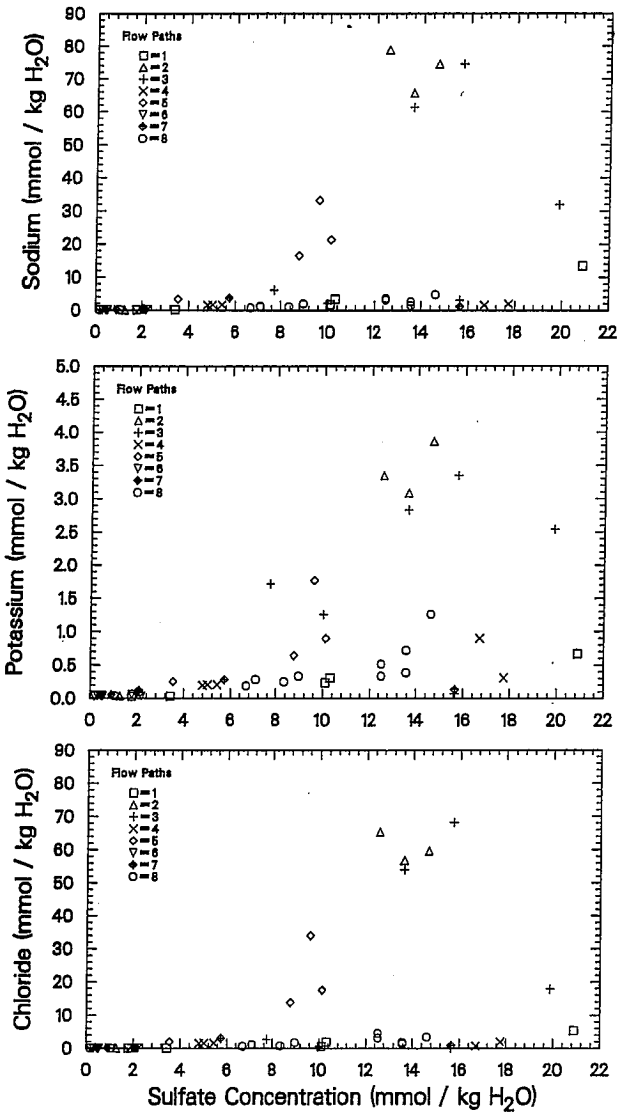

Fig. 11. Comparison of concentrations of sodium, potassium, and chloride as a function of dissolved sulfate content for waters from the Madison aquifer.

the mass balance models. Dolomite, calcite, and anhydrite are included to quantify the dedolomitization reaction.

Dissolution of halite was indicated by the earlier analysis of trends. Sylvite has not been reported in Madison evaporites but is included in the plausible phases (Table 6) as a proxy for an evaporite source of potassium, as suggested by the covariance of sodium, potassium, and chloride (Figure 11). Sodium in excess of chloride (adjusted for potassium sources) is attributed to sodium ion exchange with calcium (and in some cases magnesium) according to the reaction

$$\mathrm{Na_2(clay)} + X_{\mathrm{Mg}}\mathrm{Mg^{2+}} + (1 - X_{\mathrm{Mg}})\mathrm{Ca^{2+}} = [\mathrm{Ca}_{(1-X_{\mathrm{Mg}})}, \mathrm{Mg}_{(X_{\mathrm{Mg}})}](\mathrm{clay}) + 2\mathrm{Na^{+}} \quad (10)$$

where X_{Mg} varies between 0 and 1 for pure Ca/Na and pure Mg/Na cation exchange, respectively.

Carbon dioxide gas was included among the plausible phases to provide an additional constraint on the modeling. Near-zero values for the CO_2 gas mass transfer were expected for the deep, confined groundwater system. Although the aquifer system is expected to be closed to CO_2 gas mass transfer, this does not preclude the possibility of reactions producing or consuming CO_2 within the aquifer, such as through oxidation of organic matter accompanying sulfate reduction, methanogenesis, or carbonate mineral dissolution or precipitation, all of which were considered. Calculated nonzero values of the CO_2 gas mass transfer refer to implied amounts of CO_2 that enter the aquifer from an external source such as the soil zone or cross-formational leakage or leave the aquifer, such as through outgassing. Deviations from zero of several tenths of a millimole per kilogram H_2O in CO_2 gas mass transfer can be expected from uncertainties in the analytical data, but larger deviations have been attributed to uncertainties in the sulfur isotopic composition of anhydrite or to uncertainties in total inorganic carbon in recharge areas. The computed CO_2 gas mass transfer is linked to the sulfur isotopic composition of anhydrite through the sulfate reduction reaction, which affects the carbon mass balance. As a criterion to the mass balance modeling, the sulfur isotopic composition of anhydrite was treated as an adjustable parameter, which was varied to bring the CO_2 gas mass transfer near zero.

Mass Balance Model

For the 10 plausible phases in Table 6, 10 equations of the form of (3), (4), and (6) are needed to calculate the mass transfer coefficients (α_p). These equations are

(1) mass balance

$$\alpha_{\mathrm{calcite}} + 2\alpha_{\mathrm{dolomite}} + \alpha_{\mathrm{CH_2O}} + \alpha_{\mathrm{CO_2}} = \Delta m_{T,\mathrm{C}} \quad (11)$$

$$\alpha_{\mathrm{anhydrite}} + 2\alpha_{\mathrm{pyrite}} = \Delta m_{T,\mathrm{S}} \quad (12)$$

$$\alpha_{\mathrm{calcite}} + \alpha_{\mathrm{dolomite}} + \alpha_{\mathrm{anhydrite}} - (1 - X_{\mathrm{Mg}})\alpha_{\mathrm{exchange}} = \Delta m_{T,\mathrm{Ca}} \quad (13)$$

$$\alpha_{\mathrm{dolomite}} - X_{\mathrm{Mg}}\alpha_{\mathrm{exchange}} = \Delta m_{T,\mathrm{Mg}} \quad (14)$$

$$\alpha_{\mathrm{halite}} + 2\alpha_{\mathrm{exchange}} = \Delta m_{T,\mathrm{Na}} \quad (15)$$

$$\alpha_{\mathrm{sylvite}} = \Delta m_{T,\mathrm{K}} \quad (16)$$

$$\alpha_{\mathrm{halite}} + \alpha_{\mathrm{sylvite}} = \Delta m_{T,\mathrm{Cl}} \quad (17)$$

$$\alpha_{\mathrm{FeOOH}} + \alpha_{\mathrm{pyrite}} = \Delta m_{T,\mathrm{Fe}} \quad (18)$$

where X_{Mg} is the fraction of Mg/Na ion exchange,

(2) conservation of electrons

$$4\alpha_{\mathrm{calcite}} + 8\alpha_{\mathrm{dolomite}} + 6\alpha_{\mathrm{anhydrite}} + 4\alpha_{\mathrm{CO_2}} + 3\alpha_{\mathrm{FeOOH}} = \Delta\mathrm{RS} \quad (19)$$

(note that terms for CH_2O and FeS_2 do not appear in (19) because their operational valence is zero), and

(3) sulfur isotope balance

$$\alpha_{\mathrm{anhydrite}}\delta^{34}\mathrm{S}_{\mathrm{anhydrite}} + 2\alpha_{\mathrm{pyrite}}\delta^{34}\mathrm{S}_{\mathrm{pyrite}} = \Delta m_{T,^{34}\mathrm{S}_T} \quad (20)$$

where $\Delta m_{T,^{34}\mathrm{S}_T}$ is given by (7), S_T refers to total dissolved sulfur (sulfate plus sulfide species), $\delta^{34}S_T$ is the average isotopic composition of dissolved sulfate and sulfide species

TABLE 5. Isotopic Data

Well Name	Flow Path	State	Well Number	Tritium, TU	$\delta^{18}O$, ‰	δD, ‰	$\delta^{34}S_{SO_4}$, ‰	$\delta^{34}S_{H_2S}$, ‰	$\delta^{13}C$, ‰	^{14}C, % modern
Lewistown Big Spring	R1	MT	10	0.8	−18.25	−139.20	14.93	···	−4.97	35.80
Hanover Flowing Well	F1	MT	8	0.0	−18.25	−140.45	17.48	···	−5.32	25.40
Vanek Warm Spring	F1	MT	9	5.3	−18.35	−139.65	17.78	···	−5.18	29.30
Landusky Spring	F1	MT	12	21.9	−18.25	−138.75	21.33	···	−7.46	···
Lodgepole Warm Spring	F1	MT	13	31.8	−17.80	−134.75	23.86	···	−7.04	28.00
Sleeping Buffalo	F1	MT	18	···	−18.40	−138.35	21.95	···	−3.22	4.20
Bozeman Fish Hatchery	R2	MT	4	115.0	−18.90	−143.70	3.34	···	−8.98	84.10
Big Timber Fish Hatchery	R2	MT	7	124.0	−18.60	−142.65	−4.46	···	−14.11	103.90
Mcleod Warm Spring	F2	MT	6	45.5	−18.50	−140.70	17.95	···	−7.57	52.50
Sumatra	F2	MT	17	···	−16.90	−136.15	17.01	−2.60	−3.61	···
Keg Coulee	F2	MT	15	···	−16.80	−136.40	17.75	···	−1.68	1.00
Texaco C115X	F2	MT	16	···	···	···	18.69	−0.22	···	···
Mock Ranch	R3	WY	1	35.4	−18.35	−138.00	···	···	−7.10	57.70
Denius 1	R3	WY	2	19.8	−18.50	−137.85	9.73	···	−6.88	8.40
Colstrip	F3	MT	21	···	−19.05	−146.05	14.67	···	−2.67	···
Sarpy Mine	F3	MT	19	···	−19.80	−151.40	13.79	−9.20	−2.33	3.30
Gas City	F3	MT	26	···	···	···	···	···	···	···
Bluewater Spring	F3	MT	11	0.5	−19.35	−146.90	···	···	−9.51	···
Moore	F3	MT	22	···	−18.00	−141.75	17.06	−7.73	−2.40	1.60
Mysse Flowing Well	F3	MT	20	···	−18.25	−141.50	16.30	−22.09	−2.34	0.80
Story Fish Hatchery	R4	WY	6	107.0	−18.35	−138.95	···	···	−7.82	88.80
Mobil	R4	WY	7	56.7	−17.45	−132.00	11.51	···	−9.75	62.20
Mock Ranch	R4	WY	1	35.4	−18.35	−138.00	···	···	−7.10	57.70
Denius 1	R4	WY	2	19.8	−18.50	−137.85	9.73	···	−6.88	8.40
HTH 1	F4	WY	14	5.4	···	···	11.60	···	−6.63	12.70
Ranch Creek	F4	MT	23	···	−18.10	−137.60	11.75	···	−6.17	10.00
Belle Creek	F4	MT	24	···	−18.25	−137.90	11.71	···	−6.02	9.50
Delzer 1	F4	SD	7	0.0	−19.66	···	15.20	···	−4.60	4.60
Delzer 2	F4	SD	8	0.0	−18.13	···	14.67	−17.37	−2.61	2.80
Hole in The Wall	R5	WY	5	0.5	−18.30	−139.10	···	···	−10.77	87.40
Barber Ranch Spring	R5	WY	12	53.0	−18.20	−137.65	7.75	···	−11.74	83.70
Conoco 175	F5	WY	11	0.8	−19.25	−145.50	8.23	···	−6.23	13.90
Conoco 44	F5	WY	8	0.0	−20.10	−154.05	8.41	···	−5.14	1.80
MKM	F5	WY	10	0.2	−19.70	−152.05	8.52	···	−4.66	2.60
Shidler	F5	WY	9	1.2	−20.15	−153.65	8.64	···	···	6.20
Mallo Camp	R6	WY	24	···	···	···	···	···	−8.00	92.90
Rhoads Fork	R6	SD	4	62.2	−17.22	−125.00	6.22	···	−11.00	92.90
Seeley	F6	WY	19	0.8	···	−133.50	9.94	···	−7.82	61.40
Coronado 2	F6	WY	16	0.0	−17.60	−133.30	···	···	−7.51	36.00
Newcastle	F6	WY	21	0.1	−17.66	−130.00	9.84	···	−10.40	46.20
Osage	F6	WY	17	0.5	−18.15	−135.00	10.44	···	−10.00	54.70
Upton	F6	WY	15	···	−18.18	−133.00	12.16	···	−8.20	14.70
Devils Tower	F6	WY	13	1.5	−17.85		11.68	···	−6.80	59.00
Rhoads Fork	R7	SD	4	62.2	−17.22	−125.00	6.22	···	−11.00	92.90
Voss	F7	WY	20	2.3	−17.40	−130.65	10.09	···	−7.26	44.50
Self	F7	WY	22	0.0	−17.60	−131.80	10.49	···	−6.60	31.20
JBJ	F7	WY	18	0.3	−17.95	−130.65	11.68	···	−4.24	4.80
Evans Plunge	F7	SD	10	···	−16.71	−121.00	11.62	···	−9.70	28.50
Cascade Spring	F7	SD	9	···	−15.48	−118.00	12.50	···	−9.10	19.40
Jones Spring	R8	SD	12	276.0	−14.61	−110.00	6.67	···	−11.60	100.00
Kaiser	R8	SD	11	27.7	−12.13	···	9.00	···	−8.36	81.10
Cleghorn Spring	R8	SD	16	182.0	−13.23	−103.00	5.75	···	−9.60	91.60
Lein	F8	SD	17	16.6	−14.19	···	−3.20	···	−8.03	68.50
McNenney	F8	SD	2	11.4	−17.43	−127.00	11.36	···	−11.50	79.60
Ellsworth AFB	F8	SD	18	···	−14.13	−107.00	···	···	−9.10	5.80
Fuhs	F8	SD	6	65.6	−16.13	···	4.50	···	−9.96	53.80
Philip	F8	SD	19	···	−17.55	−125.00	14.52	···	−7.20	2.80
Kosken	F8	SD	1	0.1	−16.75	−126.60	12.93	···	−6.20	7.80
Midland	F8	SD	24	···	−17.62	−128.00	14.96	···	−6.20	2.40
Murdo	F8	SD	25	1.3	−17.35	−131.45	14.56	−19.12	−5.50	3.20
Prince	F8	SD	26	···	−17.87	···	15.58	···	−4.72	4.00
Hilltop Ranch	F8	SD	22	0.0	−17.60	−132.40	12.96	···	−6.63	4.60
Hamilton	F8	SD	21	···	−17.74	···	15.22	−12.22	−3.50	2.40
Eagle Butte	F8	SD	23	0.6	−18.25	−137.10	15.99	−7.21	−2.40	2.20
Dupree	F8	SD	20	10.2	−19.00	−143.65	16.31	−4.77	−2.05	2.80

TU, tritium units; one TU is one atom of tritium in 10^{18} atoms of hydrogen. Per mil values of $\delta^{18}O$ and δD are reported relative to Vienna-SMOW. $\delta^{13}C$ and $\delta^{34}S$ are in per mil relative to the PDB (peedee belemnite) and CDT (Canyon Diablo troilite) standards, respectively. Carbon 14 is in percent modern of the National Bureau of Standards 1950 oxalic acid standard. Three dots indicate that data are not available. Sulfur isotope data for dissolved SO_4 and H_2S were obtained for two additional waters from the Madison aquifer and used in defining the correlation of Figure 12. These are Bough Ranch (MT, 5): $\delta^{34}S_{SO_4}$ = 19.99‰, $\delta^{34}S_{H_2S}$ = −26.21‰; and Buckhorn Exeter (MT, 27): $\delta^{34s}SO_4$ = 17.38‰, $\delta^{34}S_{H_2S}$ = −4.23‰. The letter in front of the flow path number indicates whether the well or spring was used for recharge (R) or on the flow path (F). The states are designated by MT, Montana; SD, South Dakota; and WY, Wyoming.

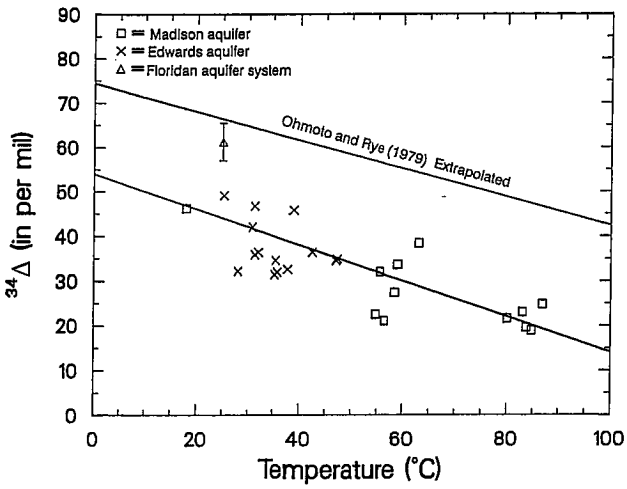

Fig. 12. Trend in $^{34}\Delta$ ($\equiv \delta^{34}S_{SO_4} - \delta^{34}S_{H_2S}$) as a function of groundwater temperature for sulfate and sulfide bearing waters of the Floridian aquifer system [*Rye et al.*, 1981] and Edwards (F. J.Pearson, Jr., and P. L. Rettman, unpublished data, 1976) and Madison aquifers. The waters from the Floridan aquifer system approach apparent isotopic equilibrium, while the sulfur isotopic composition of waters from the Madison and Edwards aquifers are probably influenced by kinetic biochemical fractionation. The error bar shows the range of values observed in the Floridian aquifer system [*Rye et al.*, 1981].

in solution, and the subscripts initial and final refer to the recharge and end point compositions along the flow path.

For an assumed value of X_{Mg} and estimates of the sulfur isotopic composition of anhydrite and pyrite, (11)–(20) provide the 10 independent equations required to solve for the unknown mass transfer coefficients (α_p). The algebraic solutions to (11)–(20), which define the mass transfers of anhydrite, pyrite, KCl, NaCl, [Ca + Mg]/Na ion exchange, dolomite, FeOOH, calcite, CO_2 gas, and CH_2O, are

$$\alpha_{\text{anhydrite}} = \frac{\Delta m_{T,^{34}S_T} - \delta^{34}S_{\text{pyrite}}\Delta m_{T,S}}{(\delta^{34}S_{\text{anhydrite}} - \delta^{34}S_{\text{pyrite}})} \quad (21)$$

$$\alpha_{\text{pyrite}} = (\Delta m_{T,S} - \alpha_{\text{anhydrite}})/2 \quad (22)$$

$$\alpha_{\text{KCl}} = \Delta m_{T,K} \quad (23)$$

$$\alpha_{\text{NaCl}} = \Delta m_{T,Cl} - \alpha_{\text{KCl}} \quad (24)$$

$$\alpha_{\text{exchange}} = (\Delta m_{T,Na} - \alpha_{\text{NaCl}})/2 \quad (25)$$

TABLE 6. Selected Phases for Mass Balance Reaction Modeling

Phase	Composition	Redox State (u_p)
Calcite	$CaCO_3$	4.0
Dolomite	$CaMg(CO_3)_2$	8.0
Anhydrite	$CaSO_4$	6.0
Organic matter	CH_2O	0.0
Carbon dioxide	CO_2	4.0
Ferric hydroxide	FeOOH	3.0
Pyrite	FeS_2	0.0
Cation exchange	(Ca + Mg)/Na	0.0
Halite	NaCl	0.0
"Sylvite"	KCl	0.0

$$\alpha_{\text{dolomite}} = \Delta m_{T,Mg} + X_{Mg}\alpha_{\text{exchange}} \quad (26)$$

$$\alpha_{\text{FeOOH}} = \Delta m_{T,Fe} - \alpha_{\text{pyrite}} \quad (27)$$

$$\alpha_{\text{calcite}} = \Delta m_{T,Ca} + (1 - X_{Mg})\alpha_{\text{exchange}} - \alpha_{\text{anhydrite}} - \alpha_{\text{dolomite}} \quad (28)$$

$$\alpha_{CO_2\text{gas}} = (\Delta RS - 3\alpha_{\text{FeOOH}} - 4\alpha_{\text{calcite}} - 8\alpha_{\text{dolomite}} - 6\alpha_{\text{anhydrite}})/4 \quad (29)$$

$$\alpha_{CH_2O} = \Delta m_{T,C} - \alpha_{CO_2\text{gas}} - 2\alpha_{\text{dolomite}} - \alpha_{\text{calcite}} \quad (30)$$

To facilitate the calculations, (11)–(20) were solved for each pair of recharge-discharge water samples using the computer program BALANCE [*Parkhurst et al.*, 1982].

Criteria Used in Reaction Modeling

In preparing the mass transfer models the initial set of plausible reactants and products was maintained (Table 6), whereas the isotopic composition of dissolving anhydrite was varied. The carbon isotopic composition of the final water was modeled by solving the Rayleigh distillation equations of *Wigley et al.* [1978, 1979] for the computed mass transfer. Equilibrium fractionation factors for the carbonate system were from *Vogel et al.* [1970], *Mook et al.* [1974], and *Mook* [1980]. The one input-one fractionating output case was used to model ^{13}C evolution of the dissolved HCO_3^- of the waters from the Madison aquifer, where the ^{13}C content of incoming carbon was adjusted for the average mass fraction of dolomite and organic matter entering solution. The modeled $\delta^{13}C$ at the end point of the reaction is a function of the initial and final total molalitites of dissolved inorganic carbon, the initial value of $\delta^{13}C$ in the recharge water, the fractionation between the precipitating calcite and solution, the mass transfers of carbon, and the average isotopic composition of incoming carbon from dolomite and CH_2O.

Although the CO_2 gas term was minimized in the modeling exercise (through adjustment of the sulfur isotopic composition of anhydrite), the final value was not always zero. For cases requiring input of CO_2 gas, its mass transfer was added to the total incoming carbon from CH_2O and dolomite and the average $\delta^{13}C$ of incoming carbon adjusted using the $\delta^{13}C$ value of soil gas for the particular flow path. The $\delta^{13}C$ value of soil gas for the flow path was solved by an application of carbon isotope mass balance to the reaction of rain (identical with pure water) with soil CO_2, calcite, dolomite, and anhydrite to form the recharge water. The value of $\delta^{13}C$ of soil gas is determined from the mass balance using the measured $\delta^{13}C$ of the recharge water and the assumption of zero values of $\delta^{13}C$ for calcite and dolomite in the recharge waters. The modeled values of $\delta^{13}C$ for soil gas CO_2 on flow paths 1–8 are −9.44, −20.49, −13.36, −14.64, −20.24, −17.39, −19.90 and −17.16‰, respectively.

In cases where the mass balance model indicated outgassing of CO_2, the modeled $\delta^{13}C$ of the final water was calculated using the one input-two fractionating output Rayleigh distillation equation of *Wigley et al.* [1978, 1979].

The following requirements were met in preparing the mass transfer models:

1. It was assumed that the sulfur isotopic composition of

Madison Limestone anhydrites is variable within the study area. Mississippian-age marine anhydrites show considerable variation in $\delta^{34}S$, decreasing through the Mississippian from about 25‰ in the early Mississippian to about 15‰ in late Mississippian [*Claypool et al.*, 1980]. These values may be further modified by diagenetic processes (see later discussion). Because of the large variation in $\delta^{34}S$ reported for Mississippian-age marine anhydrites, initial local estimates of $\delta^{34}S$ of anhydrite were obtained from extrapolations to zero sulfate content on plots of $\delta^{34}S$ of dissolved SO_4 versus dissolved SO_4 concentration for each flow path. These initial estimates of $\delta^{34}S$ of anhydrite were generally lighter than Mississippian marine anhydrites worldwide [*Claypool et al.*, 1980] and were 17.1, 14.7, 11.8, 10.3, 7.9, 9.5, 10.0, and 11.0‰ for flow paths 1–8, respectively.

2. The value of $\delta^{34}S$ anhydrite was always equal to or less than the value of $\delta^{34}S_{SO_4}$ for each well or spring. That is, in the absence of sulfate reduction, $\delta^{34}S_{SO_4}$ for each well or spring would be equal to $\delta^{34}S$ of anhydrite.

3. The initial value of $\delta^{34}S$ of anhydrite was varied in order to minimize, and decrease to zero if possible, the CO_2 gas mass transfer. The final modeled estimates of $\delta^{34}S$ of anhydrite tend to be larger than the initial estimates. CH_2O was maintained as a reactant.

4. Only wells or springs with measured values of $\delta^{34}S_{SO_4}$ were modeled. The value of $\delta^{34}S_{H_2S}$ used was either the measured value or, if missing, calculated from (9) using the measured temperature and $\delta^{34}S_{SO_4}$.

5. Pyrite was maintained as a product and FeOOH as a reactant. For example, in some cases in order to decrease the α_{CO_2} term to zero it was necessary to increase the value of $\delta^{34}S$ of anhydrite to the point that mass balance calculations showed pyrite as a reactant and FeOOH as a product. In these cases the value of $\delta^{34}S$ anhydrite was decreased until pyrite appeared as a product and FeOOH as a reactant. Pyrite is a product because of the presence of H_2S. In laboratory studies of the reactions of H_2S with goethite to form pyrite at 22°–24°C, fine-grained pyrite was found to be 0.8‰ lighter than the H_2S source [*Price and Shieh*, 1979]. We have no data on the sulfur isotopic composition of pyrite in the Madison, but because the fractionation between H_2S and pyrite is negligibly small, the sulfur isotopic content of pyrite was assumed to be equal to that of dissolved H_2S.

6. For wells or springs where the CO_2 gas and pyrite mass transfers are not sensitive to $\delta^{34}S$ of anhydrite, the selected criteria for $\delta^{34}S$ anhydrite was the agreement between the measured and calculated values of $\delta^{13}C$ in the final solution.

7. The value of $\delta^{13}C_{CH_2O}$ was varied between −20 to −25‰ but usually chosen to be −25‰.

8. The value of $\delta^{13}C$ dolomite was varied between 0.0 and 4.0‰ but usually chosen as 2.0‰. Twenty-one determinations of $\delta^{13}C$ of Madison dolomites from eight cores in the Madison Limestone from NE Wyoming and Montana range between 1.0 and 5.0‰ and average 3.1 ± 1.2‰. These values of $\delta^{13}C$ of Madison dolomites are within the range of values reported by *Budai et al.* [1987] for dolomites of the Madison Group in the Wyoming-Utah Overthrust Belt, west of the study area. In the modeling exercise the value of $\delta^{13}C$ of dolomite was adjusted to obtain agreement between observed $\delta^{13}C$ in the final water and the modeled value. The reaction model was not rejected if the estimated $\delta^{13}C$ of dolomite was within the observed range for Madison dolomites.

9. Ion exchange is an important reaction along flow paths 2 and 3, based on the analysis of the chemical trends. A variable $(Ca^{2+} + Mg^{2+})/Na^+$ ion exchange reaction was considered in which the fraction of magnesium exchange, X_{Mg}, was adjusted in the range $0.0 \le X_{Mg} \le 1.0$. Values of $X_{Mg} > 0.0$ were necessary to model many of the observed heavy $\delta^{13}C$ values for wells along flow paths 2 and 3. Cases of extensive Mg^{2+}/Na^+ ion exchange are indicative of formation of magnesium-enriched minerals such as sepiolite or stevensite but were not explicitly modeled as such.

10. In a few cases the magnitude of the ion exchange term was not sufficient to increase the calculated value of $\delta^{13}C$ to a value similar to the measured value; and for these the possibilities of methanogenesis and carbon isotope exchange were considered. Within the uncertainty of the available chemical and isotopic data it is not possible to completely exclude carbon isotope exchange with calcite and dolomite as a reaction in accounting for some of the heavier ^{13}C contents in waters from the Madison aquifer (Table 5) near −2‰ $\delta^{13}C$. But because there is a close correspondence in modeled and observed $\delta^{13}C$ for most of the waters from the Madison aquifer, consistent with reasonable, known carbon isotopic contents of Madison dolomites and organic matter, isotopic exchange is probably not occurring to a great extent in the Madison aquifer. If the waters from the Madison aquifer were influenced by extensive carbon isotope exchange with the average dolomite ($\delta^{13}C = 3.1 \pm 1.2$‰), the ^{13}C values of dissolved inorganic carbon would approach 2‰, which is not observed.

Although the sulfur isotope data were included in the mass balance equations, in cases where the calculated α_{CO_2} is zero, identical mass transfer results would be obtained by excluding CO_2 gas and solving the mass balance and electron balance equations. For example, the algebraic solution to (3) and (4) for the plausible phases (excluding CO_2 gas) defines the anhydrite mass transfer as

$$\alpha_{\text{anhydrite}} = \tfrac{1}{7}[3\Delta m_{T,S} - 6\Delta m_{T,Fe} + 2\Delta RS - 8\Delta m_{T,Mg} - 8\Delta m_{T,Ca} - 4(\Delta m_{T,Na} - \Delta m_{T,Cl} + \Delta m_{T,K})] \quad (31)$$

which is numerically identical to (21) when the aquifer is closed to external sources or sinks of CO_2 gas ($\alpha_{CO_2} \equiv 0$). If CO_2 gas is excluded in the modeling, the sulfur isotopic composition of Madison Limestone anhydrites could be found by solving (21) using the measured sulfur isotopic composition of the dissolved sulfur species, the assumption that $\delta^{34}S_{Pyrite} = \delta^{34}S_{H_2S}$, and the mass balance results obtained from (31).

Subtle differences between the two approaches of either defining α_{CO_2} to be zero or minimizing α_{CO_2} via the sulfur isotope data enter into the modeling when likely uncertainties in the analytical data are considered. This is particularly true for the uncertainties resulting from selecting an appropriate recharge water composition for a given flow path. The data of Table 4 show a range of total inorganic carbon concentrations of 3.31–5.73 (mmol/kg H_2O) for the defined recharge waters for the eight Madison flow paths. From inspection of (21)–(30), erroneous values for the analytical data, such as for $\Delta m_{T,C}$, can lead to substantial uncertainties in the calculated mineral mass transfer. In the case $\alpha_{CO_2} = 0$,

TABLE 7a. Summary of Modeling Alternatives Applied to the Mysse Flowing Well (Well 20 in Montana): Modeling Parameters

Case	$\delta^{34}S$,* ‰	Ion Exchange X_{Mg}†	Proportion of Carbon Dioxide in Gas‡	Methane Fractionation,§ ‰	$\delta^{13}C$, ‰	
					Organic Matter	Dolomite
1	11.8	0.0	1.0	···	−25.0	+2.0
2	11.8	1.0	1.0	···	−25.0	+2.0
3	11.8	0.0	0.8	−60.	−25.0	+2.0
4	11.8	1.0	0.8	−60.	−25.0	+2.0
5	15.5	0.0	1.0	···	−25.0	+2.0
6	15.5	0.0	1.0	···	−25.0	+4.0

Parts per thousand, ‰.
*Dissolving anhydrite.
†X_{Mg} is the fraction of magnesium/sodium ion exchange: 0.0 is pure calcium/sodium ion exchange and 1.0 is pure magnesium/sodium ion exchange.
‡Proportion of carbon dioxide gas in a carbon dioxide methane mixture: 1.0 is pure carbon dioxide gas and 0.0 is pure methane gas.
§Modeled carbon isotopic fractionation of methane relative to the carbon isotopic composition of the dissolved inorganic carbon.

analytical error may result in violating some of the modeling criteria. For example, if α_{CO_2} is forced to be identically equal to zero, pyrite may become a reactant; a thermodynamically impossible situation in hydrogen sulfide-bearing waters of the Madison aquifer.

As discussed earlier, the CO_2 gas mass transfer is expected to be near zero, and the magnitude of this term has been used as a criterion in refining the mass balance models. The results below show that for most of the waters modeled the CO_2 gas mass transfer is 0.0 ± 0.5 mmol/kg H_2O which, taking into account the modeling assumptions, reasonably supports the conclusion of a closed system.

Example

As an example of the modeling exercise, several modeling alternatives to the Mysee Flowing Well (well 20, flow path 3 in Montana) were examined. The data in Table 7 show that for the initial modeling conditions of Ca^{2+}/Na^+ exchange, no methanogenesis, an initial assumed value of +11.8‰ for $\delta^{34}S$ anhydrite, $\delta^{13}C$ dolomite equal to 2.0‰, and $\delta^{13}C_{CH_2O}$ equal to −25.0‰, the calculated value of δ^{13}(−9.39‰) is substantially lighter than the measured value (−2.34‰), and a significant quantity of CO_2 outgassing (1.97 mmol/kg H_2O) is indicated (case 1, Table 7).

Before adjusting $\delta^{34}S$ anhydrite, several other modeling alternatives were considered. By providing a sink for magnesium as, for example, a pure Mg^{2+}/Na^+ exchange reaction in place of pure Ca^{2+}/Na^+ exchange, the dolomite and calcite mass transfers are almost tripled (Table 7), but there is no change in the large calculated quantity of CO_2 outgassed. Although the calculated value of $\delta^{13}C$ (−4.31‰) in this simulation is closer to the measured value (−2.34‰), the added magnesium sink leads to a calculated ^{14}C value less than the measured value (case 2, Table 7), which is not possible and therefore invalidates this model.

Another modeling alternative is the possibility of methanogenesis. Biological fractionation of ^{13}C accompanies methanogenesis, resulting in the formation of isotopically light CH_4, (typically 40 ± 20‰ lighter in ^{13}C than the CH_2O from which it was derived). Methane as light as −80‰ is not uncommon [*Hoefs*, 1973]. The CO_2-CH_4 equilibrium fractionation factor is about 70‰ at 25°C and decreases to 50‰ at about 90°C [*Bottinga*, 1969].

Only traces of dissolved CH_4 were found in the dissolved gases of 12 wells completed in the Madison aquifer [*Busby et al.*, 1983]. The maximum concentrations (0.45–0.87 mg/L) were in water from wells along flow paths 2 and 3. The modeling of the mass transfer along flow paths 2 and 3 indicates that this concentration of methane is insufficient to significantly affect the calculated value of $\delta^{13}C$. Larger concentrations of CH_4 are required to increase the calculated value of $\delta^{13}C$, which would necessitate a system open to both CO_2 and CH_4 outgassing.

Returning to the modeling example of the Mysse Flowing

TABLE 7b. Summary of Modeling Alternatives Applied to the Mysse Flowing Well: Calculated Results

Case	Mass Transfer, mmol/kg					$\delta^{13}C$, ‰		^{14}C, % Modern	
	Dolomite	Calcite	Anhydrite	Organic Matter	Carbon Dioxide Gas	Calculated	Measured	Adjusted*	Measured
1	3.54	−7.53	22.35	5.00	−1.97	−9.39	−2.34	5.79	0.80
2	11.82	−24.09	22.35	5.00	−1.97	−4.31	−2.34	0.28	0.80
3	3.54	−7.53	22.35	6.31	−3.28	−7.90	−2.34	4.56	0.80
4	11.82	−24.09	22.35	6.31	−3.28	−3.78	−2.34	0.22	0.80
5	3.54	−7.53	20.15	0.87	−0.04	−3.57	−2.34	12.30	0.80
6	3.54	−7.53	20.15	0.87	−0.04	−2.20	−2.34	12.30	0.80

*Carbon 14 content of the Mysse Flowing Well adjusted for reaction effects but not radioactive decay.

TABLE 8. Summary of Mass Transfer Results

Well Name	Flow Path	State	Well Number	Dolomite	Calcite	Anhydrite	CH_2O	FeOOH	Pyrite	Ion Exchange	NaCl	KCl	CO_2 gas
Hanover Flowing Well	F1	MT	8	0.04	−0.20	0.40	0.16	0.04	−0.04	0.02	−0.02	0.01	0.06
Vanek Warm Spring	F1	MT	9	0.49	−1.20	2.10	0.23	0.06	−0.06	0.02	0.01	0.01	0.21
Landusky Spring	F1	MT	12	2.93	−7.36	9.76	2.07	0.55	−0.55	0.70	0.27	0.21	−0.07
Lodgepole Warm Spring	F1	MT	13	2.80	−7.41	10.13	2.36	0.63	−0.63	0.89	1.56	0.28	−0.14
Sleeping Buffalo	F1	MT	18	3.80	−8.26	19.73	0.56	0.15	−0.15	4.37	4.68	0.64	−0.40
Mcleod Warm Spring	F2	MT	6	0.27	−0.95	1.12	0.25	0.07	−0.07	−0.07	−0.02	−0.01	−0.33
Sumatra	F2	MT	17	5.72	−12.10	13.97	3.29	0.15	−0.15	8.32	61.92	3.30	−0.17
Keg Coulee	F2	MT	15	7.39	−14.95	15.08	3.46	0.03	−0.03	5.88	53.65	3.04	−0.36
Texaco C115X	F2	MT	16	10.70	−22.52	18.59	8.34	0.14	−0.15	9.23	55.74	3.82	−4.70
Colstrip	F3	MT	21	2.68	−6.35	7.97	0.78	0.15	−0.15	2.54	1.00	1.69	−0.52
Sarpy Mine	F3	MT	19	2.18	−5.35	10.23	0.72	0.16	−0.15	1.36	−0.66	1.23	−1.06
Moore	F3	MT	22	6.61	−16.07	17.81	4.28	0.84	−0.84	4.81	64.80	3.32	0.29
Mysse Flowing Well	F3	MT	20	3.54	−5.33	20.15	0.87	0.09	−0.09	8.28	15.31	2.52	−0.04
HTH 1	F4	WY	14	0.96	−2.36	4.87	0.36	0.19	−0.09	0.09	1.33	0.17	0.01
Ranch Creek	F4	MT	23	1.04	−2.33	5.03	0.25	0.07	−0.07	0.12	1.37	0.18	−0.01
Belle Creek	F4	MT	24	1.12	−2.61	5.46	0.27	0.07	−0.07	0.10	1.40	0.18	−0.02
Delzer 1	F4	SD	7	3.68	−8.81	17.62	1.97	0.66	−0.52	0.86	−0.20	0.88	−2.70
Delzer 2	F4	SD	8	3.68	−9.14	18.26	1.19	0.41	−0.31	0.16	1.58	0.29	−0.02
Conoco 175	F5	WY	11	0.70	−2.47	3.38	0.09	0.06	−0.02	0.72	1.69	0.21	−1.26
MKM	F5	WY	10	0.64	−3.85	9.73	0.65	0.29	−0.16	0.40	32.16	1.73	0.26
Shidler	F5	WY	9	0.97	−2.48	10.16	0.47	0.16	−0.12	2.28	16.60	0.86	−2.38
Conoco 44	F5	WY	8	1.47	−3.59	8.58	0.05	0.02	−0.01	1.59	13.17	0.60	0.14
Seeley	F6	WY	19	0.14	−0.18	0.15	0.01	0.00	−0.00	0.01	−0.01	0.01	−0.07
Newcastle	F6	WY	21	0.23	−0.60	0.47	0.01	0.00	−0.00	0.04	−0.01	0.03	0.01
Osage	F6	WY	17	0.14	−0.41	0.51	0.02	0.01	−0.01	0.03	−0.02	0.02	0.17
Upton	F6	WY	15	0.72	−1.87	1.86	0.22	0.06	−0.06	0.05	−0.04	0.04	0.00
Devils Tower	F6	WY	13	0.60	−1.62	2.27	0.20	0.05	−0.05	0.04	0.03	0.02	−0.21
Voss	F7	WY	20	0.25	−0.71	0.42	0.01	0.00	−0.00	0.03	0.01	0.03	0.04
Self	F7	WY	22	0.33	−1.00	0.88	0.02	0.01	−0.01	0.03	0.01	0.04	−0.41
JBJ	F7	WY	18	−0.04	−1.77	2.16	0.20	0.05	−0.05	0.17	0.10	0.11	−1.88
Evans Plunge	F7	SD	10	0.74	−2.64	5.93	0.44	0.12	−0.12	0.44	2.83	0.27	−0.42
Cascade Spring	F7	SD	9	2.48	−7.33	16.91	2.42	0.65	−0.65	0.19	0.75	0.12	−0.90
McNenney	F8	SD	2	0.18	−0.31	0.91	0.03	0.01	−0.01	−0.06	−0.03	−0.02	0.20
Kosken	F8	SD	1	1.17	−3.55	7.10	0.30	0.08	−0.08	0.05	0.84	0.23	−0.93
Philip	F8	SD	19	1.58	−4.34	6.98	0.86	0.23	−0.23	0.06	0.43	0.13	−0.79
Midland	F8	SD	24	1.91	−5.00	8.66	0.88	0.23	−0.24	0.16	0.54	0.19	−1.12
Murdo	F8	SD	25	1.87	−4.70	9.19	0.71	0.21	−0.19	0.19	1.38	0.28	−1.18
Hilltop Ranch	F8	SD	22	2.36	−7.75	12.70	0.63	0.18	−0.17	−0.36	4.18	0.28	0.49
Prince	F8	SD	26	2.61	−6.47	12.94	1.07	0.29	−0.28	0.16	2.59	0.46	−1.70
Hamilton	F8	SD	21	2.90	−7.15	13.56	0.30	0.11	−0.06	0.14	0.97	0.33	−0.40
Eagle Butte	F8	SD	23	3.72	−8.22	13.58	0.33	0.12	−0.07	0.66	1.06	0.66	−0.69
Dupree	F8	SD	20	3.07	−8.17	14.74	0.53	0.13	−0.13	1.22	2.13	1.20	0.00

All mineral and gas mass transfers are in millimoles per kilogram of water. Negative for precipitation, positive for dissolution. The states are designated by MT, Montana; SD, South Dakota; and WY, Wyoming.

Well, the mass transfer to this well was calculated assuming the formation of a gas containing 20% CH_4 and 80% CO_2 (Table 7, cases 3 and 4). The CH_4 produced was assumed to be 60‰ lighter than the $\delta^{13}C$ of the aqueous solution. The remainder of the modeling parameters were as before: Ca^{2+}/Na^+ exchange (case 3) or pure Mg^{2+}/Na^+ exchange (case 4), with $\delta^{34}S$ of anhydrite equal to 11.8‰ and $\delta^{13}C_{CH_2O}$ and $\delta^{13}C_{dolomite}$ of −25.0 and 2.0‰, respectively.

Inclusion of methanogenesis significantly increases the calculated quantity of outgassing. As expected, the quantity of organic matter oxidized is increased, and there is only minor improvement in the calculated value of $\delta^{13}C$. The combined effect of pure Mg^{2+}/Na^+ exchange and methanogenesis (case 4, Table 7) differs little from that of Mg^{2+}/Na^+ exchange alone (case 2). Substantial methanogenesis is not known to occur in the presence of dissolved sulfate [*Claypool and Kaplan*, 1974; *Fenchel and Blackburn*, 1979; *Lovley and Klug*, 1986; *Grossman et al.*, 1989]. Because many of the waters are almost saturated with respect to anhydrite, methanogenesis is not expected to be an important process in the Madison aquifer.

The data in Table 7 show that for the Mysse Flowing Well (case 5) the calculated CO_2 outgassing is near 0.0 mmol/kg of water if $\delta^{34}S$ of anhydrite is increased to 15.5‰. Using this heavier value of $\delta^{34}S$ of anhydrite, the CH_2O mass transfer is decreased from 5.00 to 0.87 mmol/kg of water, and the calculated value of $\delta^{13}C$ is only 1.23‰ lighter than the measured value.

Minor variations in many of the other modeling parameters can lead to almost identical calculated and measured

TABLE 9. Summary of Model Parameters and Carbon Isotope Results

Well Name	Flow Path	State	Well Number	$\delta^{34}S$, ‰ Anhydrite	$\delta^{13}C$, ‰ Organic Matter	$\delta^{13}C$, ‰ Dolomite	Ion Exchange X_{Mg}	$\delta^{13}C$, ‰ Calculated	$\delta^{13}C$, ‰ Measured	^{14}C, % modern Adjusted	^{14}C, % modern Measured	Apparent Age, Years
Hanover Flowing Well	F1	MT	8	17.10	−25.00	2.00	0.0	−5.84	−5.32	49.09	25.40	5446.
Vanek Warm Spring	F1	MT	9	17.10	−25.00	1.00	0.0	−5.19	−5.18	37.38	29.30	2013.
Landusky Spring	F1	MT	12	17.10	−25.00	0.00	0.0	−7.33	−7.46	5.66	...	...
Lodgepole Warm Spring	F1	MT	13	20.00	−25.00	2.00	0.0	−7.05	−7.04	5.45	28.00	modern
Sleeping Buffalo	F1	MT	18	21.90	−25.00	0.00	0.0	−3.22	−3.22	3.63	4.20	modern
Mcleod Warm Spring	F2	MT	6	17.00	−25.00	2.00	0.0	−10.15	−7.57	45.29	52.50	modern
Sumatra	F2	MT	17	15.00	−20.00	4.00	0.6	−3.72	−3.61	2.92	...	...
Keg Coulee	F2	MT	15	14.70	−20.00	5.00	1.0	−1.85	−1.68	1.66	1.00	4185.
Texaco C115X	F2	MT	16	14.70	−20.00	5.00	1.0	−3.19	...	0.15	...	...
Colstrip	F3	MT	21	14.00	−20.00	4.00	1.0	−2.64	−2.67	10.97	...	...
Sarpy Mine	F3	MT	19	13.00	−20.00	4.00	0.8	−2.41	−2.33	12.75	3.30	11173.
Moore	F3	MT	22	14.00	−20.00	6.70	1.0	−2.47	−2.40	2.43	1.60	3448.
Mysse Flowing Well	F3	MT	20	15.50	−25.00	4.00	0.0	−2.21	−2.34	12.30	0.80	22588.
HTH 1	F4	WY	14	10.30	−25.00	1.20	0.0	−6.66	−6.63	30.59	12.70	7266.
Ranch Creek	F4	MT	23	10.90	−25.00	0.90	0.0	−6.18	−6.17	30.61	10.00	9247.
Belle Creek	F4	MT	24	10.90	−25.00	1.00	0.0	−6.01	−6.02	28.72	9.50	9147.
Delzer 1	F4	SD	7	12.60	−27.00	0.00	0.0	−4.58	−4.60	1.99	4.60	modern
Delzer 2	F4	SD	8	13.60	−22.00	4.00	0.0	−2.60	−2.61	5.49	2.80	5560.
Conoco 175	F5	WY	11	7.90	−25.00	2.50	0.0	−6.29	−6.23	34.84	13.90	7597.
MKM	F5	WY	10	7.90	−20.00	2.00	0.0	−11.59	−4.66	33.08	2.60	21026.
Shidler	F5	WY	9	7.90	−25.00	2.00	0.0	−4.69	...	25.32	6.20	11631.
Conoco 44	F5	WY	8	8.30	−25.00	4.00	0.0	−5.10	−5.14	27.79	1.80	22624.
Seeley	F6	WY	19	9.50	−25.00	2.00	0.0	−8.86	−7.82	51.80	61.40	modern
Newcastle	F6	WY	19	9.50	−25.00	2.00	0.0	−8.77	−10.40	50.14	46.20	677.
Osage	F6	WY	17	9.50	−25.00	2.00	0.0	−9.33	−10.00	51.68	54.70	modern
Upton	F6	WY	15	9.50	−25.00	0.50	0.0	−8.19	−8.20	40.09	14.70	8294.
Devils Tower	F6	WY	13	9.50	−25.00	2.00	0.0	−7.79	−6.80	41.85	59.00	modern
Voss	F7	WY	20	10.00	−25.00	2.00	0.0	−10.17	−7.26	50.62	44.50	1065.
Self	F7	WY	22	10.00	−25.00	2.00	0.0	−9.28	−6.60	48.68	31.20	3677.
JBJ	F7	WY	18	10.00	−25.00	2.00	0.0	−9.92	−4.24	53.57	4.80	19942.
Evans Plunge	F7	SD	10	10.00	−25.00	0.00	0.0	−9.67	−9.70	38.04	28.50	2386.
Cascade Spring	F7	SD	9	9.00	−25.00	1.00	0.0	−9.08	−9.10	13.72	19.40	modern
McNenney	F8	SD	2	11.00	−25.00	2.00	0.0	−9.51	−11.50	53.02	79.60	modern
Kosken	F8	SD	1	12.40	−25.00	2.00	0.0	−6.14	−6.20	28.01	7.80	10568.
Philip	F8	SD	19	12.90	−25.00	2.00	0.0	−7.20	−7.20	21.49	2.80	16847.
Midland	F8	SD	24	13.70	−25.00	2.00	0.0	−6.18	−6.20	17.31	2.40	16332.
Murdo	F8	SD	25	13.30	−25.00	2.00	0.0	−5.52	−5.50	18.40	3.20	14461.
Hilltop Ranch	F8	SD	22	12.30	−25.00	2.00	0.0	−6.72	−6.63	15.35	4.60	9960.
Prince	F8	SD	26	14.30	−25.00	2.00	0.0	−4.73	−4.72	10.26	4.00	7784.
Hamilton	F8	SD	21	15.00	−25.00	2.00	0.0	−3.59	−3.50	12.01	2.40	13310.
Eagle Butte	F8	SD	23	15.80	−25.00	2.00	0.0	−2.35	−2.40	8.53	2.20	11203.
Dupree	F8	SD	20	16.00	−25.00	4.90	0.0	−2.07	−2.05	10.29	2.80	10763.

Parts per thousand, ‰. Adjusted ^{14}C assumes no radioactive decay. The states are designated by MT, Montana; SD, South Dakota; and WY, Wyoming.

values of $\delta^{13}C$. For example, if $\delta^{13}C$ of the dissolving dolomite is about 4.0‰ rather than 2.0‰ (case 6, Table 7), the calculated $\delta^{13}C$ value at the Mysse Flowing Well is similar to the measured value. Other factors, which separately or combined would result in similar calculated and measured values of $\delta^{13}C$, are (1) lighter $\delta^{34}S_{H_2S}$, (2) variation in $\delta^{13}C_{dolomite}$, (3) variation in $\delta^{13}C_{CH_2O}$, (4) $(Ca^{2+} + Mg^{2+})/Na^+$ ion exchange, and (5) minor uncertainties in the analytical data. It is apparent that an almost unlimited number of minor variations in reaction parameters can lead to close agreement in calculated and measured values of $\delta^{13}C$. Clearly then, the modeling results are not unique. But, through all of these changes, the overall mass transfer results are changed only slightly and are similar to those of case 5 (Table 7).

Of the three modeling alternatives investigated (Mg^{2+}/Na^+ ion exchange, methanogenesis, and variation in $\delta^{34}S$ anhydrite), only varying the value of $\delta^{34}S$ anhydrite minimizes the calculated CO_2 outgassing, indicating the expected closed system. In so doing, the calculated $\delta^{13}C$ value is heavier and similar to the measured values; and the calculated ^{14}C activity, corrected for reaction affects, is significantly larger than the measured value, which results in more reasonable age estimates.

On the basis of this analysis of modeling alternatives, the single most significant factor contributing to error in model-

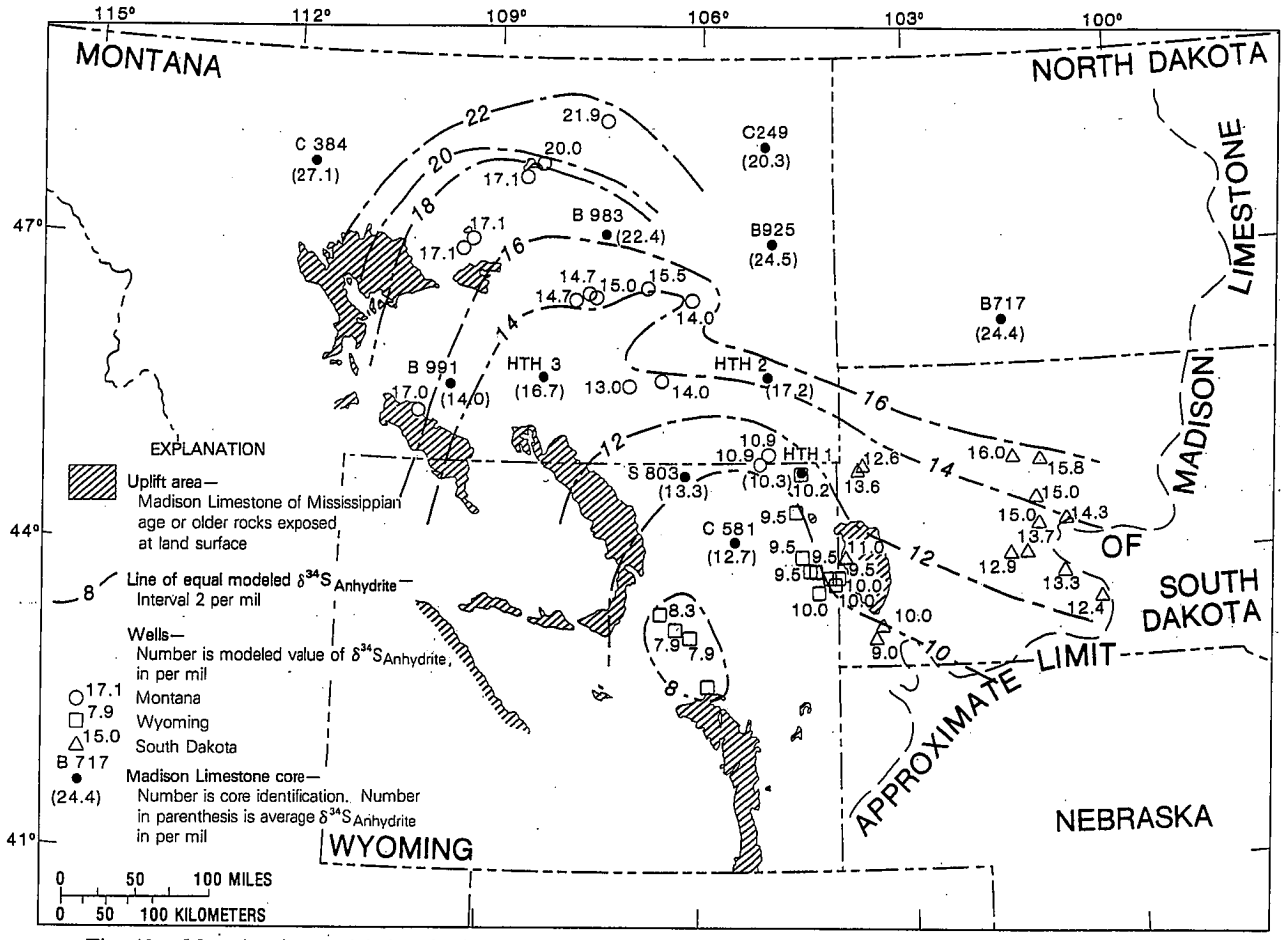

Fig. 13. Map showing modeled sulfur isotopic composition of Madison Limestone anhydrites (contours) compared with average values for anhydrites from Madison Limestone cores (solid circles). See Table 10.

ing results is uncertainty in the sulfur isotopic composition of dissolving anhydrite. Insufficient data are available to define the sulfur isotopic composition of anhydrite throughout the study area. Substantially more data are available on the sulfur isotopic composition of dissolved sulfate than for anhydrites in the Madison Limestone. Therefore the mass transfer models as described above have been solved and tested by comparing predicted values of $\delta^{34}S$ of anhydrite with the limited sulfur isotopic data for Madison anhydrites determined in this study.

Mass Transfer Results

The mass transfers of dolomite, calcite, anhydrite, CH_2O, FeOOH, pyrite, ion exchange, NaCl, KCl, and CO_2 gas, in millimoles per kilogram of water, are listed in Table 8 for 42

TABLE 10. Summary of Sulfur Isotope Data for Anhydrites in the Madison Limestone

Well	State	Location	Elevation*	Total Depth, ft	Interval Sampled	Average $\delta^{34}S$ Anhydrite, ‰	1 Standard Deviation, ‰	Number of Samples
S803	WY	57°N 78°W 11 NWSE	4165.	12215.	10991.–11160.	13.3	1.6	12
C581	WY	49°N 72°W 3 NWSE	4653.	10532.	10497.–10505.	12.7	0.4	2
HTH1	WY	47°N 65°W 15 NESE	3618.	6718.	2480.–2805.	10.2	4.4	6
HTH2	MT	1°N 54°E 18 SESE	2809.	10709.	6521.–7404.	17.2	3.1	6
B991	MT	1°N 17°E 22 NWSE	4632.	8580.	6752.–6807.	14.0	2.1	7
HTH3	MT	2°N 27°E 35 NWSE	3039.8	8462.8	4374.–5315.5	16.7	1.7	11
B983	MT	15°N 33°E 12	3335.	8133.	6675.–6687.	22.4	2.5	5
C384	MT	25°N 1°W 30 SESESE	3585.	4161.	3120.–3165.	27.1	1.8	2
B925	MT	16°N 54°E 17 SWNW	2532.	9990.	7765.	24.5	···	1
C249	MT	28°N 51°E 14 NWNW	2167.	6248.	5746.–5752.	20.3	0.9	4
B717	ND	134°N 87°W 16 NESESE	2273.	9470.	6030.–6071.	24.4	2.0	9

*Elevation of Kelly Bushing, in feet. One foot = 0.3048 m. The states are designated by MT, Montana; ND, North Dakota; and WY, Wyoming.

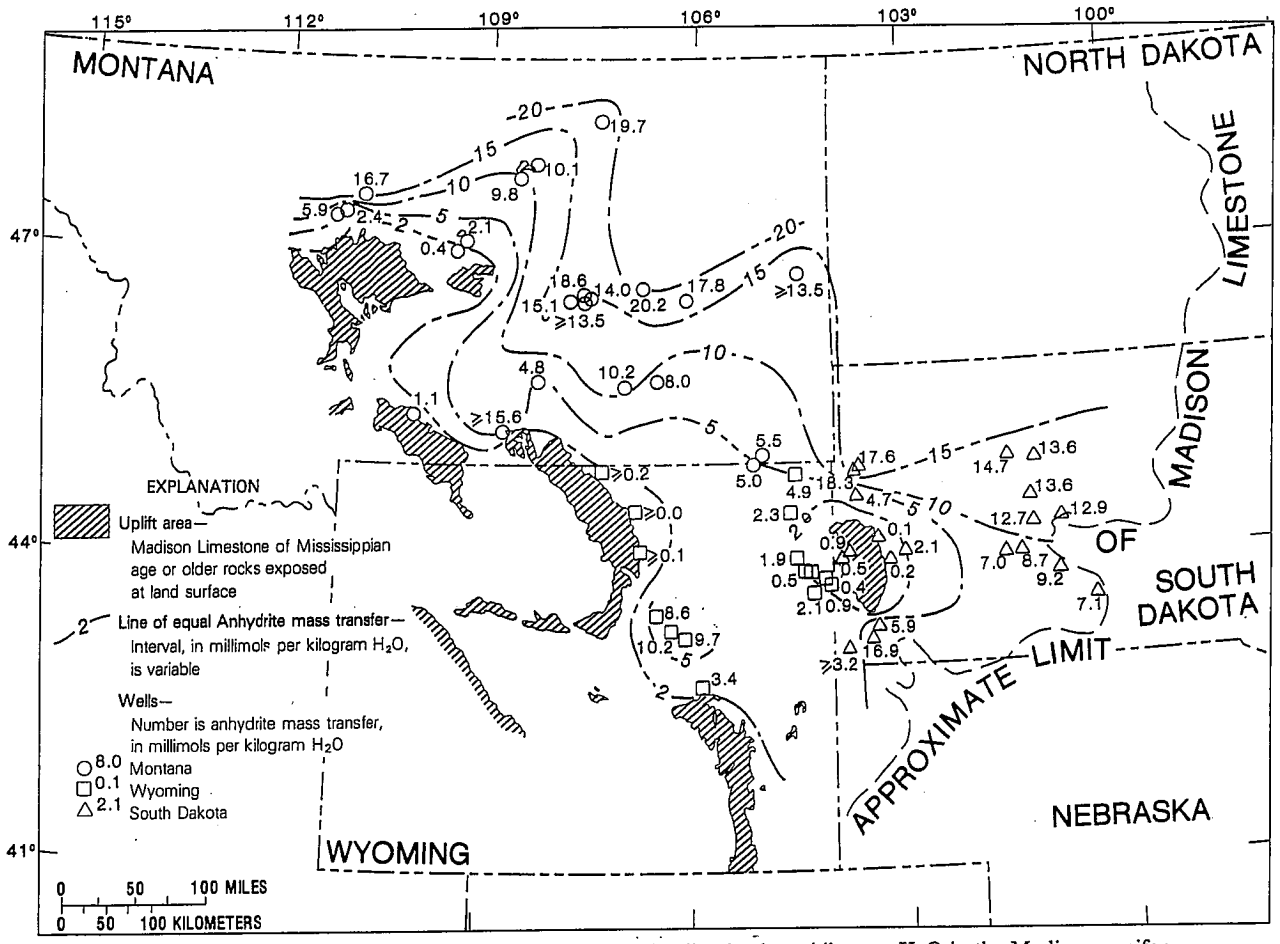

Fig. 14. Contours showing calculated amounts of anhydrite dissolved per kilogram H_2O in the Madison aquifer.

wells or springs in the Madison aquifer. The carbon and sulfur isotopic values used and the nature of the ion exchange reaction considered are summarized in Table 9. The calculated and measured $\delta^{13}C$ values are also compared in Table 9. The few examples of dissimilarity between calculated and measured values of $\delta^{13}C$ such as the Voss well (well 20 in Wyoming) usually correspond to wells near recharge areas where modeling is particularly sensitive to uncertainties in the starting $\delta^{13}C$ conditions.

Regional Pattern in Sulfur Isotopic Content of Anhydrite

The best estimates of the sulfur isotopic composition of dissolving anhydrite in the Madison aquifer are given in Table 9. The lightest values (about 8‰) are calculated in northeast Wyoming and eastward through the Black Hills (9–10‰). As shown in Figure 13, these model-derived values of $\delta^{34}S$ of anhydrite (contours) increase progressively to heavier values northward through east central Montana and to the northeast through western South Dakota. The lighter sulfur isotopic values for dissolved sulfate in northeastern Wyoming have previously been interpreted as indicating leakage of waters from overlying Pennsylvanian and Permian rocks in response to extensive pumpage from the Madison aquifer [*Busby et al.*, 1983]. This study suggests that the values in northeast Wyoming (Figure 13) are not necessarily anomalous but are, instead, part of a regional pattern in the Madison rocks.

As a means of testing the validity of the computed mass transfer models, the modeled sulfur isotopic composition of anhydrite was compared with measured values from all available cores from the Madison Limestone from Wyoming and Montana (10 cores) in the U.S. Geological Survey core library, Arvada, Colorado. No cores were available from South Dakota, however, one core was sampled from southwest North Dakota. A total of 65 samples of anhydrite from 11 Madison cores were analyzed for $\delta^{34}S$ of anhydrite and summarized in Table 10, showing the average value, standard deviation, and number of samples for each core. Many of the measurements of $\delta^{34}S$ of Madison anhydrites are within the range of marine Mississippian anhydrites [*Claypool et al.*, 1980], but some values as light as 10‰ were observed in northeast Wyoming and southeast Montana (Table 10). For example, the sulfur isotopic composition of 12 Madison anhydrite samples from core S803 in northeast Wyoming vary between 10.5 and 15.4‰ over an interval of 170 ft (51.8 m). In contrast, two Madison anhydrite samples from northwest Montana (core C384) have sulfur isotopic compositions of 28.4 and 25.8‰ at depths of 3120. and 3165 ft (951.0 and 964.7 m), respectively. The average measured rock values of $\delta^{34}S$ anhydrite are plotted on Figure 13 for comparison with the model-predicted sulfur isotopic content of anhydrite (contours). Although the agreement is not

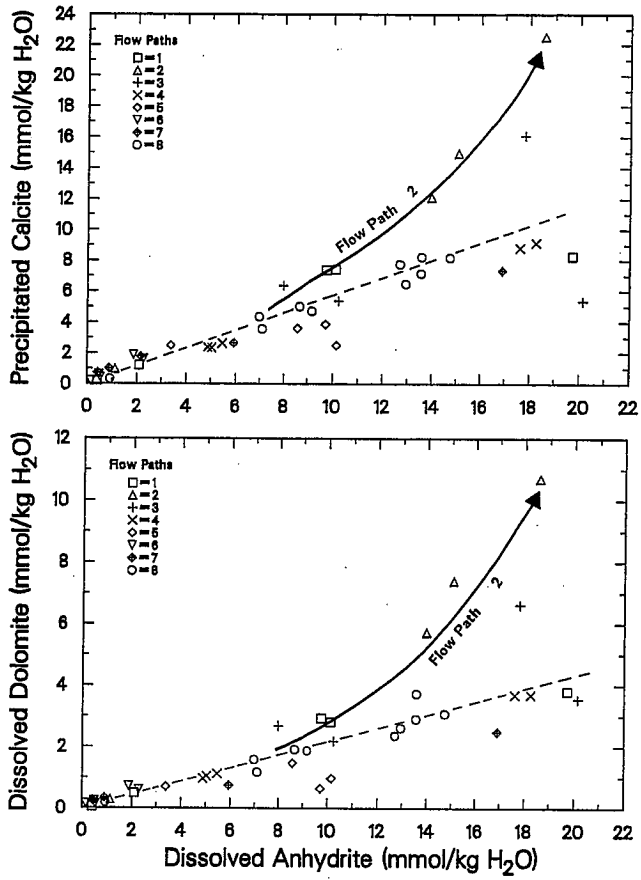

Fig. 15. Comparison of the calcite and dolomite mass transfers as a function of the amount of anhydrite dissolved. Two trends are evident primarily due to dedolomitization alone and dedolomitization combined with cation exchange reactions along flow path 2.

perfect, the measured values strongly support the modeled results. The broad pattern of light values of $\delta^{34}S$ of anhydrite in northeastern Wyoming increasing northeast, north, and northwest is also observed for the anhydrite samples. Most of the contours are within several per mil or better of the average measured anhydrite values. This comparison of modeled and measured sulfur isotopic content of anhydrite strongly supports the mass transfer models of Tables 8 and 9.

Several explanations can be offered for the differences in the observed sulfur isotope pattern in Madison rocks relative to established marine evaporite isotopic data [*Claypool et al.*, 1980]. The marine values may be modified by a terrigenous source of sulfur in northeast Wyoming and southwest South Dakota. According to *Sando* [1976*b*], land masses associated with the Transcontinental arch were emergent in southeast Wyoming and northeast Nebraska throughout the Mississippian and could have contributed light sulfur (presumably from pyrite) to deposits in northeastern Wyoming and southwestern South Dakota. The inferred trend to heavier sulfur isotopic composition of anhydrite northward through western South Dakota and through east central Montana may correspond to a decrease in deposition of terrigenous sulfur and more influence of a marine evaporite environment.

Alternatively, the observed pattern in sulfur isotopic content of anhydrite may be related to the primary deposition of organic matter in Madison sediment. Areas of greater deposition of organic matter would promote more extensive sulfate reduction and formation of isotopically lighter pyrite. Subsequent oxidation of pyrite in the sediment and evaporative precipitation of gypsum from mixed sulfur sources could lead to a direct correlation of isotopically lighter gypsum and organic matter.

Although the processes responsible for the sulfur isotopic pattern in the Madison anhydrites are unknown, the observed geographic distribution of $\delta^{34}S_{Anhydrite}$ is similar to the modeled values. We may therefore examine the mass transfer results (Table 8) with some confidence.

Summary of Chemical Reactions in the Madison Aquifer

The data in Table 8 indicate that dedolomitization, that is, dissolution of anhydrite and dolomite accompanied by precipitation of calcite, is the predominant process throughout the entire Madison aquifer. The extent to which this process proceeds appears to be a function of both distance of flow (age) and availability of anhydrite for reaction. The anhydrite mass transfer reaches about 20 mmol dissolved per kilogram of water along flow paths 1, 2, 3, and 4. Along flow path 8 the quantity of anhydrite dissolved increases northward normal to the eastward direction of flow, indicating that the increased availability of anhydrite northward toward the Williston basin is a more dominant cause of mass transfer than distance down the flow path. Other waters show little or no anhydrite dissolution (flow path 6), indicating low abundance of the mineral there and/or more rapid flow velocities. The importance of mineral availability for reaction is further demonstrated by the fact that some of the largest quantities of anhydrite dissolution are found in some of the youngest (flow paths 1 and 7) and oldest (flow paths 2 and 3) waters.

There are systematic variations in the regional pattern of anhydrite dissolution in the Madison aquifer, based on mass transfer calculations (Figure 14). The quantity of anhydrite dissolved is affected by distance from recharge areas; progressive increases in anhydrite dissolution occur with distance downgradient. This is most noticeable in the Madison aquifer surrounding the Black Hills. As expected for dedolomitization, the dolomite and calcite mass transfers are related to the anhydrite mass transfer. The data in Figure 15 indicate nearly linear relations between the mass transfers of anhydrite and dolomite and between anhydrite and calcite. The slopes of points in Figure 15 indicate that for flow paths 1–8, about 0.2 mmol/kg of water of dolomite dissolves for every millimole per kilogram of water of anhydrite dissolved, causing the precipitation of approximately 0.5 mmol/kg of water of calcite. These mass transfers are similar to those calculated from thermodynamic simulations of hypothetical dedolomitization using the geochemical mass transfer program PHREEQE [*Parkhurst et al.*, 1980].

The only significant exceptions to these determinations in the calcite and dolomite mass transfers are several wells along flow path 2 where substantial ion exchange was indicated. Here the dissolved-dolomite and precipitated-calcite mass transfers were larger than the trend shown for the rest of the Madison aquifer (Figure 15).

Regionally, the dolomite mass transfer (Figure 16) is similar to the anhydrite dissolution pattern (Figure 14). The quantity of dolomite dissolved also is found to increase normal to the direction of flow along flow path 8, in response

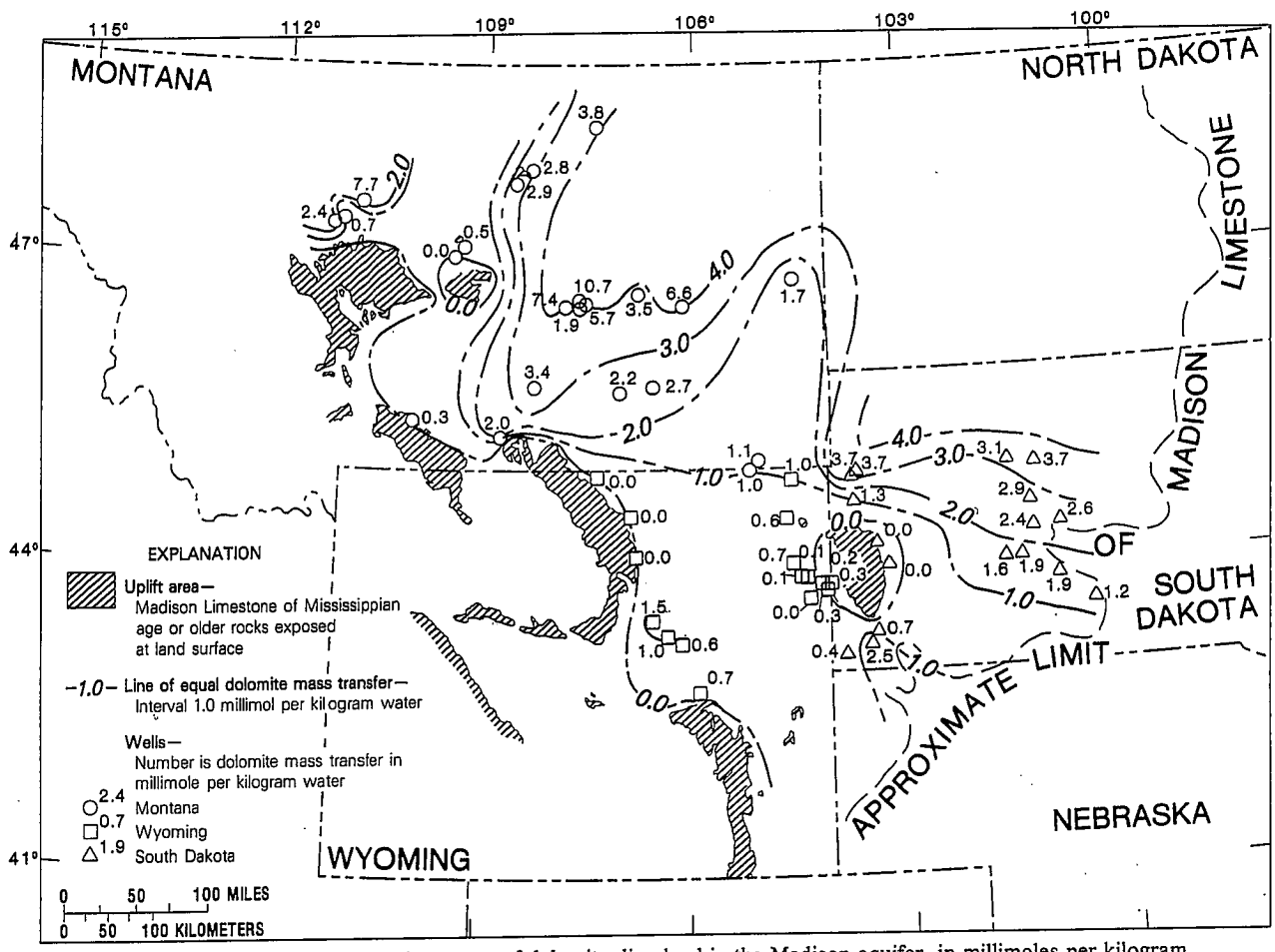

Fig. 16. Map showing calculated amounts of dolomite dissolved in the Madison aquifer, in millimoles per kilogram H_2O.

to the irreversible dissolution of anhydrite. Similar variations exist for the calcite mass transfer.

Occurring with the dedolomitization reaction is some organic matter oxidation, dissolution of ferric hydroxide, and pyrite authigenesis. Several flow paths, notably 5, 6, and 7, show little or no evidence of sulfate reduction, whereas water from wells in the Central Montana trough (flow paths 2 and 3) and points along flow paths 4 and 8 indicate greater sulfate reduction. For example, in water from wells in the Central Montana trough, the model indicates that as much as 4–8 mmol of organic matter are oxidized per kilogram of water. Elsewhere in the Madison aquifer most values for organic matter oxidation are less than 0.5 mmol/kg of water.

Accompanying the relatively substantial sulfate reduction along flow path 2 is small amounts of pyrite precipitation and dissolution of FeOOH. This probably reflects lesser quantities of detrital FeOOH deposited in the Central Montana trough. Here most of the reduced sulfur species remain in solution. Elsewhere in the Madison aquifer, sulfate reduction accompanies proportionately larger quantities of FeOOH and greater pyrite mass transfer.

Halite dissolution and cation exchange are significant only in limited parts of Montana and Wyoming, presumably influenced by the availability of halite and clay minerals there.

Cation exchange occurs along flow paths 1, 2, 3, 5, and 8 but is significant only along flow paths 2 and 3. There are systematic variations in the degree of cation exchange, increasing significantly northeastward from central Montana. Dissolution of halite is very important along flow paths 2, 3, and 5 and minor to absent throughout the rest of the Madison aquifer. Halite dissolution contributes about 1 mmol chloride per kilogram of water or less to most of the waters of the Madison aquifer, except in east central Montana, where; very abruptly, water from most wells has more than 50 mmol of NaCl dissolved per kilogram of water. The addition of a potassium chloride phase always accompanies halite dissolution but at mass transfer levels of only 5% that of halite.

As discussed earlier, the CO_2 gas mass transfer is expected to be near zero, and the magnitude of this term has been used as a criterion in refining the mass balance models. For most of the wells modeled the CO_2 gas mass transfer is 0.0 ± 0.5 mmol/kg of water, which, taking into account the modeling assumptions, reasonably supports the conclusion of a closed system. Other wells show larger CO_2 gas mass transfers that are attributed to uncertainties in the composition of recharge waters or other errors in the modeling parameters.

CARBON 14 AGE OF GROUNDWATER IN THE MADISON AQUIFER

On the basis of the reaction models of Tables 8 and 9, adjusted ^{14}C ages for many of the waters from the Madison aquifer have been computed. The primary concerns in the

TABLE 11. Comparison of Calculated Prenuclear Detonation ^{14}C Values, A_0 for Recharge Waters from the Madison Aquifer (Percent Modern)

Flow Path	Modified Tamers This Work	Tamers	Ingerson-Pearson	Fontes-Garnier	Eichinger
1	52.9	53.1	34.7	16.1	32.7
2	56.4	52.3	63.3	74.8	59.5
3	52.3	53.5	43.4	33.3	40.7
4	54.1	54.6	47.4	39.9	44.0
5	55.5	55.0	62.0	69.1	57.3
6	54.6	54.3	54.4	54.6	50.6
7	55.2	55.7	60.9	66.6	56.3
8	57.4	55.1	55.9	56.8	51.7

Fractionation factors are those of the original sources (see text for references). Water chemistry and isotope data for the recharge waters are given in Tables 4 and 5. Calculation of A_0 assumes $\delta^{13}C_{CO_2} = -20‰$, $\delta^{13}C_{carbonates} = 3‰$, $^{14}C_{CO_2} = 100\%$, and $^{14}C_{carbonates} = 0\%$. See Tables 8 and 9 for further reaction adjustments to A_0 in defining A_{nd}.

^{14}C dating analysis are (1) reliability of the estimated prenuclear detonation ^{14}C content in the recharge areas, A_0, and (2) the accuracy of the derived mass transfer and reaction corrections in adjusting the estimated recharge value for reaction effects along the flow path to the final well. This latter correction defines A_{nd}, the ^{14}C content expected at the final well if no radioactive decay occurred.

Calculation of A_0 and A_{nd}

The prenuclear detonation ^{14}C content of the recharge waters was estimated using a modified Tamers calculation [*Tamers*, 1967, 1975; *Tamers and Scharpenseel*, 1970] which included a chemical mass balance for calcite, dolomite, anhydrite, and CO_2 gas in the recharge water, and assumed a 100% modern source of CO_2 gas and 0% modern carbonate mineral sources. The modeled ^{14}C contents of the recharge waters (prenuclear detonation), A_0, for flow paths 1–8 are 52.68, 56.37, 52.34, 53.88, 55.63, 55.64, 55.29, and 57.39% modern, respectively. These values were further adjusted for the modeled mass transfer to the final well in a calculation based on the equations of *Wigley et al.* [1978, 1979], similar to equations used to estimate $\delta^{13}C$ in the final water. The ^{14}C values, adjusted for reaction but not radioactive decay, A_{nd}, were used with the measured ^{14}C content of the final water, A, in estimating water age, according to the radioactive decay equation

$$\Delta t = \frac{5730}{\ln 2} \ln\left(\frac{A_{nd}}{A}\right) \tag{32}$$

where Δt is the travel time, in years, since the groundwater became isolated from the soil ^{14}C reservoir [*Wigley et al.*, 1978; *Wigley and Muller*, 1981]. Values of A_{nd} and A (in percent modern) are given in Table 9 along with the calculated travel time. For nine of the waters, A_{nd} was smaller than the measured ^{14}C content (Table 9), indicating possibly mixed waters containing a modern component mixed with older water and/or uncertainties in estimating A_{nd}. Estimation of A_{nd} is carried out in two steps: (1) estimation of A_0 in the recharge waters, and (2) adjustment of A_0 for reaction effects along the flow path to the final well, which defines A_{nd}.

In estimating A_0 we have assumed a closed system evolution of soil-derived CO_2 (100% modern) reacting with ^{14}C-depleted limestones and dolostones in the recharge areas. A modified Tamers model correcting dissolved Ca for (minor) anhydrite sources in the recharge areas was used. As such, A_0 is systematically 50–55% modern for the eight recharge areas considered. *Deines et al.* [1974] demonstrated closed system evolution for carbonate waters in Pennsylvania. *Reardon et al.* [1980] found open system conditions in shallow sandy calcareous soil (≈2 m), but for unsaturated zone depths greater than 5 m some degree of closed system isotopic evolution was evident. Several other models have been proposed for estimating A_0 [*Ingerson and Pearson*, 1964; *Tamers*, 1967, 1975); *Tamers and Scharpenseel*, 1970; *Mook*, 1972, 1976, 1980; *Fontes and Garnier*, 1979; *Eichinger*, 1983], all requiring various assumptions about the physical nature of the recharge process. The reader is referred to *Fontes and Garnier* [1979] and the original sources for explanation of the various models considered here for estimating A_0. Table 11 summarizes values of A_0 estimated for the recharge waters for each flow path based on the models of *Tamers* [1967, 1975], *Ingerson and Pearson* [1964], *Fontes and Garnier* [1979], and *Eichinger* [1983] and compared with the modified Tamers model used in this study. In the calculations of Table 11, $\delta^{13}C_{CO_2} = -20‰$, $\delta^{13}C_{carbonates} = 3‰$, $^{14}C_{CO_2} = 100\%$ modern, and $^{14}C_{carbonates} = 0\%$ modern. Fractionation factors were those used in the original sources. Values of A_0, based on the model of *Mook* [1980] are not included in Table 11 because they vary widely and are unrealistic, reflecting, at least in part, lack of appropriate chemical and isotopic data in the unsaturated zone of the recharge areas. For the remaining models the results of Table 11 show some degree of consistency, supporting values of A_0 in the recharge waters near 50% modern. The range of uncertainty in estimated A_0 values leads to uncertainties of several thousand years in ^{14}C ages. Further uncertainties in estimating the ^{14}C age of Madison waters depend on the validity of the reaction corrections applied to A_0 in estimating A_{nd}.

The maximum error in ^{14}C age dating of waters from the Madison aquifer follows from uncertainty in A_0 and is considered to be approximately one half-life (5730 years). That is, if the waters evolved under open system conditions, the A_0 value of the recharge water at the point on the flow path where the water became isolated from the soil ^{14}C reservoir would be approximately 102% modern (see, for

example, *Mook* [1980]) rather than the closed system case considered here. Recharge waters partially open to the ^{14}C reservoir would have intermediate A_0 values, between approximately 50 and 102% modern, and uncertainties in age relative to the closed system model of 0–5700 years.

We are unable to determine whether the waters from the Madison aquifer actually evolved primarily as open or closed systems at the time of recharge, but for consistency in comparing results, all waters have been treated similarly using the modified Tamers model. As a result, Madison waters could be consistently as much as 5700 years older than reported in Table 9 if recharge waters formed under open system conditions.

Regarding uncertainties in the mass transfer and reaction corrections, the ^{14}C ages in Table 9 may be used with varying degrees of confidence. The most reliable ages were determined for waters that have undergone only the dedolomitization reaction. The tritium data (Table 5) indicate that some waters, particularly those near recharge areas, may be partially contaminated with modern ^{14}C.

As discussed earlier, the mass transfer and resulting adjusted ^{14}C ages are particularly sensitive to the sulfur isotopic composition of dissolving anhydrite and to the extent to which a magnesium sink, such as Mg^{2+}/Na^{+} exchange, is present. Through the modeling process, lighter values of $\delta^{34}S$ of anhydrite cause calculation of more sulfate reduction and thus oxidation of more (^{14}C-depleted) organic matter. This additional dilution of the ^{14}C leads to smaller calculated (reaction-corrected) ^{14}C values and younger adjusted ages. Similarly, an additional sink for magnesium causes calculation of more extensive dissolution of ^{14}C depleted dolomite, which again results in younger adjusted ages. Consequently, some of the more uncertain ^{14}C ages are those along flow paths 2 and 3 where extensive sulfate reduction and Mg^{2+}/Na^{+} exchange have been included in the reaction models.

The importance of the reaction model corrections to ^{14}C dating of the waters, however, cannot be overlooked. The variation in the measured ^{14}C content of all wells and springs along flow paths 1–8, as a function of the computed anhydrite mass transfer, is shown in Figure 17. An abrupt and systematic decrease is seen in the ^{14}C content as anhydrite dissolves. This decrease is, in part, due to radioactive decay because the older waters generally have greater concentrations of dissolved anhydrite. However, the measured ^{14}C values are further decreased by dilution from dissolution of dolomite and oxidation of CH_2O as well as incorporation of ^{14}C in secondary calcite precipitated via the dedolomitization reaction.

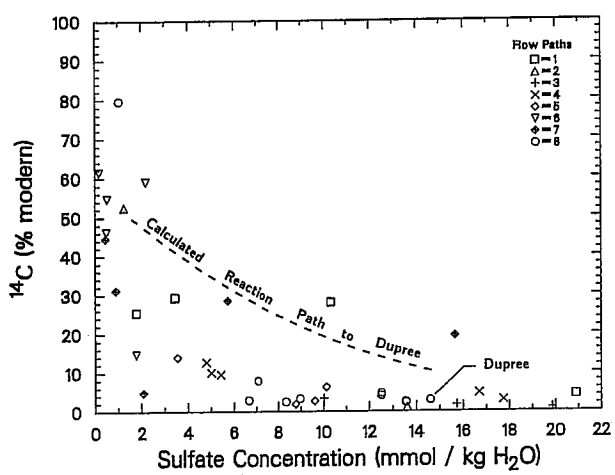

Fig. 17. Comparison of measured ^{14}C content as a function of dissolved sulfate content. The dashed curve shows the path of adjusted ^{14}C content due to chemical reaction at the Dupree well.

Examples

Taking the well at Sleeping Buffalo (well 18 in Montana) as an example, the measured ^{14}C content of 4.20% modern is equivalent to an age of 26,000 years if no corrections for reaction are made; that is, the unadjusted age is equal to (5730/ln 2) ln (100/measured percent modern). Correcting for an assumed congruent dissolution of carbonate minerals to the final well, the model of *Ingerson and Pearson* [1964] (see also *Pearson and White* [1967]) results in an age for water from the Sleeping Buffalo well of about 17,000–20,000 years (assuming $\delta^{13}C$ of CO_2 gas is −9.44‰ and $\delta^{13}C$ of dolomite is 0 and 3.1‰, respectively; see above for mass balance estimates of ^{13}C values of soil gas CO_2). When the data are corrected for incongruent dissolution of carbonate minerals and sulfate reduction using the Rayleigh distillation equations of *Wigley et al.* [1978, 1979] and the final calculated mass transfer (Table 8), the water at Sleeping Buffalo is found to be approximately modern (probably less than 5000 years old). On the basis of the proximity of the Sleeping Buffalo well to the recharge area and the digital simulation results of *Downey* [1984] a young age is expected. Clearly, large errors in ^{14}C age dating can result if adjustments are applied indiscriminately to ^{14}C data without proper evaluation of chemical reaction effects.

Not all examples are as extreme as the water from the Sleeping Buffalo well. For example, the Mysse well (well 20 in Montana) has an unadjusted ^{14}C age of 40,000 years. By correcting for an assumed congruent reaction (applying the model of *Ingerson and Pearson* [1964] and *Pearson and White* [1967] to the Mysse water) the ^{14}C age is decreased to 30,800 years ($\delta^{13}C_{dolomite}$ = 3.1‰, $\delta^{13}C_{CO_2}$ = −13.36‰, see above for mass balance estimates of soil gas ^{13}C), which compares with 22,500 years (Table 9), based on the incongruent mass transfer (Table 8) and equations of *Wigley et al.* [1978, 1979].

In an earlier publication [*Back et al.*, 1983], several waters from the Madison aquifer in the vicinity of the Black Hills were ^{14}C dated by correcting for incongruent dissolution only (the dedolomitization reaction). This led to a ^{14}C age at the Philip well (well 19 in South Dakota), for example, of 20,000 years. When both the dedolomitization reactions and sulfate reduction were evaluated, the water from the Philip well was found to be about 3000 years younger, with an adjusted age of about 16,800 years (Table 9).

The curve in Figure 17 shows the adjusted ^{14}C content, A_{nd}, along a hypothetical reaction path to the Dupree well (well 20 in South Dakota). The adjusted ^{14}C content was calculated using the computed mass transfer to the Dupree well, assuming constant relative rates of reaction in proportion to the computed mass transfer. Although the curve in Figure 17 is based on the mass transfer to the Dupree well, similar variation is expected for other waters that are affected predominantly by the dedolomitization reaction. Modern waters will have measured ^{14}C contents similar to

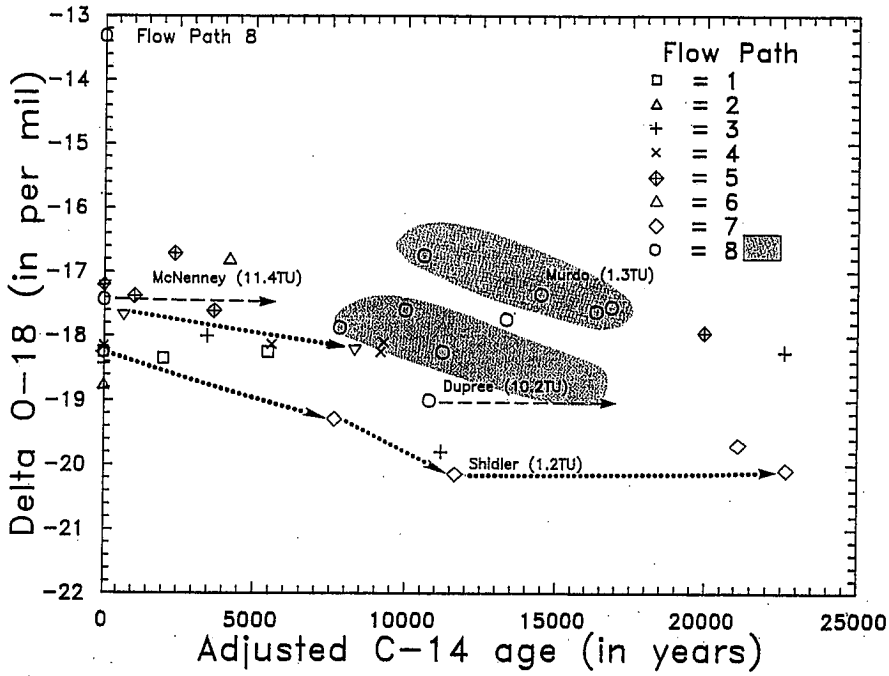

Fig. 18. Variation in $\delta^{18}O$ of waters from the Madison aquifer as a function of adjusted ^{14}C age. The upper and lower shaded zones show two parallel trends to lighter $\delta^{18}O$ values with increasing age for waters on flow path 8. Waters from the upper shaded zone originate primarily along the northern and northwestern flanks of the Black Hills, and those in the lower shaded zone were recharged primarily along the south and southwest portions of the Black Hills (see text). The horizontal dashed lines indicate expected older ages for waters from the Madison aquifer at McNenny and Dupree, if corrected for contamination by modern water, as suggested by the measured tritium content (TU). The dotted curves show observed trends to isotopically lighter $\delta^{18}O$ values of waters on flow paths 5 and 6.

those along the curve, as a function of anhydrite dissolution. Older waters have ^{14}C values that plot below the curve. The ratio of the adjusted and measured ^{14}C at the Dupree well results in an estimated age of about 10,800 years. This is a minimum estimate of water age because, in this case, the Dupree water is contaminated with tritium (10.8 TU), indicating a mixed water. Judging from its relation in the flow system to other wells in the Madison aquifer, the Madison aquifer at Dupree is possibly some 5000 years older than the adjusted age indicates. Waters with large anhydrite mass transfers and relatively large values of measured ^{14}C such as Cascade Spring and the Evans Plunge Spring are interpreted to be either virtually modern or possibly mixtures of older waters which have been contaminated in part with soil gas containing modern CO_2. Unfortunately, no tritium data are available for these two waters to check for contamination. Waters from Lodgepole Warm Spring and McNenney are contaminated with tritium (31.8 and 11.4 TU, respectively, Table 5), indicating a modern water or mixtures of older waters and modern sources.

Variations in $\delta^{18}O$ With Adjusted ^{14}C Age

Several flow paths suggest trends to lighter stable isotopic compositions of water with increasing adjusted ^{14}C age, as seen in the $\delta^{18}O$ content (Figure 18). The average value of $\delta^{18}O$ of the recharge water for each flow path (zero age) is shown on Figure 18, and except for the well at McNenney (flow path 8), waters that appear to be modern after adjustment of ^{14}C for reaction effects are omitted. Wells containing a portion of tritiated water (>1 TU) are identified on Figure 18. The portion of these tritiated waters from the Madison aquifer is expected to be shifted to greater age, as the arrows indicate for the wells at McNenney and Dupree (Figure 18).

Water on flow path 5 which flows into the Powder River Basin in NE Wyoming shows a decrease of about 2‰ in $\delta^{18}O$ over the past 11,000 years (Figure 18). Water along flow path 6, originating on the west flank of the Black Hills and flowing north and northeast and joining flow path 4, shows a decrease of about 1‰ in $\delta^{18}O$ over approximately the past 8000 years (Figure 18).

Back et al. [1983] noted that recharge waters on the eastern flank of the Black Hills were isotopically heavier than those on the western side of the Black Hills. They attributed this difference (of nearly 4‰) to differences in storm tracks, the eastern flank of the Black Hills receiving a greater proportion of isotopically heavier water originating in the Gulf of Mexico. If waters on flow path 8 are recharged primarily along the eastern flank of the Black Hills, the older Madison waters in western South Dakota are shifted some −4‰ in $\delta^{18}O$ relative to modern recharge. However, as the flow vector map (Figure 5) suggests, waters on flow path 8 in western South Dakota originate from three sources. Water recharged on the western side of the Black Hills diverts to the north and south before flowing eastward into western South Dakota, where it mixes with water recharged on the eastern side of the Black Hills.

Two parallel trends are evident in the $\delta^{18}O$ data for the waters sampled on flow path 8 in western South Dakota (Figure 18). The four southernmost wells on flow path 8 (Kosken, Murdo, Philip, and Midland) are probably a mixture of water originating on the eastern and south-

southwestern sides of the Black Hills. Waters from the four northern wells on flow path 8 in western South Dakota (Prince, Hilltop Ranch, Eagle Butte, and Dupree) probably contain a greater proportion of water originating on the west-northwest side of the Black Hills and portions of water on flow path 4 (Figure 5). As a result, two separate but parallel groupings of wells in western South Dakota suggest trends to lighter $\delta^{18}O$ values with increasing adjusted ages of 8000–16,000 years (Figure 18). Water from the well at Hamilton (well 21, MT, flow path 8) plots midway between these two groups (Figure 18) and probably represents a mixture of all three waters.

Although several flow paths of the Madison aquifer suggest (presumably paleoclimatic) trends in the stable isotopic composition of recharge water with age, no trends in $\delta^{18}O$ are evident for the relatively younger waters on flow paths 1, 4, and 7. The water at Keg Coulee is actually some 2‰ heavier in $\delta^{18}O$ than modern recharge on flow path 2, possibly due to uncertainty in identification of recharge area for flow path 2 (Figure 5). Water between Moore (3500 years) and Sarpy Mine (11,000 years) on flow path 3 shows a decrease of nearly 2‰ in $\delta^{18}O$ consistent with similar trends observed on flow paths 5 and 8, however, this trend is not observed consistently throughout flow path 3. Further interpretation of the stable isotopic data is not possible without more details on the nature of the flow system, identification of recharge areas, and effects of mixing due to, for example, fracture flow conditions.

Estimation of Regional Hydraulic Conductivity

The regional hydraulic conductivity ($K_{^{14}C}$), in feet per second, was estimated from the adjusted ^{14}C ages. The flow lines used in this analysis were selected to be orthogonal to the potentiometric surface, with the exception of those in southern Wyoming where the flow lines were selected to follow the dissolved-solids gradient.

The calculation of regional hydraulic conductivity ($K_{^{14}C}$), based on the work of *Hanshaw et al.* [1964], uses the Darcy equation in the form

$$K = \frac{V\Theta}{\Delta h/\Delta L} \tag{33}$$

where K is the hydraulic conductivity, in feet per second; V is the average linear flow velocity, in feet per second; Θ is the effective porosity, dimensionless; Δh is the change in hydraulic head, in feet; and ΔL is the length of the flow path, in feet (1 foot = 0.3048 m).

Most of the available measurements of hydraulic properties of the Madison aquifer are summarized by *Cooley et al.* [1986]. Reported horizontal hydraulic conductivities, based on measured hydraulic properties, range from 1.0×10^{-4} ft/s in the Newcastle area of Wyoming to 2.8×10^{-7} ft/s in southeast Montana and 8.7×10^{-6} ft/s in east central Wyoming, though another reported value in southeast Montana is 7.1×10^{-5} ft/s [*Cooley et al.*, 1986]. For comparison with the regional hydraulic conductivity values, based on the adjusted ^{14}C data $K_{^{14}C}$, the regional hydraulic conductivity K_{Hyd} was calculated by dividing the transmissivity obtained from either aquifer tests or model simulation by the aquifer thickness, using data from *Downey* [1984, Figure 30]. Both the thickness and transmissivities were distance weighted averages along the length of the flow path.

Substituting into (33) for the average ^{14}C velocity,

$$K_{^{14}C} = \frac{\Delta L^2 \Theta}{\Delta t \Delta h} \tag{34}$$

where t is water age in seconds. The values for hydraulic conductivities ($K_{^{14}C}$) derived from (34) assume an average effective porosity of 3% [*Busby et al.*, 1990] and are compared to the horizontal hydraulic conductivities (K_{Hyd}) derived from analysis of the transmissivity maps described by *Downey* [1984] in Table 12. Uncertainties in the evaluation of hydraulic conductivities from ^{14}C water ages along hydrologic flow paths were considered by *Konikow* [1985], *Back et al.* [1985], and *Busby et al.* [1990]. *Konikow* [1985] concluded that the average effective porosity in the Madison aquifer probably lies between 3.5 and 7.5%. *Miller* [1976] reports laboratory measurements of porosity for the Madison Limestone in a well in southeast Montana that vary from about 1 to 20%, with many values in the vicinity of 5–6%. A doubling of the estimated effective porosity for the Madison Limestone would double the calculated hydraulic conductivities ($K_{^{14}C}$) and slightly improve the agreement with hydraulic conductivities, based on digital simulation (Figure 19).

The values of hydraulic conductivity derived from digital simulation and ^{14}C ages of groundwater are within the range of values typical of carbonate aquifer systems and show a consistency between the two sets of data, with the worst case being within a factor of 8. The $K_{^{14}C}$ values range from 1.1×10^{-6} ft/s to 29.9×10^{-6} ft/s, a factor of about 27 and reasonable for carbonate aquifers. The larger values at Dupree, Eagle Butte, Kosken, and Prince wells in South Dakota along flow path 8 are near a zone of greater permeability postulated by *Downey* [1986]. The smallest values of regional hydraulic conductivity ($K_{^{14}C}$), calculated on the basis of ^{14}C age, are found along flow path 5 in Wyoming, an area expected to have received detrital material from the Transcontinental arch during deposition [*Sando*, 1976*b*].

Sources of error in hydraulic conductivity values derived from ^{14}C data include uncertainties in hydraulic head change, length of flow path, effective porosity, and water age. Inspection of (34) shows that on a relative basis, errors in the length of flow path will be squared in comparison to uncertainties in the other parameters. If, for example, we assign uncertainties of 20% to length of flow path, hydraulic head change, and water age and an uncertainty of 70% to effective porosity, (34) indicates a maximum range of $K_{^{14}C}$ values that could be larger by a factor of 4 or smaller by a factor of 8. This range of uncertainties is similar to the range of differences observed between K_{Hyd} and $K_{^{14}C}$, as shown in the histogram of Figure 19.

Apparent Reaction Rates

The calculated mineral mass transfer (Table 8) may be combined with the adjusted ^{14}C ages (Table 9) to determine apparent rates of reaction. The rates calculated from these data are termed "apparent" because they have not been normalized to unit surface area and are averaged over long flow paths. Such rates do not account for the likely heterogeneity in mineral abundance and mineral surface area in contact with the groundwater over the length of the flow path. Some of the uncertainties associated with correcting field-derived apparent rates of reaction to unit surface area

TABLE 12. Comparison of Horizontal Hydraulic Conductivity Values Calculated From Groundwater Velocities on the Basis of Adjusted Carbon 14 Ages With Values Calculated From Digital Simulation [*Downey*, 1984]

Well	Well Number	State	Flow Path	Change in Hydraulic Head, ft	Horizontal Flow Length, mi	Hydraulic Gradient $\times 10^{-3}$	Carbon 14 Age $\times 10^{-3}$, years	Carbon 14 Velocity, ft/yr	Hydraulic Conductivity Values: Carbon 14 Age $\times 10^{-6}$, ft/s	Hydraulic Conductivity Values: Digital Simulation $\times 10^{-6}$, ft/s
Keg Coulee	15	MT	2	3002	143	3.98	23.0	32.8	7.85	6.07
Sarpy Mine	19	MT	3	3002	174	3.27	11.2	82.0	23.86	3.29
Mysse Well	20	MT	3	3097	99	5.92	22.5	23.2	3.73	3.48
HTH 1	14	WY	4	1260	40	5.97	7.3	28.9	4.61	7.81
Ranch Creek	23	MT	4	1260	68	3.51	9.2	39.0	10.58	7.09
Belle Creek	24	MT	4	1260	68	3.51	9.1	39.4	10.69	7.45
Delzer 2	8	SD	4	1499	28	10.14	5.6	26.4	2.48	6.96
Conoco 175	11	WY	5	1631	43	7.02	7.6	29.9	4.05	7.14
MKM	10	WY	5	1001	62	3.06	21.0	15.6	4.85	4.26
Shidler	9	WY	5	1001	50	3.79	11.6	22.8	5.71	4.36
Conoco 44	8	WY	5	1001	31	6.12	22.6	7.2	1.12	4.69
Upton	15	WY	6	1125	25	8.52	8.3	15.9	1.78	6.20
Evans Plunge	10	SD	7	1499	31	9.16	2.4	68.2	7.08	7.15
Kosken	1	SD	8	2539	174	2.76	10.6	86.7	29.87	5.45
Philip	19	SD	8	2241	106	4.00	16.8	33.3	7.92	3.54
Midland	24	SD	8	2342	124	3.58	16.3	40.2	10.67	6.23
Murdo	25	SD	8	2500	130	3.64	14.5	47.3	12.38	4.56
Hilltop Ranch	22	SD	8	2500	106	4.47	10.0	56.0	11.91	5.18
Prince	26	SD	8	2552	124	3.90	7.8	83.9	20.47	4.26
Hamilton	21	SD	8	2434	106	4.35	13.3	42.1	9.20	3.54
Eagle Butte	23	SD	8	2500	149	3.18	11.2	70.2	21.0	5.74
Dupree	20	SD	8	2402	124	3.67	10.8	60.6	15.71	4.00

A porosity of 3% is assumed. One foot = 0.3048 m. One mile = 1.609 km. The states are designated by MT, Montana; SD, South Dakota; and WY, Wyoming.

were considered by *Paces* [1973, 1983]. The apparent rates used here are expressed as micromoles reacted per liter of ground water per year (μmol/L/yr) and serve as the basis for preliminary comparisons of apparent rates of geochemical reactions throughout the Madison aquifer. These rates potentially have transfer value to other aquifer systems of similar physical and chemical characteristics. Examined here are the apparent rates of the dedolomitization reaction and of bacterial oxidation of organic matter.

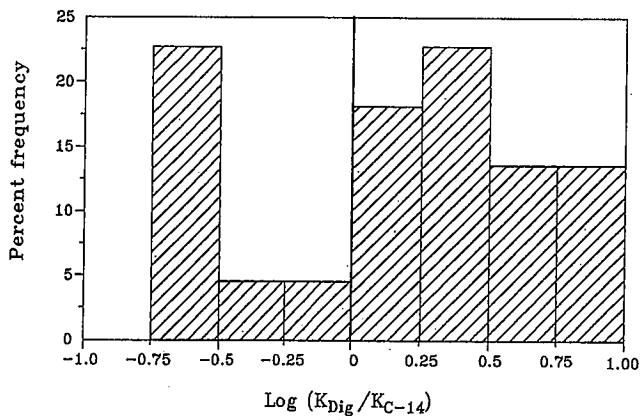

Fig. 19. Histogram showing comparison of horizontal hydraulic conductivities, based on digital simulation [*Downey*, 1984] and calculated from application of Darcy's law to adjusted ^{14}C ages of waters from the Madison aquifer.

Dedolomitization

As discussed earlier, the predominant reaction throughout the Madison aquifer is dedolomitization. Figure 15 shows that the actual mass transfers of dolomite and calcite are related by a factor of approximately 2 throughout most of the Madison aquifer where reactions other than dedolomitizations are not particularly significant. Such a relation is expected from the overall stoichiometry of the dedolomitization reaction

$$CaMg(CO_3)_2 + CaSO_4 \rightarrow 2CaCO_3 + MgSO_4(aq) \quad (35)$$

that is, in a groundwater system at equilibrium with calcite, dolomite, and anhydrite, 2 mol of calcite are precipitated and 1 mol of dolomite dissolved for every mole of $CaSO_4$ irreversibly added to solution. In most of the Madison aquifer the waters appear to be saturated with calcite and dolomite but are undersaturated with anhydrite (Figure 6). Thus the anhydrite mass transfer will increase out of proportion to the dolomite and calcite mass transfers (Figure 15). The occurrence of other reactions such as cation exchange and organic matter oxidation also cause deviations from the overall stoichiometry of reaction (35).

In determining the apparent rates of reactions the mass transfers of calcite, dolomite, and anhydrite are divided by water age, therefore we can expect a similar relationship in rate as that observed for the mass transfer. Excluding results for the Moore well which yields apparent rates tenfold those found elsewhere in the Madison aquifer, the remaining 28

wells for which we have adjusted ^{14}C ages (Table 9) indicate that the average rate of calcite precipitation is 0.59 μmol/L/yr, which is slightly more than twofold the average dolomite dissolution rate, 0.24 μmol/L/yr. The reaction rates for all wells span several orders of magnitude for calcite precipitation and dolomite dissolution: 0.037–4.67 μmol calcite precipitated per liter per year and 0.007–1.92 μmol dolomite dissolved per liter per year. The rate of anhydrite dissolution averages 0.95 μmol/L/yr and varies from 0.073 to 5.17 μmol/L/yr.

Although the dolomite and calcite mass transfers are dependent on the anhydrite mass transfer, we are justified in using the variation in the anhydrite mass transfer and dissolution rate to interpret differences in abundance (availability) of anhydrite along different flow paths in the Madison aquifer. Some of the fastest apparent rates of anhydrite dissolution are found on flow paths 2 and 3 in the Central Montana trough (3.6 μmol/L/yr at Keg Coulee, flow path 2, and 5.2 μmol/L/yr at Moore, flow path 3) and at the ends of flow paths 4 and 7 at Delzer 2 (3.3 μmol/L/yr) and Evans Plunge (2.5 μmol/L/yr), which are located north and south of the Black Hills, respectively. Some of the slower apparent rates of anhydrite dissolution occur in the immediate vicinity of the Black Hills where most of the anhydrite has been removed by dissolution. Further evidence of the influence of mineral availability on the apparent rates of anhydrite dissolution is found for the eight wells at the end of flow path 8 in western South Dakota. Here the rates of anhydrite dissolution approximately double in water moving from south to north toward the Williston Basin in a direction normal to the (present) direction of flow.

Organic Matter Oxidation

There is strong evidence that CH_2O oxidation in sediments at low temperatures requires the enzymatic catalysis of bacteria [*Lovley*, 1987; *Chapelle et al.*, 1988]. As such, rates of CH_2O oxidation are a broad measure of bacterial activity. Representing the oxidation of organic matter as

$$CH_2O + H_2O \rightarrow CO_2 + 4H^+ + 4e^- \qquad (36)$$

makes no assumptions as to the ultimate electron-accepting processes, which may be a combination of fermentation, iron reduction, sulfate reduction, and methanogenesis. The mass transfer data for CH_2O given in Table 8 define the extent of (36) in the Madison aquifer and are regarded as an overall estimate of bacterial activity. The mass balance calculations indicate that the predominant electron acceptor is sulfate and to a lesser extent ferric iron in the Madison aquifer; a result that is strongly supported by the observed carbon and sulfur isotopic data.

Estimated rates of bacterial activity using data of Tables 8 and 9 range from 0.002 μmol CH_2O/L/yr (Conoco 44) to 1.24 μmol CH_2O/L/yr (Moore well) and average 0.12 μmol CH_2O/L/yr. These estimates are of similar magnitude to bacterial CO_2 production rates of 0.01–1.0 μmol CH_2O/L/yr estimated from aquifers of Cretaceous age of the northern Atlantic Coastal Plain [*Chapelle et al.*, 1987] but are much less than estimates of 10 μmol CH_2O/L/yr for the Hawthorn aquifer in the Miocene Hawthorn Formation in the southeastern Atlantic Coastal Plain [*Chapelle et al.*, 1988]. In the Madison aquifer the amount of organic matter oxidized tends to increase with increasing dissolved sulfate content, but the rate of organic matter oxidation is probably independent of sulfate concentration. The fastest rates of organic matter oxidation are found in the Central Montana trough.

The average rate of organic matter oxidation in the Madison aquifer is three to four orders of magnitude smaller than rates observed in modern organic-rich sediments (see, for example, *Goldhaber et al.* [1977] and *Kharaka et al.* [1984]). The slower rates of organic matter oxidation in the Madison aquifer are a consequence of the relatively low abundance of organic matter remaining in the Madison rocks and of the relatively low reactivity of the remaining organic matter compared to that found in recent organic-rich sediments [*Westrich and Berner*, 1984].

SUMMARY AND CONCLUSION

In developing the geochemical mass balance models of Tables 8 and 9 we have made extensive use of carbon and sulfur isotope data in conjunction with the water chemistry and thermodynamic speciation calculations. The stable isotope data were particularly useful because they provided additional criteria linking water chemistry with mineral mass transfer. The sulfur isotope data permitted definition of the extent of sulfate reduction. Through use of the sulfur isotope data, both CO_2 and organic matter were included in the mass balance. This permitted estimation of a regional pattern in the sulfur isotopic content of anhydrite consistent with the assumption of a groundwater system closed to CO_2 gas. Sulfur isotope analyses of 65 anhydrite samples from 11 cores in the Madison Limestone in the study area strongly support the calculated sulfur isotope pattern for Madison anhydrites and therefore the mass transfer models. The mass transfer and carbon isotope data for the groundwater indicate the dissolution of relatively heavy dolomites, generally 0–5‰ in $\delta^{13}C$, which is similar to the measured range of $\delta^{13}C$ values for Madison dolomites. The modeled results of Tables 8 and 9 account for observed changes in water chemistry and are supported by measured stable isotopic content of carbon and sulfur in the water and rock. The major conclusions of the models are as follows:

1. The predominant groundwater reaction in the Madison aquifer is dedolomitization (calcite precipitation accompanying dolomite dissolution), which is driven by the irreversible dissolution of anhydrite. Sulfate reduction, $[Ca^{2+} + Mg^{2+}]/Na^+$ cation exchange, and halite dissolution are important locally, particularly in central Montana. The modeled mineral mass transfer can be mapped regionally throughout the study area.

2. The sulfur isotopic composition of dissolving anhydrite in northeastern Wyoming and southwestern South Dakota, estimated through the modeling process and observed in cores from the Madison Limestone, is significantly lighter than expected for Mississippian marine evaporites, indicating diagenetic processes or possibly contributions of sulfur from a terrigenous source. The lighter sulfur isotopic values in northeast Wyoming are thought to be part of a regional depositional pattern.

3. The carbon isotope data, coupled with the mass balance calculations, indicate that incorporation of magnesium in clay minerals through cation exchange or formation of authigenic magnesium-silicate minerals may be important in parts of central Montana and northeast Wyoming. The loss of magnesium causes additional dissolution of dolomite,

which may account for the measured heavy $\delta^{13}C$ values of some waters from the Madison aquifer (about −2.0‰).

4. Groundwater ages adjusted for the modeled mass transfer vary from virtually modern to about 23,000 years for the sampled well locations. These ^{14}C ages indicate flow velocities of 7–87 ft/yr (2.1–26.5 m/yr).

5. Hydraulic conductivities calculated from Darcy's law using the average ^{14}C flow velocities vary from 1.1×10^{-6} to 29.9×10^{-6} ft/s (0.3×10^{-6} to 9.1×10^{-6} m/s) and are similar to those based on digital simulation of the flow system.

6. The measured sulfur isotopic composition of dissolved sulfate and hydrogen sulfide demonstrated a (kinetic) biochemical fractionation of ^{34}S between dissolved sulfate and hydrogen sulfide of approximately −44‰ at 25°C, with a temperature variation of −0.4‰ per °C.

7. The average apparent rates of calcite precipitation, dolomite dissolution, anhydrite dissolution, and organic matter oxidation are 0.59, 0.24, 0.95, and 0.12 μmol/L/yr, respectively.

Acknowledgments. We have benefitted from discussions with many of our Geological Survey colleagues, particularly William Back, Leonard F. Konikow, Ruth G. Deike, Frank H. Chapelle, Briant A. Kimball, and Blair F. Jones. Ruth G. Deike assisted in sampling and description of cores from the Madison Limestone, which were made available to this study by the U.S. Geological Survey Core Library (Denver, Colorado). David A. Stanley, George W. Fleming, and Eric C. Prestemon assisted in computer calculations and computer graphics. We thank Barbara Shultz for sample preparation, Wayne C. Shanks for sulfur isotope analyses, and Carol Kendall and Tyler B. Coplen for carbon isotope data. The manuscript was improved by review comments from Joe S. Downey (USGS, Denver, Colorado), Frank H. Chapelle (USGS, Columbia, South Carolina), Ruth G. Deike (USGS, Reston, Virginia), and an anonymous reviewer.

REFERENCES

Aggarwal, P. K., W. D. Gunter, and Y. K. Kharaka, The effect of pressure on aqueous equilibria, in *Chemical Modeling of Aqueous Systems II*, *Am. Chem. Soc. Symp. Ser.*, vol. 416, edited by D. C. Melchior and R. L. Bassett, pp. 87–101, American Chemical Society, Washington, D. C., 1990.

Back, W., B. B. Hanshaw, L. N. Plummer, P. H. Rahn, C. T. Rightmire, and M. Rubin, Process and rate of dedolomitization—Mass transfer and ^{14}C dating in a regional carbonate aquifer, *Geol. Soc. Am. Bull.*, *94*(12), 1415–1429, 1983.

Back, W., B. B. Hanshaw, L. N. Plummer, P. H. Rahn, C. T. Rightmire, and M. Rubin, Process and rate of dedolomitization—Mass transfer and ^{14}C dating in a regional carbonate aquifer: Reply, *Geol. Soc. Am. Bull.*, *96*, 1098–1099, 1985.

Blankennagel, R. K., L. W. Howells, W. R. Miller, and C. V. Hansen, Preliminary data for Madison Limestone test well 3, NW-1/4 SE-1/4 sec. 35, T. 2 N., R. 27 E., Yellowstone County, Montana, *U. S. Geol. Surv. Open File Rep.*, *79-745*, 201 pp., 1979.

Bottinga, Y., Calculated fractionation factors for carbon and hydrogen isotope exchange in the system calcite-CO_2-graphite-methane-hydrogen and water vapor, *Geochim. Cosmochim. Acta*, *33*, 49–64, 1969.

Brown, D. L., R. K. Blankennagel, L. M. MacCary, and J. A. Peterson, Correlation of paleostructure and sediment deposition in the Madison Limestone and associated rocks in parts of Montana, North Dakota, South Dakota, Wyoming, and Nebraska, *U.S. Geol. Surv. Prof. Pap.*, *1273-B*, 24 pp., 1984.

Brown, E., M. W. Skougstad, and M. J. Fishman, Methods for collection and analysis of water samples for dissolved minerals and gases, laboratory analysis, *U. S. Geol. Surv. Tech. of Water-Resources Invest.*, *5*(C1), 160 pp., 1970.

Budai, J. M., K. C. Lohmann, and J. L. Wilson, Dolomitization of the Madison Group, Wyoming and Utah Overthrust Belt, *Am. Assoc. Pet. Geol. Bull.*, *71*, 909–924, 1987.

Busby, J. F., R. W. Lee, and B. B. Hanshaw, Major geochemical processes related to the hydrology of the Madison Aquifer System and associated rocks in parts of Montana, South Dakota, and Wyoming, *U. S. Geol. Surv. Water Resour. Invest. Rep.*, *83-4093*, 180 pp., 1983.

Busby, J. F., L. N. Plummer, R. W. Lee, and B. B. Hanshaw, Geochemical evolution of water in the Madison aquifer in parts of Montana, South Dakota, and Wyoming, *U. S. Geol. Surv. Prof. Pap.*, *1273-F*, in press, 1990.

Busenberg, E., and L. N. Plummer, Kinetic and thermodynamic factors controlling the distribution of SO_4^{2-} and Na^+ in calcites and selected aragonites, *Geochim. Cosmochim. Acta*, *49*, 713–725, 1985.

Busenberg, E., L. N. Plummer, and V. B. Parker, The solubility of strontianite ($SrCO_3$) in CO_2-H_2O solutions between 2 and 91°C, the association constants of $SrHCO_3(aq)$ and $SrCO_3(aq)$ between 5 and 80°C, and an evaluation of the thermodynamic properties of $Sr^{2+}(aq)$ and $SrCO_3(cr)$ at 25°C and 1 atm total pressure, *Geochim. Cosmochim. Acta*, *48*, 2021–2035, 1984.

Carothers, W. W., and Y. K. Kharaka, Aliphatic acid anions in oil-field waters and their implications for the origin of natural gas, *Am. Assoc. Pet. Geol. Bull.*, *62*, 2441–2453, 1978.

Chapelle, F. H., and L. L. Knobel, Stable carbon isotopes of HCO_3^- in the Aquia aquifer, Maryland: Evidence for an isotopically heavy source of CO_2, *Ground Water*, *23*(5), 592–599, 1985.

Chapelle, F. H., J. L. Zelibor, Jr., D. J. Grimes, and L. L. Knobel, Bacteria in deep coastal plain sediments of Maryland: A possible source of CO_2 to groundwater, *Water Resour. Res.*, *23*(8), 1625–1632, 1987.

Chapelle, F. H., J. T. Morris, P. B. McMahon, and J. L. Zelibor, Jr., Bacterial metabolism and the $\delta^{13}C$ composition of ground water, Floridian aquifer system, South Carolina, *Geology*, *16*, 117–121, 1988.

Chebotarev, I. I., Metamorphism of natural waters in the crust of weathering, *Geochim. Cosmochim. Acta*, *8*, 137–170, 198–212, 1955.

Claypool, G. E., and I. R. Kaplan, The origin and distribution of methane in marine sediments, in *Natural Gases in Marine Sediments*, edited by I. R. Kaplan, pp. 99–139, Plenum, New York, 1974.

Claypool, G. E., W. T. Holser, I. R. Kaplan, H. Sakai, and I. Zak, The age curves of sulfur and oxygen isotopes in marine sulfate and their mutual interpretation, *Chem. Geol.*, *27*, 199–260, 1980.

Cooley, R. L., L. F. Konikow, and R. L. Naff, Nonlinear regression groundwater flow modeling of a deep regional aquifer system, *Water Resour. Res.*, *22*, 1759–1778, 1986.

Deines, P., D. Langmuir, and R. S. Harmon, Stable carbon isotope ratios and the existence of a gas phase in the evolution of carbonate ground waters, *Geochim. Cosmochim. Acta*, *38*, 1147–1164, 1974.

Downey, J. S., Geohydrology of the Madison and associated aquifers in parts of Montana, North Dakota, South Dakota, and Wyoming, *U. S. Geol. Surv. Prof. Pap.*, *1273-G*, 47 pp., 1984.

Downey, J. S., Geohydrology of bedrock aquifers in the Northern Great Plains in parts of Montana, North Dakota, South Dakota, and Wyoming, *U. S. Geol. Surv. Prof. Pap.*, *1402-E*, 87 pp., 1986.

Eichinger, L., A contribution to the interpretation of ^{14}C groundwater ages considering the example of a partially confined sandstone aquifer, *Radiocarbon*, *25*, 347–356, 1983.

Fenchel, T., and T. H. Blackburn, *Bacteria and Mineral Cycling*, 225 pp., Academic, New York, 1979.

Fontes, J.-C., and J.-M. Garnier, Determination of the initial ^{14}C activity of the total dissolved carbon: A review of the existing models and a new approach, *Water Resour. Res.*, *15*, 399–413, 1979.

Foster, M. D., The origin of high sodium bicarbonate waters in the Atlantic and Gulf Coastal Plains, *Geochim. Cosmochim. Acta*, *1*, 33–48, 1950.

Freeze, R. A., and J. A. Cherry, *Groundwater*, 604 pp., Prentice-Hall, Englewood Cliffs, N. J., 1979.

Gallo, G., Equilibrio fra sulfato distronzio ed hequa alle varia temperatura, *Ann. Chim. Appl.*, *25*, 628–631, 1935.

Goldhaber, M. B., R. C. Aller, J. K. Cochran, J. K. Rosenfeld, C. S. Martens, and R. A. Berner, Sulfate reduction, diffusion, and

bioturbation in Long Island Sound sediments, Report of the FOAM group, *Am. J. Sci.*, *277*, 193–237, 1977.

Grossman, E. L., B. K. Coffman, S. J. Fritz, and H. Wada, Bacterial production of methane and its influence on ground-water chemistry in east-central Texas aquifers, *Geology*, *17*, 495–499, 1989.

Grossman, I. G., Origin of the sodium sulfate deposits of the northern Great Plains of Canada and the United States, *U. S. Geol. Surv. Prof. Pap.*, *600-B*, B104–B109, 1968.

Hanshaw, B. B., W. Back, and M. Rubin, Radiocarbon determinations for estimating groundwater flow velocities in central Florida, *Science*, *148*(3669), 494–495, 1964.

Hanshaw, B. B., J. Busby, and R. W. Lee, Geochemical aspects of the Madison aquifer system, in *Montana Geological Society 24th Annual Conference Williston Basin Symposium, Guideb.*, pp. 385–389, Montana Geological Society, Billings, Mont., 1978.

Harvie, C. E., and J. H. Weare, The prediction of mineral solubilities in natural waters—The Na-K-Mg-Ca-Cl-SO_4-H_2O system from zero to higher concentrations at 25°C, *Geochim. Cosmochim. Acta*, *44*, 981–997, 1980.

Hoefs, J., *Stable Isotope Geochemistry*, 140 pp., Springer-Verlag, New York, 1973.

Ingerson, E., and F. J. Pearson, Jr., Estimation of age and rate of motion of groundwater by the ^{14}C-method, in *Recent Researches in the Fields of Hydrosphere, Atmosphere and Nuclear Geochemistry*, pp. 263–283, Maruzen, Tokyo, 1964.

Kharaka, Y. K., S. W. Robinson, L. M. Law, and W. W. Carothers, Hydrochemistry of Big Soda Lake, Nevada: An alkaline meromictic desert lake, *Geochim. Cosmochim. Acta*, *48*, 823–835, 1984.

Konikow, L. F., Process and rate of dedolomitization: Mass transfer and ^{14}C dating in a regional carbonate aquifer: Extended interpretation, *Geol. Soc. Am. Bull.*, *96*, 1096–1098, 1985.

Lee, R. W., and D. J. Strickland, Geochemistry of groundwater in Tertiary and Cretaceous sediments of the southeastern coastal plain in eastern Georgia, South Carolina, and southeastern North Carolina, *Water Resour. Res.*, *24*, 291–303, 1988.

Lovley, D. K., Organic matter mineralization with the reduction of ferric iron: A review, *Geomicrobiol.*, *5*, 375–399, 1987.

Lovley, D. K., and M. J. Klug, Model for the distribution of sulfate reduction and methanogenesis in freshwater sediments, *Geochim. Cosmochim. Acta*, *50*, 11–18, 1986.

MacCary, L. M., E. M. Cushing, and D. L. Brown, Potentially favorable areas for large-yield wells in the Red River Formation and Madison Limestone in parts of Montana, North Dakota, South Dakota, Wyoming, and Nebraska, *U. S. Geol. Surv. Prof. Pap.*, *1273-E*, E1–E13, 1983.

Marshall, W. L., and R. Slusher, Thermodynamics of calcium sulfate dihydrate in aqueous sodium chloride solutions, 0–110°, *J. Phys. Chem.*, *70*, 4015–4027, 1966.

Miller, W. R., Water in carbonate rocks of the Madison Group in Southeastern Montana—A preliminary evaluation, *U. S. Geol. Surv., Water Supply Pap.*, *2043*, 51 pp., 1976.

Millero, F. J., The effect of pressure on the solubility of minerals in water and sea water, *Geochim. Cosmochim. Acta*, *46*, 11–22, 1982.

Mook, W. G., On the reconstruction of the initial ^{14}C content of groundwater from the chemical and isotopic composition, in *Proceedings of Eighth International Conference on Radiocarbon Dating*, vol. 1, pp. 342–352, Royal Society of New Zealand, Wellington, 1972.

Mook, W. G., The dissolution-exchange model for dating groundwater with ^{14}C, in *Interpretation of Environmental Isotope and Hydrochemical Data in Groundwater Hydrology*, pp. 213–225, International Atomic Energy Agency, Vienna, 1976.

Mook, W. G., Carbon-14 in hydrogeological studies, in *Handbook of Environmental Isotope Geochemistry*, vol. 1, *The Terrestrial Environment*, *A*, edited by P. Fritz and J.-C. Fontes, pp. 49–74, Elsevier, New York, 1980.

Mook, W. G., J. C. Bommerson, and W. H. Staverman, Carbon isotope fractionation between dissolved bicarbonate and gaseous carbon dioxide, *Earth Planet. Sci. Lett.*, *22*, 169–176, 1974.

Ohmoto, H., and R. O. Rye, Isotopes of sulfur and carbon, in *Geochemistry of Hydrothermal Ore Deposits*, edited by A. L. Barnes, pp. 509–567, Wiley Interscience, New York, 1979.

Olson, G. J., W. S. Dockins, G. A. McFeters, and W. P. Iverson, Sulfate-reducing bacteria from deep aquifers in Montana, *Geomicrobiol. J.*, *2*(4), 327–340, 1981.

Paces, T., Steady-state kinetics and equilibrium between ground water and granitic rock, *Geochim. Cosmochim. Acta*, *37*, 2641–2663, 1973.

Paces, T., Rate constants of dissolution derived from the measurements of mass balance in hydrological catchments, *Geochim. Cosmochim. Acta*, *47*, 1855–1863, 1983.

Parker, V. B., D. D. Wagman, and W. H. Evans, Selected values of chemical thermodynamic properties, *Tech. Note 270-6*, 106 pp., Natl. Bur. of Stand., Gaithersburg, Md., 1971.

Parkhurst, D. L., D. C. Thorstenson, L. N. Plummer, PHREEQE—A computer program for geochemical calculations, *U. S. Geol. Surv. Water Resour. Invest.*, *80-96*, 210 pp., 1980.

Parkhurst, D. L., L. N. Plummer, and D. C. Thorstenson, BALANCE—A computer program for calculating mass transfer for geochemical reactions in ground water, *U. S. Geol. Surv. Water Resour. Invest. Rep.*, *82-14*, 29 pp., 1982.

Pearson, F. J., Jr., and C. T. Rightmire, Sulphur and oxygen isotopes in aqueous sulphur compounds, in *Handbook of Environmental Isotope Geochemistry*, vol. 1, *The Terrestrial Environment*, *A*, edited by P. Fritz and J. -C. Fontes, pp. 227–258, Elsevier, New York, 1980.

Pearson, F. J., Jr., and D. E. White, Carbon-14 ages and flow rates of water in Carrizo Sand, Atascosa County, Texas, *Water Resour. Res.*, *3*(1), 251–261, 1967.

Peterson, J. A., Subsurface geology and porosity distribution, Madison Limestone and underlying formations, Powder River basin, northeastern Wyoming and southeastern Montana and adjacent areas, *U. S. Geol. Surv. Open File Rep.*, *78-783*, 32 pp., 1978.

Peterson, J. A., Stratigraphy and sedimentary facies of the Madison Limestone and associated rocks in parts of Montana, Nebraska, North Dakota, South Dakota, and Wyoming, *U. S. Geol. Surv. Prof. Pap.*, *1273-A*, 34 pp., 1981.

Plummer, L. N., Geochemical modeling: A comparison of forward and inverse methods, in *First Canadian/American Conference on Hydrogeology, Practical Applications of Ground Water Geochemistry*, edited by B. Hitchon and E. I. Wallick, pp. 149–177, National Water Well Association, Worthington, Ohio, 1984.

Plummer, L. N., and W. Back, The mass balance approach: Applications to interpreting the chemical evolution of hydrologic systems, *Am. J. Sci.*, *280*, 130–142, 1980.

Plummer, L. N., and E. Busenberg, The solubilities of calcite, aragonite, and vaterite in CO_2-H_2O solutions between 0 and 90°C, and an evaluation of the aqueous model for the system $CaCO_3$-CO_2-H_2O, *Geochim. Cosmochim. Acta*, *46*, 1011–1040, 1982.

Plummer, L. N., B. F. Jones, and A. H. Truesdell, WATEQF—A FORTRAN IV version of WATEQ, a computer program for calculating chemical equilibria of natural waters, *U. S. Geol. Surv. Water Resour. Invest. Rep.*, *76-13*, 61 pp., 1976.

Plummer, L. N., D. L. Parkhurst, and D. C. Thorstenson, Development of reaction models for groundwater systems, *Geochim. Cosmochim. Acta*, *47*, 665–685, 1983.

Price, F. T., and Y. N. Shieh, Fractionation of sulfur isotopes during laboratory synthesis of pyrite at low temperatures, *Chem. Geol.*, *27*, 245–253, 1979.

Reardon, E. J., A. A. Mozeto, and P. Fritz, Recharge in northern clime calcareous sandy soils: Soil water chemical and carbon-14 evolution, *Geochim. Cosmochim. Acta*, *44*, 1723–1735, 1980.

Robie, R. A., B. S. Hemingway, and J. R. Fisher, Thermodynamic properties of minerals and related substances at 298.15°K and 1 bar (10^5 pascal) pressure and at higher temperatures, *U. S. Geol. Surv. Bull.*, *1452*, 456 pp., 1978.

Rye, R. O., W. Back, B. B. Hanshaw, C. T. Rightmire, and F. J. Pearson, Jr., The origin and isotopic composition of dissolved sulfide in groundwater from carbonate aquifers in Florida and Texas, *Geochim. Cosmochim. Acta*, *45*, 1941–1950, 1981.

Sando, W. J., Ancient solution phenomena in the Madison Limestone (Mississippian) of north-central Wyoming, *U. S. Geol. Surv. J. Res.*, *2*(2), 133–141, 1974.

Sando, W. J., Madison Limestone, east flank of Bighorn Mountain, Wyoming, *28th Annual Field Conference Guidebook*, pp. 45–52, Wyoming Geological Association, Casper, 1976*a*.

Sando, W. J., Mississippian history of the northern Rocky Mountains regions, *U. S. Geol. Surv. J. Res.*, *4*(3), 317–338, 1976*b*.
Seidell, W., *Solubilities of Inorganic and Metal-Organic Compounds*, American Chemical Society, Washington, D. C., 1958.
Smith, D. L., Depositional cycles of the Lodgepole Formation (Mississippian) in central Montana, *21st Annual Field Conference Guidebook*, pp. 27–36, Montana Geological Society, Billings, 1972.
Smith, H. J., On equilibrium in the system: Ferrous carbonate, carbon dioxide, and water, *J. Am. Chem. Soc.*, *40*, 879–885, 1918.
Smith, R. M., and A. E. Martell, *Critical Stability Constants*, vol. 4, *Inorganic Complexes*, 257 pp., Plenum, New York, 1976.
Surdam, R. C., L. J. Crossey, E. S. Hagen, and H. P. Heasler, Organic-inorganic interactions and sandstone diagenesis, *Am. Assoc. Pet. Geol. Bull.*, *73*, 1–23, 1989.
Tamers, M. A., Surface-water infiltration and groundwater movement in arid zones of Venezuela, in *Isotopes in Hydrology*, pp. 339–351, International Atomic Energy Agency, Vienna, 1967.
Tamers, M. A., Validity of radiocarbon dates on groundwater, *Geophys. Surv.*, *2*, 217–239, 1975.
Tamers, M. A., and H. W. Scharpenseel, Sequential sampling of radiocarbon in groundwater, in *Isotope Hydrology 1970*, pp. 241–256, International Atomic Energy Agency, Vienna, 1970.
Thayer, P. A., Petrology and petrography for U.S. Geological Survey test wells 1, 2, and 3 in the Madison Limestone in Montana and Wyoming, *U. S. Geol. Surv. Open File Rep.*, *81-221*, 82 pp., 1981.
Thorstenson, D. C., D. W. Fisher, and M. G. Croft, The geochemistry of the Fox Hills-Basal Hell Creek aquifer in southwestern North Dakota and northwestern South Dakota, *Water Resour. Res.*, *15*(6), 1479–1498, 1979.
Vogel, J. C., P. M. Grootes, and W. G. Mook, Isotope fractionation between gaseous and dissolved carbon dioxide, *Z. Phys.*, *230*, 225–238, 1970.
Westrich, J. T., and R. A. Berner, The role of sedimentary organic matter in bacterial sulfate reduction: The G model tested, *Limnol. Oceanogr.*, *29*, 236–249, 1984.
Wigley, T. M. L., and A. B. Muller, Fractionation corrections in radiocarbon dating, *Radiocarbon*, *23*(2), 173–190, 1981.
Wigley, T. M. L., L. N. Plummer, and F. J. Pearson, Jr., Mass transfer and carbon isotope evolution in natural water systems, *Geochim. Cosmochim. Acta*, *42*, 1117–1139, 1978.
Wigley, T. M. L., L. N. Plummer, and F. J. Pearson, Jr., Errata, *Geochim. Cosmochim. Acta*, *43*, 1395, 1979.
Wood, W. W., Guidelines for collection and field analysis of ground-water samples for selected unstable constituents, *U. S. Geol. Surv. Tech. Water Resour. Invest.*, (1)D2, 24 pp., 1976.

J. F. Busby, U.S. Geological Survey, 55 N. Interregional Highway, Austin, TX 78702.
B. B. Hanshaw, U.S. Geological Survey, 917 National Center, Reston, VA 22092.
R. W. Lee, U.S. Geological Survey, A-413 Federal Building, U.S. Courthouse, Nashville, TN 37203.
L. N. Plummer, U.S. Geological Survey, 432 National Center, Reston, VA 22092.

(Received March 27, 1989;
revised November 29, 1989;
accepted January 8, 1990.)